The Dissertation Committee for Eric Thomas Ritschdorff Certifies that this is the approved version of the following dissertation:

Applications of Multiphoton-Excited Photochemistry to Microsecond Capillary Electrophoresis, Photolithography, and the Development of Smart Materials

Committee:

Jason B. Shear, Supervisor

James A. Holcombe

Keith J. Stevenson

David A. Vanden Bout

Christine Schmidt

Applications of Multiphoton-Excited Photochemistry to Microsecond Capillary Electrophoresis, Photolithography, and the Development of Smart Materials

by

Eric Thomas Ritschdorff, B.S.

Dissertation

Presented to the Faculty of the Graduate School of

The University of Texas at Austin

in Partial Fulfillment

of the Requirements

for the Degree of

Doctor of Philosophy

The University of Texas at Austin
August 2010

Dedication

This dissertation is dedicated to my parents, John and Joanne

Acknowledgements

I must thank my advisor, Jason Shear, for a tremendous amount of help, support, and patience. I would like to thank Dr. James Holcombe, Dr. Keith Stevenson, Dr. David Vanden Bout, and Dr. Christine Schmidt for their time and consideration while serving as members of my committee. I owe many thanks to former and current Shear lab members. I thank Dr. Matt Plenert for sharing his knowledge of laser beam alignment and capillary electrophoresis, and for laying the groundwork for the experiments presented in Chapter 2. I thank Drs. Ryan Hill, Rex Nielson, and Bryan Kaehr for being a source of help, friendship, and (sometimes) good ideas. I thank current lab members Stephanie Seidlits, Samira Moorjani, Eric Spivey, Todd Hoppe, Michelle Fox, Maryam Ali, and Derek Hernandez. I thank Jodi Connell for assistance with any and all cell culture presented in this dissertation, as well as for her efforts on our collaboration for the work presented in Chapter 4. I thank Tim Hooper for turning a broken-down confocal microscope into a fully functional laser scanning system that was used for the work presented in Chapters 3 and 5. I must thank my family and friends in New York for somehow dealing with me and always putting things into perspective, and to Randy Drevland for years of friendship and lolz. Finally, to Viviene, whose love and support has helped me in more ways than she will ever know.

Applications of Multiphoton-Excited Photochemistry to Microsecond Capillary Electrophoresis, Photolithography, and the Development of Smart Materials

Publication No._____

Eric Thomas Ritschdorff, Ph.D.

The University of Texas at Austin, 2010

Supervisor: Jason B. Shear

Laser-based techniques have become essential tools for probing biological molecules in systems that demand high spatial and temporal control. This dissertation presents the development of micro-analytical techniques based on multiphoton excitation (MPE) to promote highly localized, three-dimensional (3D) photochemistry of biologically relevant molecules on submicron dimensions. Strategies based on capillary electrophoresis (CE) have been developed for the rapid separation and spectroscopic analysis of short-lived photochemical reaction products. High-speed separation and analysis are achieved through a combination of very high electric fields and a laser-based optical system that uses MPE for both the generation and detection of hydroxyindole photoproducts on the time scale of microseconds. MPE was also used for the development of photolithographic techniques for the creation of microstructured protein-based materials with highly defined three-dimensional (3D) topographies. Specifically, a

multiphoton lithographic (MPL) technique was developed that used a low-cost microchip laser for the rapid prototyping of 3D microarchitectures when combined with dynamic optical masking. Furthermore, MPL was used to create novel "smart" biomaterials that reproducibly respond with tunable actuation to changes in the local chemical and thermal environment. The utility of these materials for creating biocompatible cellular microenvironments was demonstrated and presents a novel approach for studying small populations of microorganisms. Finally, through the development of a multifocal approach that used multiple laser beams to promote the photocrosslinking of biological molecules, the speed and versatility of MPL was extended to allow both the parallel fabrication of 3D microstructures and the rapid creation of large-scale biomaterials with highly defined spatial features.

Table of Contents

List of Figures

Chapter 1: Introduction

With the invention of the laser 50 years ago, substantial technological advancements have been realized in the fields of chemistry, biology, physics, medicine, and industrial processes. These advancements originate from a laser's ability to achieve high-intensity, coherent radiation over a broad spectral range (X-ray to far IR) with high spectral purity and high temporal resolution. Laser-based techniques have been crucial for elucidating information from biological systems at levels ranging from multicellular organisms to single biomolecules using tools such as fluorescence microscopy (e.g., confocal [1, 2] and multiphoton [3-5]), scattering-based techniques (e.g., coherent anti-Stokes Raman scattering (CARS) microscopy [6, 7]), and, as is the focus of this dissertation, laser-induced nonlinear photochemistry (e.g., dye uncaging [8, 9] and photolithography [10]). The development of laser-based micro-analytical techniques that rely on exciting photochemistry for probing complex biologically related systems requires high-resolution tools capable of three-dimensional (3D) spatial control and high temporal control.

Restricting photochemistry to high-resolution 3D coordinates as a result of laser excitation is most easily achieved through multiphoton excitation (MPE). Typically, this is accomplished by using high numerical aperture (NA) optics to focus a high-peak power laser to a very small focal spot. This can result in the generation of an excitation focal volume (voxel) with physical dimensions of $< 1\ \mu m^3$ (1 fl) and excitation intensities in the terawatt (10^{12} W cm^{-2}) range.

1

MPE has broad applications to the study of biological systems because of is its inherent ability to localize photochemistry in three-dimensions without the extensive scatter and photodamage associated with single-photon processes. Using MPE, fluorescence recovery after photobleaching (FRAP) has been used to determine the diffusion coefficient of a dye molecule by intentionally photobleaching a 3D volume of known dimensions and monitoring the fluorescence that is generated as dye molecules diffuse into the bleached area [11]. MPE has also been used for the localized uncaging of bound calcium [12] and for laser axotomy for studying nerve regeneration in earthworms [13].

When applied to traditional analytical separation techniques such as capillary electrophoresis (CE), multiphoton-excited photochemistry has enabled for the rapid examination of transient photochemical reaction products on millisecond and microsecond timescales [14-16]. I have worked to expand on this by integrating MPE with CE to develop strategies that allow for the rapid separation and spectroscopic analysis of short-lived transient photodegredation products. High-speed separation and analysis are achieved through a combination of very high electric fields and a laser-based optical system that uses MPE for both the generation and detection of hydroxyindole photoproducts on the time scale of microseconds.

By tightly focusing high peak power laser into a solution of protein and photosensitizer, sufficient intensities can be reached that promotes the photochemical crosslinking of oxidizable amino acid residues. This direct-write photofabrication approach allows for the creating of novel, biocompatible materials [10, 17] with feature

sizes on the order of hundreds of nanometers [10, 18] that respond to environmental cues [19]. I have employed MPE for the development of 3D multiphoton photolithography (MPL) techniques. Specifically, the MPL capabilities of low-cost microchip lasers have been assessed for the fabrication of biological and acrylic-based materials. MPL has been used for the design and creation of novel "smart" biomaterials that reproducibly respond to environmental cues. These smart biomaterials are capable of integrating with single cells and have shown to be useful for the study of bacterial group behavior. Using multiple laser beams, dynamic masked-based MPL has been multiplexed to improve the speed and versatility of this technique, allowing for the rapid parallel prototyping of biocompatible microstructures.

1.1 MULTIPHOTON EXCITATION

MPE is an alternate form of electronic excitation that requires high peak intensities for the simultaneous absorption of two or more photons. Originally postulated in 1931 by Maria Göppert-Mayer [20], MPE was not experimentally realized until the invention of the laser in 1961 [21]. While MPE can occur with the use of continuous-wave lasers [22], the requirement of high peak intensities limits their use, and the widespread adoption of MPE in the biosciences did not occur until the introduction of the femtosecond pulsed titanium:sapphire (Ti:S) laser in 1991 [23].

With a one-photon absorption event, the energy absorbed by a molecule equals the energy gap between the ground state and the excited state (Figure 1.1). For a multiphoton absorption event to occur, two or more photons of lower energy must be

simultaneously absorbed in a high photon flux regime. The first of these lower energy photons excites the molecule to a virtual state, whereby a second must be absorbed prior to the decay this virtual state for electronic excitation to occur (Figure 1.1). This virtual state is not quantized; rather it is a superposition of electronic states that can exist for a short period of time (~1 fs) due to broadening of the energy levels.
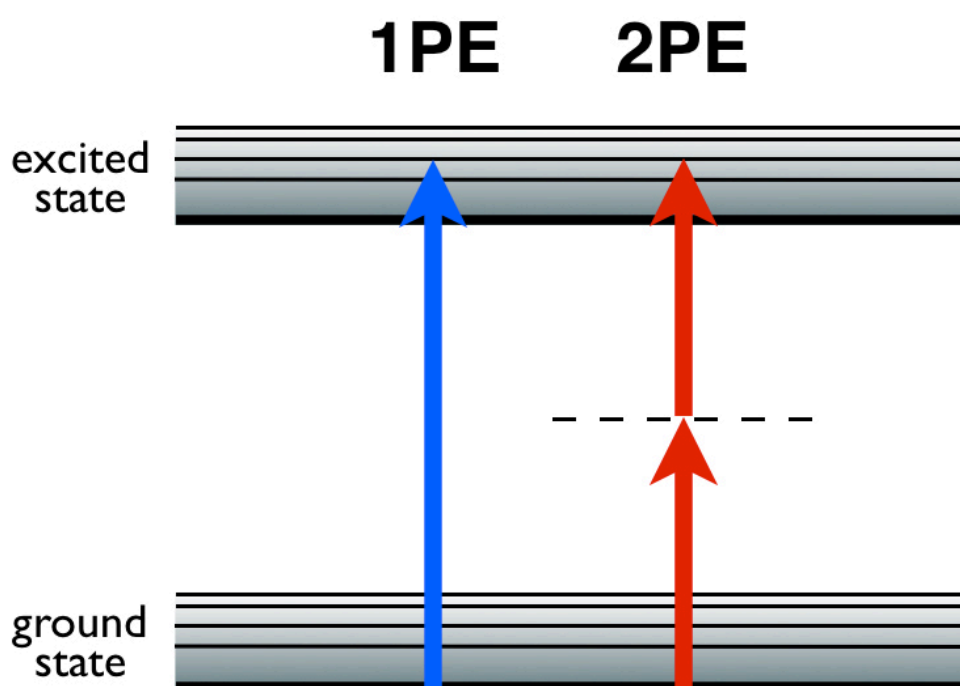
Figure 1.1:   Multiphoton excitation. A simplified Jablonski diagram showing one-photon (1PE) and two-photon (2PE) excitation. In a 1PE regime, a single photon is absorbed that is equal to the energy gap between the ground and excited states. In 2PE, that gap is bridged by a virtual state through which two lower energy photons pass when simultaneously absorbed.

The photonic absorption by a molecule can be expressed in the notation of a chemical reaction [24]:

$$M + n(hv) \rightleftharpoons M*,$$ [1.1]

where M and M* are the ground and excited states of a molecule, hv is a photon, and n is the number of photons absorbed that excites the molecule from the ground state to an excited state. The rate of the reaction for the generation of M* can be described as:

$$\frac{d[M*]}{dt} = k[hv]^n[M] = \delta I^n[M],$$ [1.2]

where k is the rate constant, I is the instantaneous intensity of the excitation light (in units of photons s^{-1} cm^{-2}), and δ is the excitation cross-section (in units of $cm^{2n}(s/photon)^{n-1}$). Achieving sufficient intensities (high photon flux) to excite a chromophore in a multiphoton regime requires the use of high peak power lasers in conjunction with optics capable of focusing the laser light to a very small focal spot. When using high NA, diffraction-limited optics, this localized increase in intensity results in the generation of a 3D focal volume with submicron to micron dimensions (< 1 μm^3) that is ellipsoidal in shape (prolate spheroid) [25].

The probability of an excitation event for a particular molecule is proportional its cross-section (δ) [Equation 1.2]. The fraction of light absorbed in a MPE event is generally extremely small and difficult to measure directly. As a consequence, the multiphoton fluorescence 'action' cross-section is commonly used, which is a product of

5

the absolute cross-section (δ) and the fluorescence quantum yield (ϕ), with base units of $cm^{2n} s^{n-1} photon^{-(n-1)}$, where n is equal to the number of photons involved in the excitation process. To simplify the representation of a two-photon cross-section, the unit Göppert-Mayer (GM) has been defined as $10^{-50} cm^4 s photon^{-1}$. A good two-photon absorber such as fluorescein has a two-photon fluorescence action cross-section of ~40 GM at 780 nm (H_2O, pH 11), a common operating wavelength for the Ti:S laser [26].

The most commonly used laser for MPE is the high repetition rate (75 – 80 MHz) Ti:S oscillator, which produces femtosecond pulses (20 – 250 fs) with high peak powers (kW). With a low duty cycle (10^{-5}), only low to moderate average powers are required for MPE, resulting in little damage to the specimen in the planes outside of the focus of the laser. Peak intensities sufficient for most multiphoton-excited processes can be achieved in the terawatt range ($10^{12} W cm^{-2}$) for a mode-locked Ti:S oscillator operating at 780 nm with an average power of ~ 30 mW using a 1.3 NA microscope objective.

While Ti:S oscillators offer great tunability at wavelengths that allow for deep penetration into biological samples (690 – 1000 nm), they are not the only pulsed laser source capable of promoting MPE. Recent developments in microchip lasers have produced sources capable of exciting MPE and photofabricating biological and acrylic materials [18, 27]. These lasers (frequency-doubled (532-nm) Q-switched Nd:YAG) generate low-microjoule pulses (500 ps) at moderate repetition rates (~7 – 40 kHz), producing peak powers and focused peak intensities comparable to the Ti:S at 3% of the total cost.

1.2 MULTIPHOTON PROTEIN FABRICATION

With the widespread availability of the Ti:S laser in the early 1990s, MPE-related technologies have since seen a revolution, beginning with the development of two-photon microscopy by Webb [3]. A more recent technology that takes advantage of the intrinsic 3D properties of MPE is multiphoton fabrication. This technology has allowed for the direct-write, 3D patterning of a wide range of materials that cannot be performed using single-photon, UV-initiated photolithography. The 3D patterning of acrylic-based resins using multiphoton fabrication has lead to advances in micromachines [28-30], micro-optics [31, 32], and microfluidics [33, 34]. Intricate, 3D microforms have been formed, including microscopic cattle [30], chimpanzee skulls [35], and bacteria houses [33]. While feature sizes have been reduced to tens of nanometers using acrylic resins [36], these materials do not have any native biological activity. Although resins can be doped with bio-molecules [37], they cannot be fabricated in the presence of live cell cultures because of the toxic acrylate monomers and solvents used to dissolve the monomers.

The photopolymerization of biological molecules occurs naturally and many proteins contain photo-oxidizable amino acid residues (e.g., Cys, Trp, Tyr, His) capable of crosslinking when exposed to UV light, as what occurs with some types of cataract formation in the eyes [38] and wrinkling of the skin [39]. The first demonstration of crosslinking between protein monomers as initiated by MPE was by Pitts *et al.*, where it was shown that solid protein material could be created from a solution of protein (bovine serum albumin (BSA) and photosensitizer (rose bengal) [17]. Since this initial

presentation, the Shear group has exploited this technique for the study of biological systems using a variety of approaches [10, 18, 19, 40]

Multiphoton-excited protein crosslinking is typically performed using high NA optics to tightly focus a high peak power pulsed laser into a solution of concentrated protein (e.g., BSA, avidin, lysozyme, cytochrome-c) containing a photosensitizer (e.g. rose bengal, methylene blue, flavin adenine dinucleotide (FAD)). This results in the localized excitation of the photosensitizer, leading to crosslinking of the protein within the fabrication voxel. A photosensitizer acts to catalyze the photochemical crosslinking of protein monomers to form a solid protein matrix. This photosensitization process can occur either through a type I or type II mechanism, and this designation depends on the interaction between the sensitizer molecule and the protein [41]. A type I mechanism involves the excitation of a photosensitizing molecule to a triplet state, where it then interacts directly with an oxidizable residue resulting in hydrogen abstraction, generating reactive free radicals. A type II sensitization results in the generation of a singlet oxygen ($^1O_2$) species that can then interact with amino acid residues. Of the commonly used photosensitizers for MPE protein crosslinking, FAD is known to act through a type I process, whereas rose bengal and methylene blue sensitize via type II mechanisms [41].
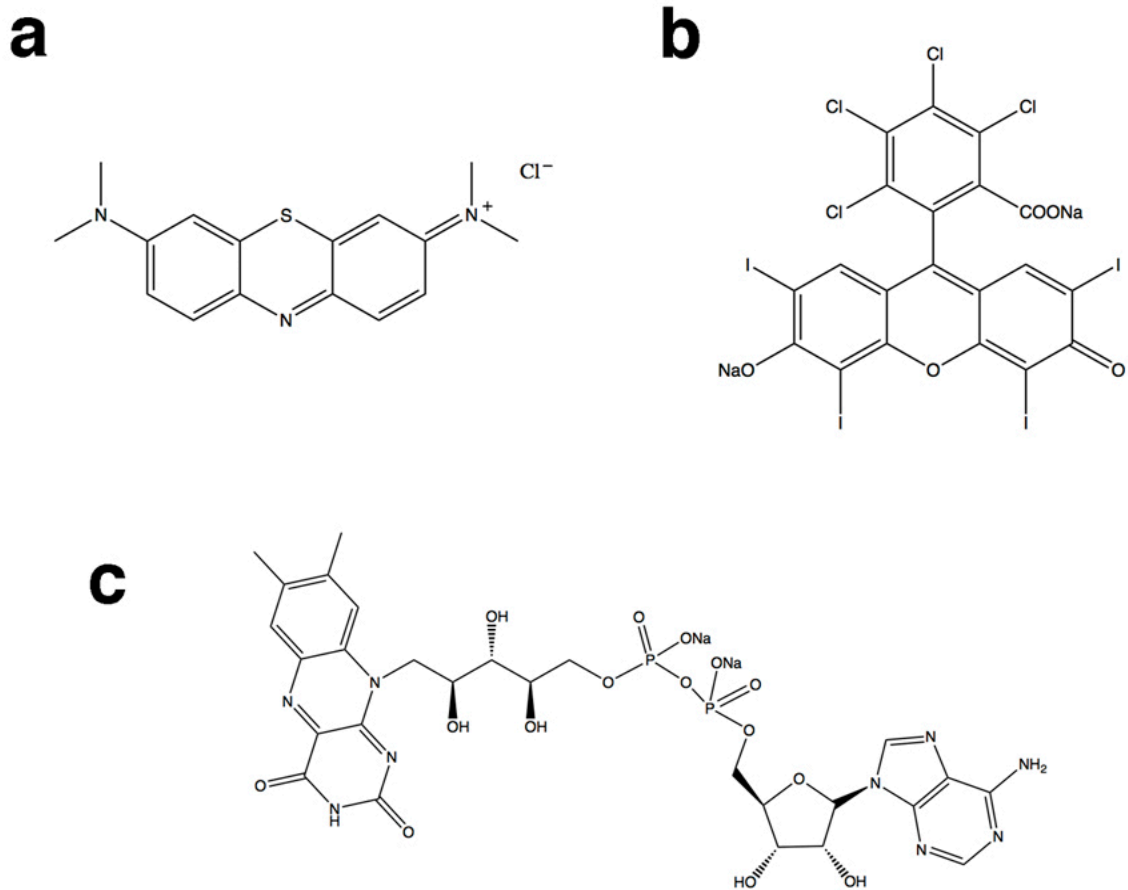
Figure 1.2: Chemical structures of common photosensitizers used for protein multiphoton fabrication: (a) methylene blue (b) rose bengal (c) flavin adenine dinucleotide (FAD).

Lines of solid protein material can be created by scanning the microscope stage relative to the focused laser beam using 3D vector-based movements, thus creating protein lines in a direct-write approach. (Figure 1.3, a, b). Alternatively, galvanometer-driven scan mirrors can be used to raster scan the focused laser beam relative to the sample, resulting in the creation of a protein fabrication plane. Tall, tower-like protein

structures (e.g., Figure 1.3, c) can be fabricated by translating the focus of the raster-scanned beam axially into solution, thereby creating structures in a plane-by-plane fashion with the maximum height of the structure being limited by the working distance of the microscope objective. Through either method, protein microarchitectures can be formed rapidly with high-resolution while maintaining biofunctionality and biocompatibility.
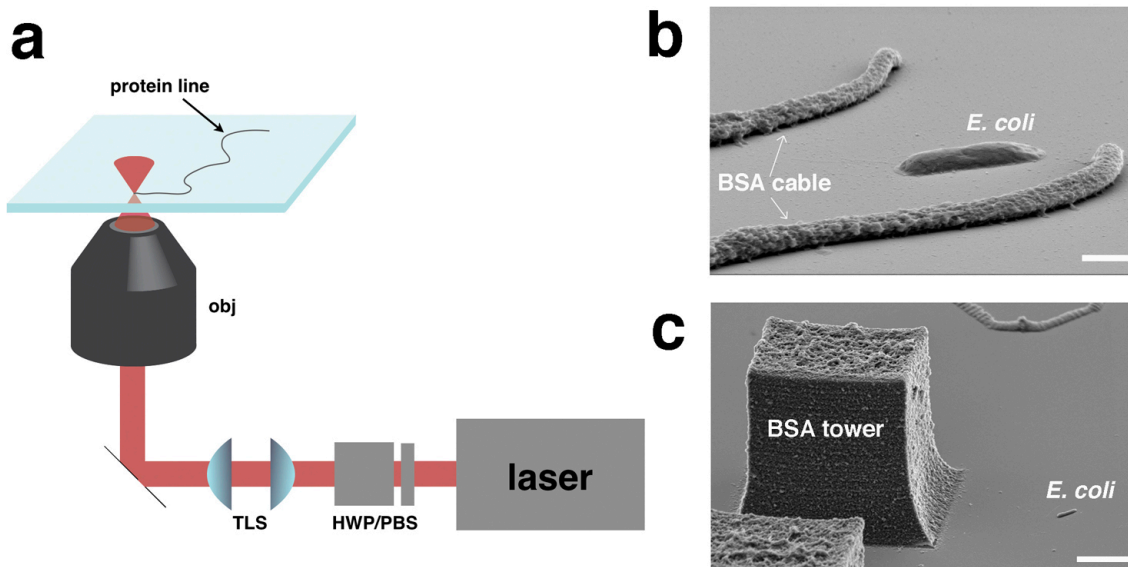
Figure 1.3: Protein microfabrication. (a) A simplified protein photofabrication setup. The output of a high peak power laser is first sent through a halfwave plate/polarizing beam splitter pair (HWP/PBS) that allows for the attenuation of the laser power. The beam is then passed through a telescoping lens set for beam collimation before being sent into the back aperture of an infinity corrected, high numerical aperture microscope objective that tightly focuses the laser beam into a solution of protein and photosensitizer. The microscope stage can then be translated to photofabricate solid protein material in a direct-write fashion. (b) A scanning electron micrograph showing a bovine serum albumin (BSA) cable fabricated using a 36.6 kHz frequency-doubled (532 nm) Nd:YAG laser from a solution of 400 mg mL^{-1} BSA and 10 mM FAD. This cable was fabricated by focusing the laser from below the glass substrate up and into solution, creating a free-floating cable that eventually settled on the glass surface. (c) SEM image of a BSA tower. By using a galvo-driven mirror to rapidly scan the laser in a two-dimensional plane, a tower can be easily fabricated by simply focusing the scanning laser beam deeper into solution at prescribed distances. This tower was fabricated to a total height of 20 μm using the same laser and protein solution as in (b) with prescribed optical axis stage increments of 1.0 μm between fabrication layers. A single *Escherichia coli* cell, added after fabrication, is shown for scale in both (b) and (c). Scale bars: b, 1 μm; c, 5 μm.

Although vector-based, point-by-point fabrication is effective for producing microstructures having arbitrary 3D topographies, it is time consuming and does not generally allow for the rapid 3D prototyping of microarchitectures that would enable researchers to rapidly iterate their fabricated designs. For the purpose of rapid design and photofabrication, the Shear lab has developed techniques that allow for the rapid fabrication and prototyping of biological and acrylic-based materials. Initially, Kaehr and Shear developed a MPL technique that relies on the use of a simple over-head transparency to act as a photomask [42]. When placed in the path of a focused, raster-scanning Ti:S laser beam in a plane conjugate to the microscope objective image plane, a one-to-one mapping occurs between the mask plane and the microscope image plane, resulting in the photofabrication of the masked object at a magnification roughly equal to the power of the microscope objective. By changing the mask, structures can be fabricated in an iterative process, allowing the creation of microforms within minutes. These microforms can be used for the capture of single or small numbers of bacteria for studying cell cultures on the microscale. However, this mask-based process becomes arduous when multiple masks corresponding to different fabrication patterns in different axial planes are needed to complete a single structure, as careful mask alignment is required.

To overcome the limitations associated with transparency-based masking, Nielson *et al.* developed a dynamic masked-based MPL technique that uses a digital micromirror device (DMD) in place of a static mask [35]. By raster scanning a focused, pulsed Ti:S laser across the mirrored-face of a DMD aligned in an optical plane conjugate to the

microscope objective image plane, the 2D binary images presented on the DMD are rendered as a 2D photofabricated plane of material with a finite axial thickness (optical axis) that depends on the NA objective used for fabrication, among other factors. Complex 3D microstructures are created rapidly with high-resolution through the synchronization of the presentation of the 2D image slices derived from 3D objects or computer-illustrated designs on the DMD with z-axis (optical axis) stage movements. Photofabricated microstructures can be progressively prototyped by simply manipulating the 2D binary images presented to the DMD, allowing for a rapid, on-the-fly iterative process for the design of 3D microarchitectures.

1.3 CAPILLARY ELECTROPHORESIS

The Shear lab has been interested in exploiting the highly localized 3D excitation coordinates generated as a result of MPE for developing novel sample introduction strategies for high-speed CE. MPE provides a means to minimize the spatial and temporal aspects of a sample introduction plug and detection zone in CE as result of the femtoliter-sized excitation voxel formed when focusing a pulsed laser with high NA optics. By minimizing the dimensions of the injection and detection regions, separation distances have been reduced to <10 μm, thus enabling chemical separations to be performed ~100-fold faster than other methods when combined with very high electric fields [15]. This section describes the basic principles of CE providing an understanding for the experiments detailed in Chapter 2.

Separation strategies such as liquid chromatography are limited by the rate at which molecules can partition between mobile and stationary phases, which often results

in separation times of minutes to hours. With a separation strategy such as CE where there is no stationary phase, the potential exists for significantly higher-speed separations. CE is a separation technique in which analytes are separated based on differences in their charge-to-drag ratio within a viscous medium that is under a continuously applied potential. Separations are performed in open-tubular, fused silica capillaries with inner diameters typically $20 - 150$ μm that have a high surface to volume ratio and allow for efficient heat transfer. A typical experiment (Figure 1.4) uses a capillary tens of centimeters long, with each end placed in an electrolyte reservoir that contains either a high-voltage electrode or a grounded electrode. To perform a separation, the capillary is first filled with electrolyte solution and an analyte plug is injected into one end of the capillary using either electrokinesis (high voltage) or hydrodynamic (pressure) flow. The capillary is then returned to the electrolyte reservoir and a high-voltage is applied. The analytes move axially within the capillary, ideally fractionating based on their movement within the electric field prior to detection [43].
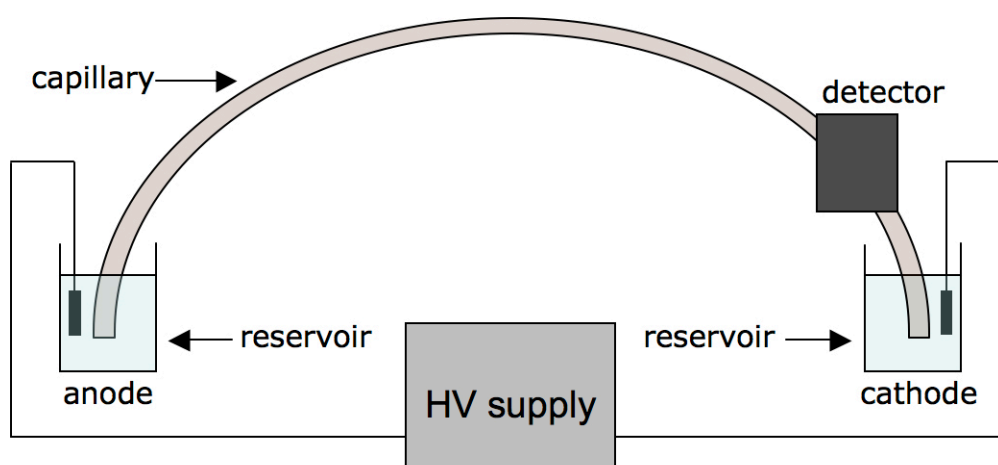
Figure 1.4: Schematic of a conventional capillary electrophoresis setup.

Analyte movement within a capillary is driven by two independent forces: electrophoresis and electroosmosis (EOF). In a system where there is no uni-directional bulk-solution flow, electrophoresis induces charged species to migrate towards electrodes of opposite charge. However, silanol groups along the inner wall of the capillary are negatively charged (above ~ pH 2.5) and solvated cations accumulate within an electrical double-layer on the negatively charged capillary surface [43]. When an electric field is applied to the capillary, these solvated cations within the electrical double layer are driven towards the cathode (negative electrode), resulting in the generation of a flat flow profile. EOF causes all species to migrate in the same direction towards the detector when conditions for EOF are present, resulting in separation of molecules of all charge states (positive, negative, and neutral). To separate analytes with the major driving force being electrophoresis, EOF can be reduced through a number of methods, most notably: increased protonation of the silanol groups by lowering the pH of the electrolyte solution, increasing the ionic strength to decrease the size of the electrical double layer, adding multivalent cations to reverse the net charge of the capillary wall, and adding high molecular weight surfactants (non-ionic) to adsorb to the capillary walls to reduce the attraction of solvated cations [43].

In contrast to liquid chromatography where a molecule is in equilibrium between the stationary and mobile phases with the kinetics ultimately limiting the speed of the separation, CE separations are performed within a single phase. Because of this, the speed at which analytes migrate through the column is limited by the separation distance and the applied electric field [15, 43, 44],

15

$$t = \frac{L}{\mu_{app}E}, \qquad [1.3]$$

where μ_{app} is the apparent electrophoretic mobility, which is the sum of the electrophoretic (μ_{ep}) and electroosmotic (μ_{os}) mobilities, L is the distance from the injection site to the detection site, and E is the applied electric field. While separation speed is important, especially if the analytes are short-lived transient species, the analytes must fractionate with sufficient resolution to distinguish them prior to detection. In an ideal electrophoretic separation where diffusion is the only contributing factor to band width, the spatial variance (σ^2) an of analyte plug migrating through a capillary is defined by the Einstein equation,

$$\sigma^2 = 2Dt, \qquad [1.4]$$

where D is the molecular diffusion coefficient and t is the migration time. Under ideal conditions, the separation efficiency, N, or the number of theoretical plates, can be defined as

$$N = \left(\frac{L}{\sigma}\right)^2 = \frac{\mu V}{2D} \qquad [1.5]$$

where σ is the spatial bandwidth and V is the applied potential [15, 44] From this relationship, it can be seen that high-speed separations can be achieved by increasing the applied potential over a shorter separation distance, thus reducing the migration time of

the analytes. However, at high electric fields, the occurrence of resistive heating (Joule heating) limits the potential that can be applied. While heating effects can be mitigated through the use of low ionic strength buffers, narrow channels, and cooling systems, the ultimate limit to the spatial variance of a migrating analyte band is the size of the injection plug and the extent of the detection regions. To overcome these limitations, the Shear lab has developed novel sample introduction and detection schemes that rely on the use of focused pulsed lasers to act as highly localized injection and detection sources [14-16], and such experiments are detailed in Chapter 2.

1.4 SUMMARY OF CHAPTERS

This dissertation describes approaches based on MPE for exciting biologically related compounds for the development of laser-based microanalytical techniques. Chapter 2 describes the development of strategies based on capillary electrophoresis that allow for the rapid separation and spectroscopic analysis of short-lived transient photochemical reaction products. Chapter 3 presents a comparison of two microchip lasers that differ in pulse repetition rate for performing MPL. Chapter 4 describes the design and creation of novel 'smart' biomaterials that reproducibly respond to environmental cues. These smart biomaterials are capable of interacting with single cells and may be useful for the study of bacterial group behavior. Chapter 5 describes the simultaneous use of multiple laser spots for performing dynamic masked-based MPL to improve the speed and versatility of this technique.

1.5 REFERENCES

1.   Korlach, J., Schwille, P. and Webb, W., *Characterization of lipid bilayer phases by confocal microscopy and fluorescence correlation spectroscopy*. Proceedings of the National Academy of Sciences, 1999. **96**: p. 8461-8466.

2.   Rajadhyaksha, M., Grossman, M. and Esterowitz, D., *In vivo confocal scanning laser microscopy of human skin: melanin provides strong contrast*. Journal of Investigative Dermatology, 1995. **104**: p. 946-952.

3.   Denk, W., Strickler, J.H. and Webb, W.W., *Two-photon laser scanning fluorescence microscopy*. Science, 1990. **248**: p. 73-76.

4.   Xu, C., Zipfel, W., Shear, J., Williams, R. and Webb, W., *Multiphoton fluorescence excitation: new spectral windows for biological nonlinear microscopy*. Proceedings of the National Academy of Sciences, 1996. **93**: p. 10763-10768.

5.   Zipfel, W.R., Williams, R.M., Christie, R., Nikitin, A.Y., Hyman, B.T. and Webb, W.W., *Live tissue intrinsic emission microscopy using multiphoton-excited native fluorescence and second harmonic generation*. Proceedings of the National Academy of Sciences, 2003. **100**: p. 7075-7080.

6.   Evans, C.L., Potma, E.O., Puorishaag, M., Cote, D., Lin, C.P. and Xie, X.S., *Chemical imaging of tissue in vivo with video-rate coherent anti-Stokes Raman scattering microscopy*. Proceedings of the National Academy of Sciences, 2005. **102**(46): p. 16807-16812.

7.   Zumbusch, A., Holtom, G. and Xie, X., *Three-dimensional vibrational imaging by coherent anti-stokes raman scattering*. Physical Review Letters, 1999. **82**: p. 4142-4145.

8.   Denk, W., *Two-photon scanning photochemical microscopy: mapping ligand-gated ion channel distributions*. Proceedings of the National Academy of Sciences, 1994. **91**: p. 6629-6633.

9.   Pettit, D.L., Wang, S.S.-H., Gee, K.R. and Augustine, G.J., *Chemical two-photon uncaging: a novel approach to mapping glutamate receptors*. Neuron, 1997. **19**: p. 465-471.

10.   Kaehr, B., Allen, R., Javier, D., Currie, J. and Shear, J., *Guiding neuronal development with in situ microfabrication*. Proceedings of the National Academy of Sciences, 2004. **101**: p. 16104-16108.

11.   Brown, E., Wu, E., Zipfel, W. and Webb, W., *Measurement of molecular diffusion in solution by multiphoton fluorescence photobleaching recovery*. Biophysical Journal, 1999. **77**: p. 2837-2849.

12. Brown, E.B., Shear, J.B., Adams, S.R., Tsien, R.Y. and Webb, W.W., *Photolysis of caged calcium in femtoliter volumes using two-photon excitation*. Biophysical Journal, 1999. **76**: p. 489-499.

13. Yanik, M.F., Cinar, H., Cinar, H.N., Chisholm, A.D., Jin, Y. and Ben-Yakar, A., *Functional regeneration after laser axotomy*. Nature, 2004. **432**: p. 822.

14. Gordon, M., Okerberg, E., Gostkowski, M. and Shear, J., *Electrophoretic characterization of transient photochemical reaction products*. Journal of the American Chemical Society, 2001. **123**: p. 10780-10781.

15. Plenert, M. and Shear, J., *Microsecond electrophoresis*. Proceedings of the National Academy of Sciences, 2003. **100**(7): p. 3853-3857.

16. Ritschdorff, E., Plenert, M. and Shear, J., *Microsecond analysis of transient molecules using bi-directional capillary electrophoresis*. Analytical Chemistry 2009. **81**: p. 8790-8796.

17. Pitts, J.D., Campagnola, P.J., Epling, G.A. and Goodman, S.L., *Submicron multiphoton free-form fabrication of proteins and polymers: studies of reaction efficiencies and applications in sustained release*. Macromolecules, 2000. **33**: p. 1514-1523.

18. Kaehr, B., Ertas, N., Nielson, R., Allen, R., Hill, R.T., Plenert, M. and Shear, J.B., *Direct-write fabrication of functional protein matrixes using a low-cost Q-switched laser*. Analytical Chemistry, 2006. **78**: p. 3198-3202.

19. Kaehr, B. and Shear, J.B., *Multiphoton fabrication of chemically responsive protein hydrogels for microactuation*. Proceedings of the National Academy of Sciences, 2008. **105**: p. 8850-8854.

20. Göppert-Mayer, M., *Elementary processes with two quantum transitions*. Annalen der Physik, 2009. **18**: p. 466-479.

21. Kaiser, W. and Garrett, C.G.B., *Two-photon excitation in $CaF_2:Eu^{2+}$*. Physical Review Letters, 1961. **7**: p. 229-231.

22. Hell, S., Booth, M., Wilms, S., Schnetter, C., Kirsch, A.K., Arndt-Jovin, D.J. and Jovin, T.M., *Two-photon near-and far-field fluorescence microscopy with continuous-wave excitation*. Optics Letters, 1998. **23**: p. 1238-1240.

23. Klein, J. and Kafka, J.D., *The Ti:Sapphire laser: The flexible research tool*. Nature Photonics, 2010. **4**(5): p. 289-289.

24. Shear, J.B., *Multi-photon excited fluorescence in bioanalytical chemistry*. Analytical Chemistry, 1999. **71**: p. 598A-605A.

25. Sun, H., Tanaka, T. and Kawata, S., *Three-dimensional focal spots related to two-photon excitation*. Applied Physics Letters, 2002. **80**: p. 3673-3675.

26. Xu, C. and Webb, W., *Measurement of two-photon excitation cross sections of molecular fluorophores with data from 690 to 1050 nm*. Journal of the Optical Society of America B, 1996. **13**: p. 481-491.

27. Wang, I., Bouriau, M., Baldeck, P., Martineau, C. and Andraud, C., *Three-dimensional microfabrication by two-photon-initiated polymerization with a low-cost microlaser*. Optics Letters, 2002. **27**(15): p. 1348-1350.

28. Bayindir, Z., Sun, Y., Naughton, M.J., Lafratta, C.N., Baldacchini, T., Fourkas, J.T., Stewart, J., Saleh, B.E.A., and Teich, M.C., *Polymer microcantilevers fabricated via multiphoton absorption polymerization*. Applied Physics Letters, 2005. **86**(6): p. 064105.

29. Galajda, P. and Ormos, P., *Complex micromachines produced and driven by light*. Applied Physics Letters, 2001. **78**: p. 249-251.

30. Kawata, S., Sun, H., Tanaka, T. and Takada, K., *Finer features for functional microdevices*. Nature, 2001. **412**: p. 697-698.

31. Sun, H., Matsuo, S. and Misawa, H., *Three-dimensional photonic crystal structures achieved with two-photon-absorption photopolymerization of resin*. Applied Physics Letters, 1999. **74**: p. 786-788.

32. Ledermann, A., Cademartiri, L. and Hermatschweiler, M., *Three-dimensional silicon inverse photonic quasicrystals for infrared wavelengths*. Nature Materials, 2006. **5**: p. 942-945.

33. Kaehr, B. and Shear, J., *High-throughput design of microfluidics based on directed bacterial motility*. Lab on a Chip, 2009. **9**: p. 2632-2637.

34. Kumi, G., Yanez, C.O., Belfield, K.D. and Fourkas, J.T., *High-speed multiphoton absorption polymerization: fabrication of microfluidic channels with arbitrary cross-sections and high aspect ratios*. Lab on a Chip, 2010. **10**(8): p. 1057-1060.

35. Nielson, R., Kaehr, B. and Shear, J., *Microreplication and design of biological architectures using dynamic-mask multiphoton lithography*. Small, 2009. **5**: p. 120-125.

36. Li, L., Gattass, R., Gershgoren, E., Hwang, H. and Fourkas, J., *Achieving {lambda}/20 resolution by one-color initiation and deactivation of polymerization*. Science, 2009. **324**: p. 910-913.

37. Correa, D.S., Tayalia, P., Cosendey, G., Santos, D.S.d., Aroca, R.F., Mazur, E. and Mendonca, C.R., *Two-photon polymerization for fabricating structures containing the biopolymer chitosan*. Journal of Nanoscience and Nanotechnology, 2009. **9**: p. 5845-5849.

38. Daviesa, M.J. and Truscottb, R.J., *Photo-oxidation of proteins and its role in cataractogenesis*. Journal of Photochemistry and Photobiology B: Biology, 2001. **63**: p. 114-125.

39.   Fisher, G.J., Dutta, S.C., Talwar, H.S., Wang, Z., Varani, J., Kang, S. and Voorhees, J.J., *Molecular bases of sun-induced premature sking ageing and retinoid antoagonism*. Nature, 1996. **379**: p. 335-339.

40.   Allen, R., Nielson, R., Wise, D. and Shear, J., *Catalytic three-dimensional protein architectures*. Analytical Chemistry, 2005. **77**: p. 5089-5095.

41.   Spikes, J.D., Shen, H., Kopeckova, P. and Kopecek, J., *Photodynamic crosslinking of proteins. 111. Kinetics of the FMN-and rose bengal-sensitized photooxidation and intermolecular crosslinking of modeI tyrosine-containing M(2-hydroxypropyI)methacryIamide copolymers*. Photochemistry and Photobiology, 1999. **70**: p. 130-137.

42.   Kaehr, B. and Shear, J., *Mask-directed multiphoton lithography*. Journal of the American Chemical Society, 2007. **129**: p. 1904-1905.

43.   Grossman, P.D. and Colburn, J.C., *Capillary Electrophoresis: Theory and Pracitce*. 1992, San Diego: Academic Press, Inc. 352.

44.   Jorgenson, J.W. and Lukas, K.D., *Capillary zone electrophoresis*. Science, 1983. **222**: p. 266-272.

Chapter 2: Transient Photochemical Analysis Using Microsecond Capillary Electrophoresis*

2.1 INTRODUCTION

The study of short-lived transient species requires tools that can rapidly distinguish similar molecules on very short time scales. Time-resolved spectroscopy has been a useful tool for performing such analyses, leading to advances in the study of transition states of conformationally changing biological macromolecules [1-3], photochemical reaction intermediates [4-6], and thermal reactions [3, 7]. However, challenges persist when reaction intermediates are in the condensed phase or when multiple analytes are present in the sample, which often leads to overlapping spectral responses. To overcome these limitations, a chemical separation could be performed prior to spectroscopic interrogation to eliminate problems associated with spectral overlap. However, this is only effective if spatial isolation occurs within the lifetime of the transient species. Because chemical separations are often slow, typically requiring analysis times that are considerably longer than the lifetimes of most transient species, there is a need for faster separation strategies that allow the rapid analysis of short-lived molecules prior to their degradation. Here, I present high-speed separation strategies based on capillary electrophoresis (CE) for the study of short-lived transient photochemical reaction products.

As discussed in Chapter 1, separation strategies such as liquid chromatography are limited by the rate at which molecules can partition between mobile and stationary

---

phases, which often results in separation times of minutes to hours. With a separation strategy such as CE where there is no stationary phase, the potential exists for significantly higher-speed separations. Chemical separations on time scales of milliseconds to low seconds have been achieved using CE in conjunction with a variety of sample gating (injection) strategies, such as optical gating and fast field switching, on microchip separation platforms that work to limit the size of the injection and detection regions [8-16]. The rapid analysis times demonstrated using these injection techniques, particularly optical injection, have brought upon great interest in their application to the study of short-lived transient solution phase molecules.

The Shear lab has been interested in developing improved gating (injection) strategies in conjunction with CE [10, 17, 18]. Hydroxyindoles act as a good model system for developing transient analysis techniques because of their unique multiphoton induced photochemistry. Hydroxyindoles (Figure 2.1), natively fluorescent in the UV region ($\lambda_{em,max} \approx 340$ nm), undergo a photodegredation process when irradiated with tightly focused pulsed Ti:S light. During this process three photons are absorbed simultaneously to form a photochemical intermediate that can subsequently absorb an additional photon, creating a photoproduct that is unable to relax to the ground state of the parent hydroxyindole [19, 20]. This photoproduct has distinct fluorescence properties from its parent compound, with $\lambda_{em} \approx 500$ nm when excited nonlinearly through the absorption of two additional photons. Because the hydroxyindole photoproduct emission is red-shifted ~ 160 nm from the parent hydroxyindole, the transient species can be

fluorescently detected independently of the parent species through the use of UV blocking filters.
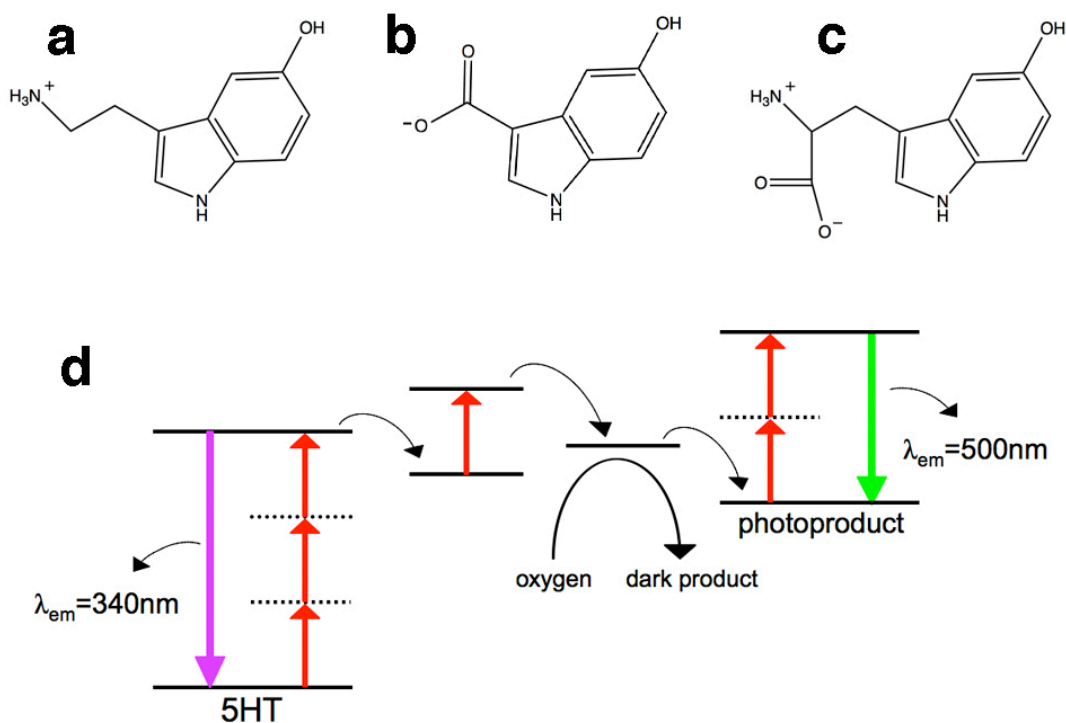
Figure 2.1: Chemical structures of hydroxyindoles examined in this work: (a) 5-hydroxytryptamine (5HT), (b) 5-hydroxyindole-2-carboxylic acid (5HI2CA), and (c) 5-hydroxytryptophan (5HTrp). (d) Multiphoton photochemistry of hydroxyindoles (5HT) proceeds initially through a three-photon absorption process that generates an intermediate that can subsequently absorb a single photon. This photoproduct can then be excited by two additional photons, resulting in improved fluorescence in the visible region [adapted from [19]].

Optical gating was introduced as means to rapidly inject analytes into a capillary for electrophoretic analysis [8]. Under a continuously applied potential, a stream of fluorescent analytes flowing through a capillary is exposed to a high intensity focused

24

laser near the inlet in a side-on approach (90° to the migration axis), resulting in the constant photobleaching of the molecules as they enter the capillary. To perform a separation, the laser beam is briefly blocked, resulting in the injection of a small plug of analytes, which are separated and then detected by another beam downstream [8]. Gordan *et al*. demonstrated the first capillary electrophoresis-based analysis of transient photochemical intermediates using a modified optical gating technique as a means to further understand the multiphoton photochemistry of hydroxyindoles [10]. Rather than continuously photobleaching with a high-intensity laser, they took advantage of the unique photochemical properties of hydroxyindoles by producing multiphoton-induced photoproducts at the capillary inlet by exposing the continuously flowing solution to a focused Ti:S laser (termed the "gate beam") for a very brief period of time. Using a second beam (termed the "probe beam") that is aligned down-stream of the gate beam, visible fluorescence from the hydroxyindole photoproduct was generated and subsequently detected with a photomultiplier. Using a separation distance of 12 μm, photoproducts were analyzed on low-millisecond timescales and it was determined that the photoproducts maintain the same charge-state as their parent molecule. However, low electric fields were generated using this approach resulting in low analyte velocity. Due to longitudinal diffusion, the slow moving analyte plug was greatly broadened resulting in low separation efficiency.

To achieve even faster separation times and greater separation efficiency, Plenert and Shear developed a novel capillary modification that resulted in the generation of increased electric fields (~0.1 MV cm^{-1}) [17]. Such high electric fields were amplified by

deforming the capillary to an hourglass shape using a pipette puller, which increases its unit-length resistance when a potential is applied following Ohm's law. Using the modified optical injection technique previously described, a binary mixture of hydroxyindoles (5-hydroxytrytamine (5HT) and 5-hydroxytryptophan (5HTrp)) was injected and separated over $\sim 10\,\mu$m in 10 μs using a modified capillary with an applied potential of 35 kV [17].

This chapter describes two strategies developed for the purpose of analyzing transient photochemical intermediates using microsecond capillary electrophoresis. The first strategy demonstrates the possibility for minimizing analysis times of oppositely charged photochemically generated transient species in which oppositely photoproducts migrate towards oppositely charged electrodes under an applied electric field, positive species towards the cathode and negative species towards the anode. In this approach, three Ti:S laser beams are aligned into a high NA microscope objective – one high-power gate beam and two lower power probe beams. The two probe beams, aligned on opposite sides of the gate beam, excite fluorescence of the photoproducts after migration of several microns from the high power gate beam.

In addition, a similar optical configuration is evaluated for tracking transient photochemical intermediates at multiple positions as the migrate down an electrophoretic channel, an approach with potential value in tracking changes in a molecule's electrophoretic mobility over short time scales (μs – ms). Here, a sequence of probe sites are positioned downstream of a gate site, providing a means to detect the mobility of a single species at multiple time points after its creation.

2.2 EXPERIMENTAL

2.2.1 Reagents and Solutions

All reagents were obtained from Sigma-Aldrich Co. (St. Louis, MO) unless otherwise noted. Stock solutions of MES buffer (pH 5.5) and HEPES buffer (pH 7.4) were prepared weekly and hydroxyindole solutions 5HT, 5HTrp, and 5HI2CA were prepared fresh daily. All solutions were filtered using 0.2 μm syringe filters (Corning, Corning, New York); buffer vials were cleaned by filling with filtered deionized H_2O and sonicated for 45 min before use.

2.2.2 Fluidics Assembly

The polyimide coating in the central 2 cm section of a 25 μm i.d., ∼10 cm long capillary (Polymicro, Technologies, Phoenix, AZ) was removed using a Bunsen burner flame. The capillary was then carefully placed into a pipet puller (P-2000, Sutter Instruments, Novato, CA) where it was pulled to produce an hourglass geometry in the central region with a waist i.d. of ∼ 5 μm. This modification resulted in a dramatic increase in the unit-length resistance within the pull region, thereby amplifying the electric field. At the applied potentials examined in this work, at least 2 V cm^{-1} were generated per volt applied to the capillary.

Pulled capillaries were secured under a milled Plexiglas block using epoxy (Epoxy 907 Adhesive System, Miller-Stephenson, Danbury, CT) so that the hourglass region coincided with a drilled access hole (Figure 2.2). A borosilicate glass coverslip (no. 0) was mounted directly beneath the capillary, and was sealed against the block to form a well surrounding the pulled region of the capillary. Refractive index matching

fluid (glycerin) was placed in the well to fill the narrow gap between the capillary and the underlying coverslip, an approach that minimized optical aberrations caused by the curved surface of the capillary. Samples were electrokinetically transported between inlet and outlet vials, which were sealed with septa to confine potentials created by platinum wire electrodes fixed permanently into the ends of the vials.
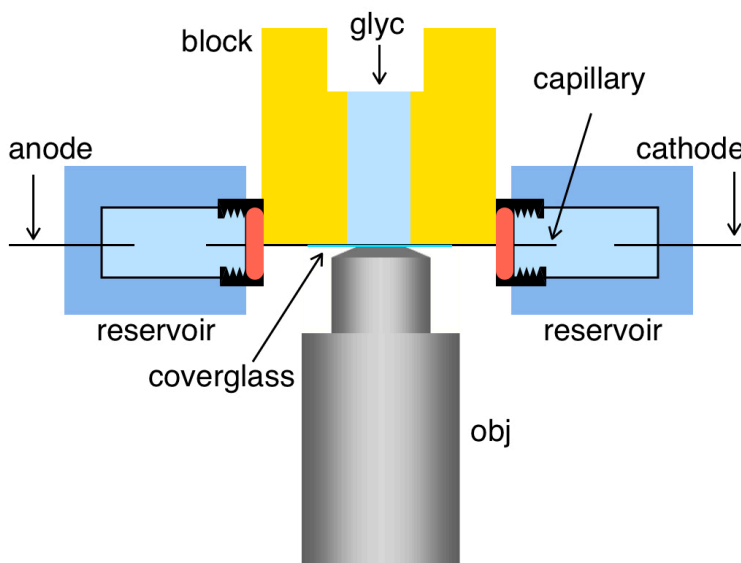
Figure 2.2: Schematic showing the fluidics assembly for bidirectional and multispot microsecond capillary electrophoresis. The microscope objective focuses multiple laser beams into the pulled region of a fused silica capillary that is sandwiched between a No. 0 coverslip and an acrylic block with near-index matching glycerin filling the small gaps between the coverslip and the capillary.

The capillary assembly, consisting of the mounted capillary and two sample reservoirs, was mounted to a 0.25 in. thick Plexiglas sheet that was bolted to a three-axis translation stage (model 562, Newport Corp., Irvine, CA) controlled by motorized actuators for stage movement and final laser alignment. Two high-voltage power supplies

were used (Series EH, Glassman High Voltage, Inc., High Bridge, NJ) to supply separation voltages of opposite polarities.

2.2.3 Instrumentation and Optical Alignment

A mode-locked titanium-sapphire (Ti:S) oscillator (Coherent Mira 900F) pumped by a 532 nm 10 W frequency-doubled neodymium-vanadate laser (Coherent Verdi) was operated at 755 nm for all experiments. This laser source produces ∼150 fs pulses with a pulse repetition rate of 76 MHz. The Ti:S output was first split using a half-wave plate and polarizing beamsplitter into gate and probe beams (Figure 2.3). The gate beam was passed through a Pockel's cell (350-50, Conoptics, Danbury, CT) that was controlled by a high-speed delay generator (DG-535, Stanford Research, Sunnyvale, CA) where it could be modulated electrooptically on microsecond time scales to create spatially narrow packets of photochemical intermediates within reagent streams. The gate was switched to high power (an average laser power of 300-400 mW, measured at the back aperture of the objective) for periods ranging from 0.7 to 1 μs. After being split from the gate beam, the probe portion of the Ti:S beam was directed through an optical rotator from a 350-50 Pockel's cell so that beams could be switched between high and low intensity (i.e., 180° out of phase with each other), enabling each probe to detect photoproduct in half of the electrophoretic repetitions as signal averaging was performed. The optical rotator was controlled using a function generator (DG-345, Stanford Research, Sunnyvale, CA) synchronized to the delay generator controlling the gate-beam Pockel's cell (see above). Switching frequencies of 2 kHz for the gate Pockel's cell and 1 kHz for the probe optical rotator were used, allowing each probe spot to excite photoproduct fluorescence after

every other gate pulse. After the optical rotator, the beam was directed through a second half-wave plate/polarizing beamsplitter pair to produce two probe beams. This configuration caused the beam to be either transmitted or reflected at the second beamsplitter, depending on whether vertically or horizontally polarized light emerged from the optical rotator. One of the probe beams was sent through another half-wave plate/polarizing beamsplitter pair to provide a means to match the power polarization to the other probe beam. The beams were then recombined slightly off-axis using a 50/50 nonpolarizing beamsplitter. Farther along the beam path, the gate beam was combined slightly off-axis with the two probe beams using a polarizing beamsplitter. All three beams were passed through a long-pass dichroic mirror (Chroma Technology Corp., 575DCXR) and reflected by a 90/10 beamsplitter into the back aperture of a 1.3 NA 100X microscope objective (Fluar, Zeiss).
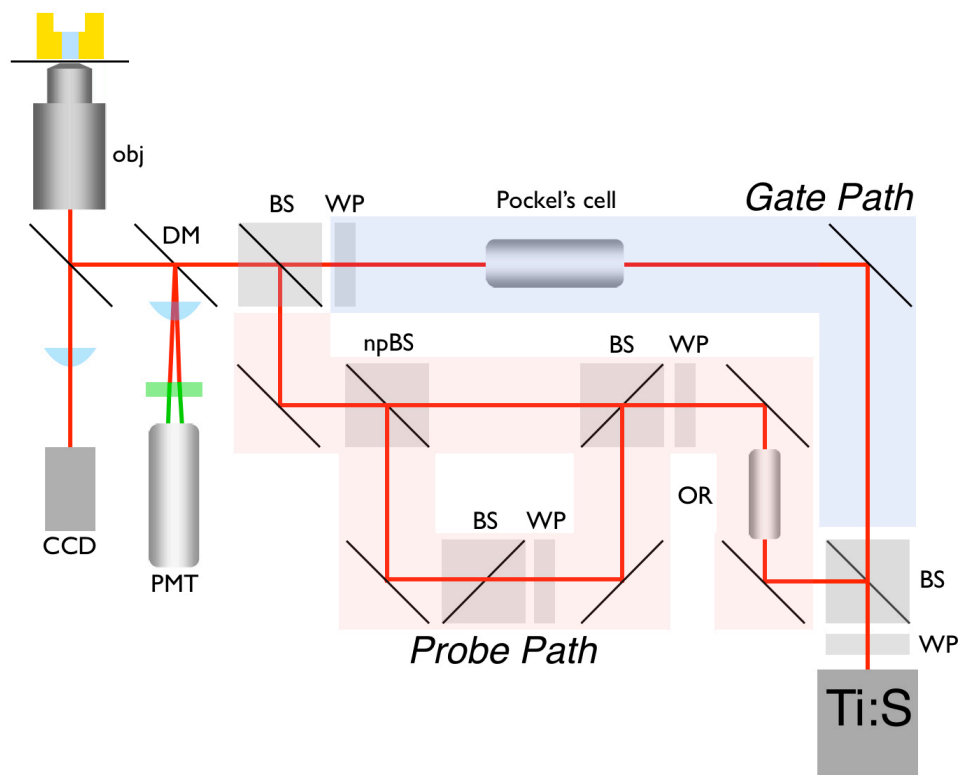
Figure 2.3: Schematic showing the optical configuration for bidirectional and multispot unidirectional microsecond capillary electrophoresis. A mode-locked titanium:sapphire (Ti:S) beam is sent through a halfwave plate (WP) and polarizing beam splitter (BS), which directs beams of orthogonal polarization to the gate path (blue) and the probe path (red). The vertically-polarized gate beam is aligned through a Pockel's cell, which generates high-intensity gate pulses of $0.7 - 1$ μs for creating fluorescent photoproduct. The gate beam is then sent through a second WP and BS before rejoining the probe beams. The horizontally-polarized probe beam is passed through an optical rotator (OR) from a 350-50 Pockel's cell that rapidly alternates its polarization. The beam is then passed through a WP and BS, creating two probe beams of opposite polarization. The reflected probe beam (vertical polarization) is passed through another WP/BS pair that rotates its polarization to the horizontal plane and allows for laser power equalization. The probe beams are recombined slight off-axis at the nonpolarizing beam splitter (npBS) before joining the gate beam at a BS. All three beams are then passed through a dichroic mirror (DM) and reflected into the back aperture of a 1.3 NA 100X Zeiss Fluar objective via a 90/10 mirror. Fluorescence is epi-collected by the same objective and reflected via the 90/10 mirror to the DM where it is passed through a 20-cm focal length plano-convex lens and through a series of optical filters before striking the photomultiplier tube (PMT).

The capillary was monitored by collecting transmitted light (from a fiber-optic illumination source) through the objective and to a tube lens, which focused the capillary image onto a video-rate CCD (KP-M1U, Hitachi Denshi, Ltd., Japan). Laser back-reflections at the interface between the coverslip and glycerol (which are nearly index matched) were imaged to guide the lateral alignment of gate and probe foci. Before performing an experiment, the capillary was adjusted using three-axis electrostrictive actuators (AD30, Newport) to position the laser foci along the central axis of the capillary near the hourglass waist.

Fluorescence emission generated from both laser foci from hydroxyindole photoproducts was epi-collected using the objective, directed back along the laser propagation path via the 90/10 beamsplitter to the dichroic mirror and passed through 20 cm focal length plano-convex lens and a series of optical filters (5 cm saturated aqueous $CuSO_4$ and two 3 mm-thick BG-39 filters) before striking the photomultiplier (PMT; HC-125, Hamamatsu, Middlesex, NJ). To improve signal-to-noise, data from rapid, sequential electrophoretic runs were summed on-the-fly using a zero-deadtime multichannel scaler with 640-ns bins (SR430, Stanford Research Systems).

2.3 RESULTS AND DISCUSSION

The Shear lab has previously shown the separation of positive and neutral photochemically generated products using CE in under 10 μs at high electric field strengths (≥ 50 kV cm^{-1}) over a very short separation distance (10 μm between a gate spot and a single probe spot) [17]. This chapter describes two similar optical configurations

for the microsecond electrophoretic analysis of transient photoproducts using a detection approach that spatially isolates photoproduct fluorescence by alternatively directing probe spots at high frequency (1 kHz).

2.3.1 Bi-directional Electrophoretic Analysis

This separation technique represents a novel electrophoretic approach for minimizing analysis times of oppositely charged photochemically generated transient species. Shown in Figure 2.4, by placing probe sites on opposites sides of a photochemical reaction site (gate), oppositely charged photoreaction products can be detected simultaneously as the positive products migrate towards one probe site and the negative species move towards the second probe site.
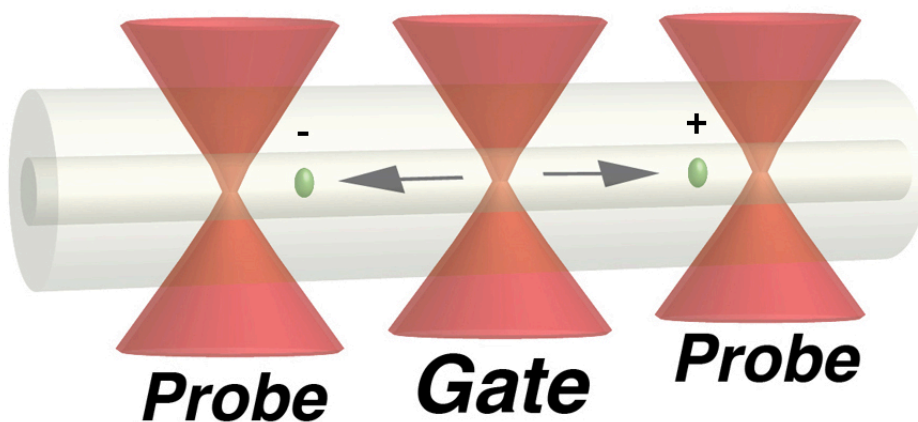
Figure 2.4: Bi-directional capillary electrophoresis. Schematic showing the centrally located gate site that is sandwiched by two probe sites that are created by tightly focusing three Ti:S laser beams using high-numerical aperture optics. Oppositely charged fluorescent hydroxyindole photoproducts are created at the gate site and subsequently transported through a fused silica capillary, primarily by electrophoretic forces, to the probe spots where they are detected via the generation of visible fluorescence.

33

To demonstrate this approach for the purpose of rapidly analyzing transient photoproducts of all charge states, a mixture of a 5HT, 5HI2CA, and 5HTrp were photochemically injected using a high power gate beam at the waist of an hourglass-shaped capillary. To ensure the predominate mode of analyte migration was electrophoretically-driven, buffer conditions were adjusted to minimize electroosmotic flow (EOF). Reductions in EOF were achieved using a slightly acidic (pH 5.5) MES buffer containing a nonionic surfactant (0.1 – 0.5% (w/v) Pluronic F-127). Pluronic F-127 is a block copolymer (consisting of propylene oxide and ethylene oxide) that previously has been used as a CE separation medium for large biomolecules [21, 22] and as a coating in microfluidic channels to reduce wall adsorption of large molecules [23], cell adhesion [15], and to modify electroosmotic flow [15, 23]. These solution modifications were found to produce a stable EOF velocity (typically $\sim$ 0.1 m s^{-1}, $\sim$ 30% of the electrophoretic velocity of the positive and negative species) for the duration of an experiment (up to 1 h), as was monitored by the migration of the neutral species, 5HTrp.
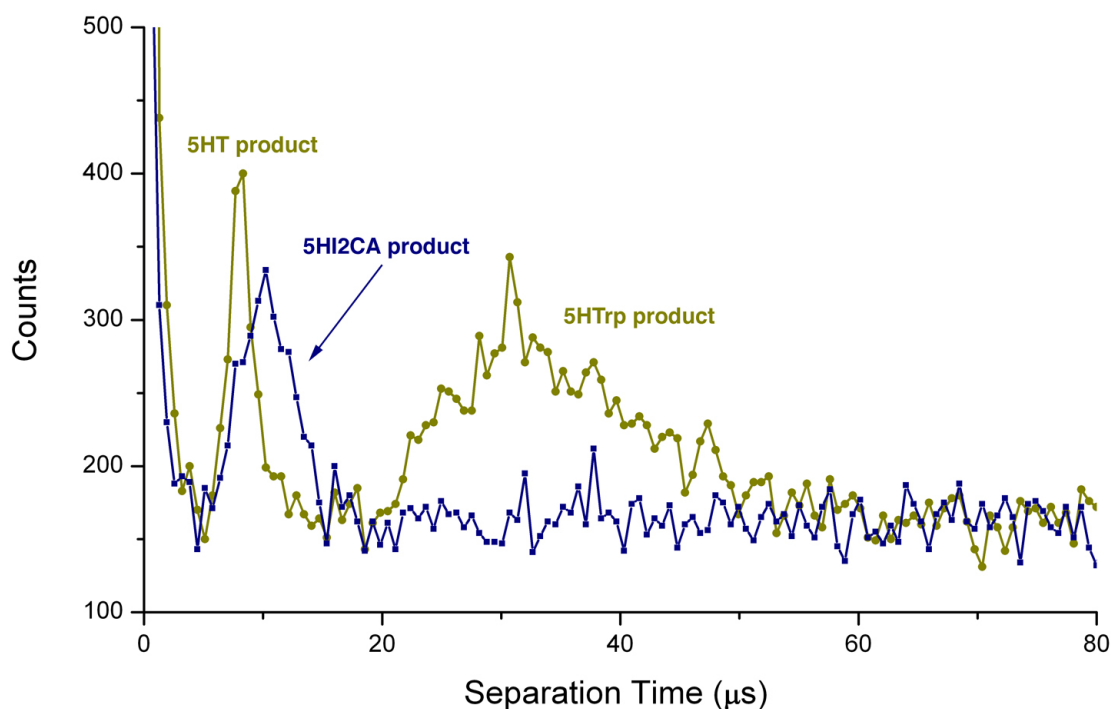
Figure 2.5: Bidirectional microsecond electrophoretic separation of a three-component mixture. A sample containing 5HT, 5HI2CA, and 5HTrp, each at 250 μM in 20 mM MES (pH 5.5) with 0.1% (w/v) Pluronic was photochemically injected using 0.7 μs gate times at a centrally located gate site and fractionated using an applied potential of 39 kV over separation distances of 3.0 μm and 2.0 μm in the direction of the cathode and anode, respectively. The plots represent the sum of 19,000 sequential electrophoretic records. 5HT and 5HI2CA photoproducts were detected in distinct channels, with an analysis time of 10 μs required to characterize mobilities of both compounds. 5HTrp photoproduct was observed in the "positive" product channel due to a residual electroosmotic flow component.

The results for this approach are shown in Figure 2.5, where a mixture of 5HT, 5HI2CA, and 5HTrp were photochemically injected and subsequently resolved within 30 μs using alternating probe spots over separation distances of 3 μm in the direction of the cathode and 2 μm in the direction of the anode. Due to residual EOF, the neutral photoproduct, 5HTrp, broadly migrated in the direction of the cathode (along with the

35

positive species, 5HT) at a velocity of $\sim$ 0.1 m s^{-1}. The electrophoretic mobilities for 5HT

and 5HI2CA were found to be identical (4.7 x 10^{-3} cm^2 V^{-1} s^{-1}), as expected due to their

similar molecular structure and charge state (+1 and -1, respectively). However, due to

the residual EOF in the direction of the cathode, 5HT migrated at a faster velocity

(0.4 m s^{-1}) and produced a narrower temporal bandwidth than 5HI2CA (0.2 m s^{-1}).

Although the separation efficiencies achieved were low (< 75 theoretical plates), the

theoretical plates generated per second were large with values of 1.8 million plates s^{-1}, 9.4

million plates s^{-1}, and 1.2 million plates s^{-1} for 5HI2CA, 5HT, and 5HTrp, respectively.

As a point of reference, conventional CE typically generates $\sim$ 1000 plates s^{-1} [24]. The

number of theoretical plates generated in a separation event is limited by a number of

factors, including the size of the injection plug relative to the separation distance,

longitudinal diffusion, and the extent of Joule heating.
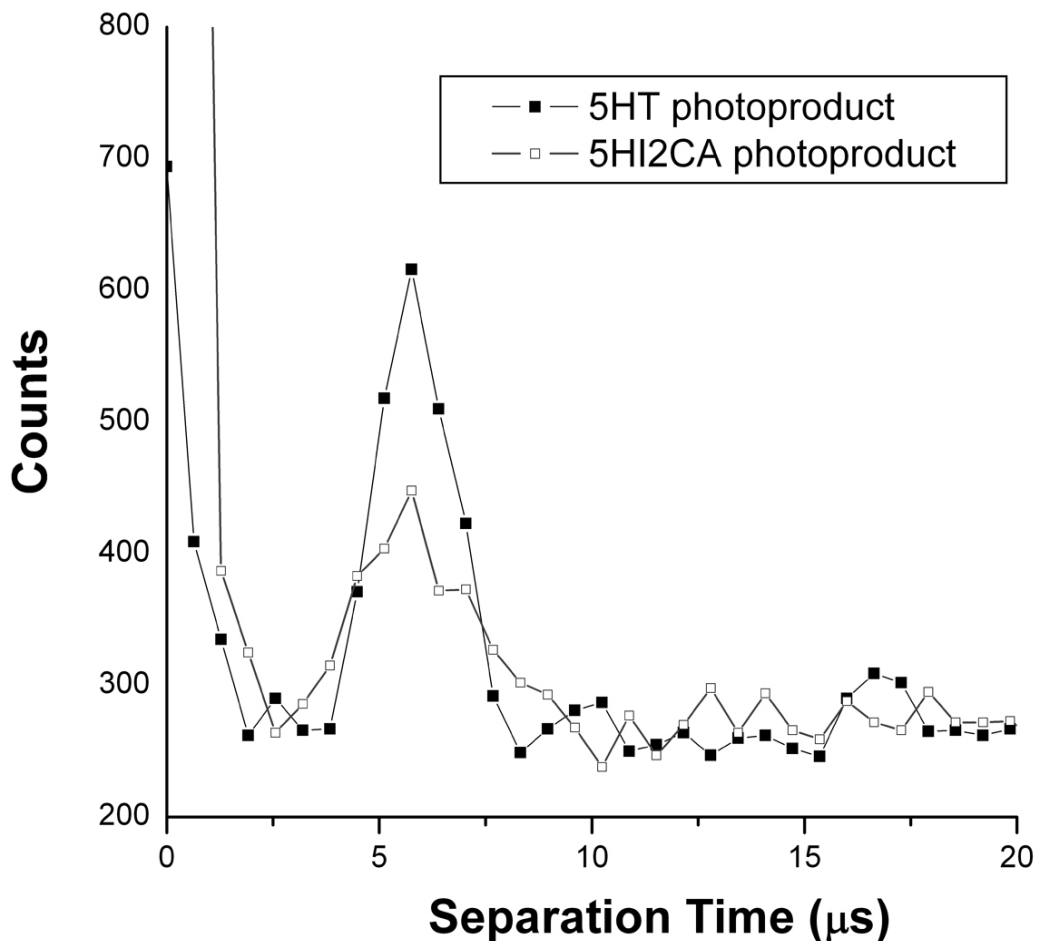
Figure 2.6: Bidirectional microsecond electrophoretic separation oppositely charged hydroxyindole photoproducts in approximately 6 μs. The sample contained 5HT and 5HI2CA, each at 500 μM in 20 mM MES (pH 5.5) with 0.1% (w/v) Pluronic. The photoproducts were photochemically injected using 0.7 μs gate times at a centrally located gate site and fractionated using an applied potential of 46 kV over separation distances of 2.2 μm and 2.0 μm in the direction of the cathode and anode, respectively. The plots represent the sum of 6000 sequential records.

As an attempt to decrease the separation time and further demonstrate the capabilities of this technique, a mixture of a positive and negative species (5HT and 5HI2CA) were photochemically injected and separated over distances of 2.2 μm and

2.0 μm in the direction of the anode and cathode, respectively. This mixture of 5HT and 5HI2CA was created and in approximately 6 μs (Figure 2.6), achieving the most rapid electrophoretic separation to date and demonstrating the resolved analysis of species that would appear to be overlapping with a continuous (non-modulated) detection scheme.

2.3.2 Multiprobe Electrophoretic Analysis

Modulating a sequence of probe spots at a high frequency also allows photoproducts to be tracked as they migrate through a separation capillary under electrophoretic and electroosmotic forces. This could potentially be applied to the study of short-lived molecules undergoing a rapid change, such as a refolding protein, as the shape or charge of transient species and photoproducts may differ from that of the original molecule, and these changes would result in different electrophoretic mobility. Techniques such as stopped-flow methods have been used to monitor transient species, for example, during protein folding; however, understanding the kinetics of such a process is difficult using traditional methods because the time resolution is low (ms) [25]. In the case of protein folding, experiments are also limited by the use of harsh denaturants [25, 26]. Alternatively, initiating the folding process of a protein has been shown to be feasible using UV excitation [26, 27]. Creating an optical trigger that responds to tightly focused Ti:S laser light could be used to initiate the folding process on the order of nanoseconds. This process could be performed within a capillary and the transient folding states could be interrogated with sequential probe spots as it migrates within microseconds through the channel. While interpreting this type of data using a multi-probe technique would be difficult, electrophoretic data could be interfaced with

computer modeling to decipher the structural characteristics of an evolving transient

species such as a refolding protein.
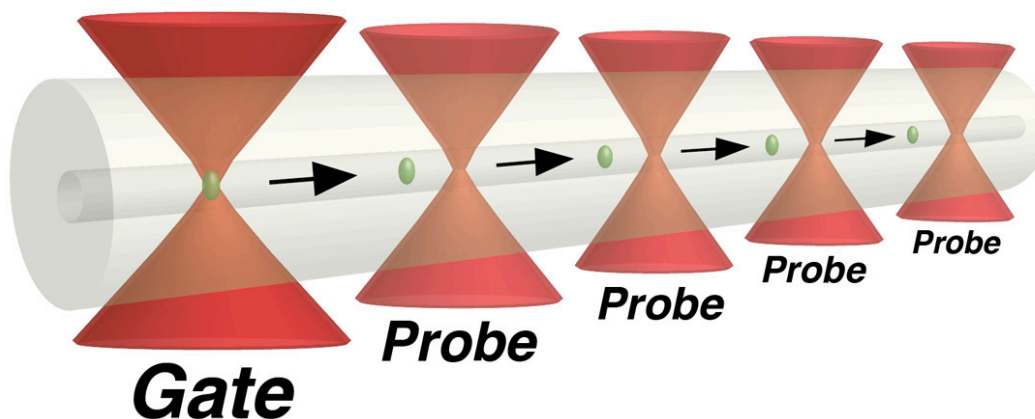
Figure 2.7: Schematic showing a multiprobe electrophoresis setup for tracking
photochemically generated analytes as they migrate down an electrophoretic
channel. The high-powered gate site is rapidly modulated to generate plugs
of fluorescent photoproducts that are sequentially probed at four probe sites
downstream. While only two probe beams are aligned into the microscope
objective, they can be translated farther downstream to achieve four distinct
probe sites.

To demonstrate this approach, 5HT photoproducts were created in a high EOF

buffer system (20 mM HEPES, pH 7.4) at the gate site within a geometrically modified

capillary and subsequently probed at four distinct locations downstream (Figure 2.7). Due

to the challenges associated with laser beam alignment and the laser power requirements

that cannot be met with our current Ti:S system, probing photoproduct fluorescence

simultaneously at four probe sites was achieved using only two probe beams. Here, two

probe beams were separated by 4 μm and aligned such that the first probe site that detected photoproduct fluorescence was 4 μm from the gate site. Using this configuration, photoproduct fluorescence was detected at two probes sites at 4 μm and 8 μm downstream from the gate site. To achieve four distinct probe sites, the probe beam configuration described above was translated 8 μm downstream from its original position, resulting in probe sites at 12 μm and 16 μm from the gate site. This procedure resulted in the creation of four probe sites at distances of 4, 8, 12, and 16 μm from the gate site. The feasibility of this approach is shown in Figure 2.8, where 5HT photoproducts were photochemically injected with a gate time of 1 μs and migrated downstream at an applied potential of 10 kV. At 10 kV, plugs of 5HT photoproduct maintained a velocity of $\sim$ 0.19 m s^{-1} at all probe sites downstream from the gate.
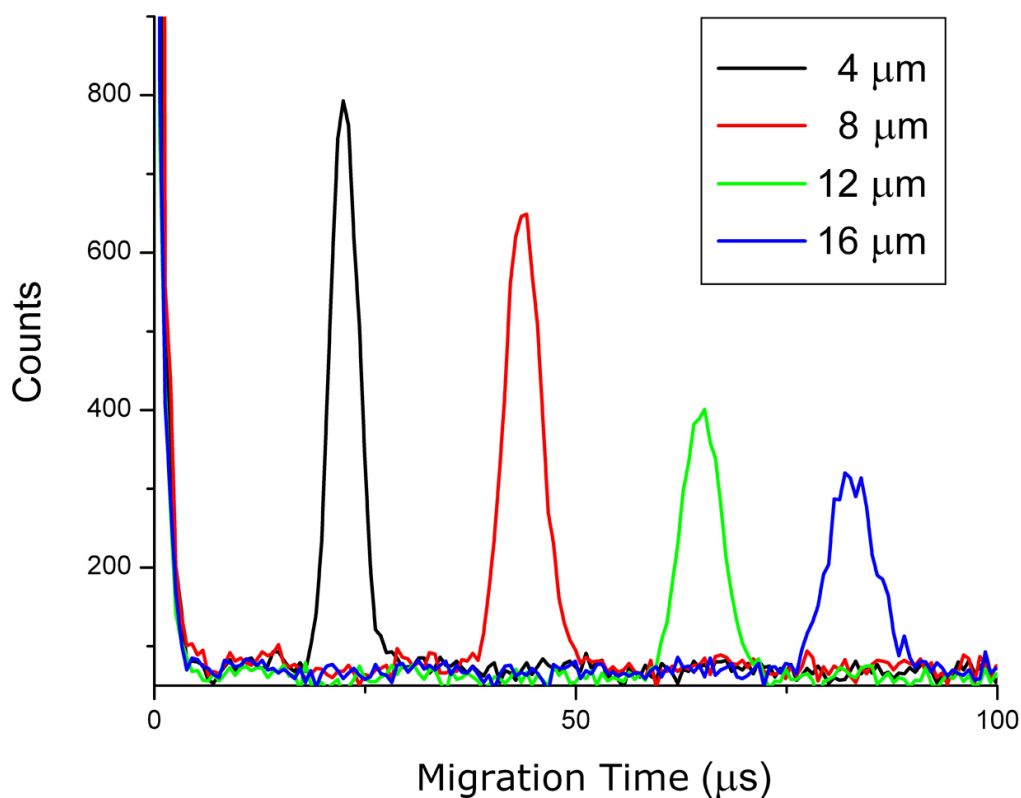
Figure 2.8. Multiprobe electrophoresis. Multiprobe electrophoretic analysis of 5HT photoproducts created with 1 μs gate times and subsequently probed at four sites within the waist of an hourglass-shaped capillary using an applied potential of 10 kV. The probe sites at 4 and 8 μm were recorded first and the beams were then translated together downstream 8 μm to record photoproduct fluorescence at 12 and 16 μm. The sample contained 500 μM 5HT in pH 7.4 HEPES buffer (20 mM) and is the result of 25000 electrophoretic records for each probe beam set (4/8 μm and 12/16 μm).

This approach demonstrates the feasibility of multiprobe monitoring of transient photoproducts as they migrate through an electrophoretic channel. As expected, in an ideal separation the signal peak height decreases at probe spots farther downstream. This is due to the spatial diffusion of photoproducts from the analyte plug into the surrounding

41

buffer, as well as photobleaching that may occur. Under ideal separation conditions where diffusion is the only source of peak broadening, the total spatial variance of a peak at any given point with the capillary is defined by the sum of the variances associated with the injection site (σ_{intro}) and detection site (σ_{det}), as well as diffusion (2Dt),

$$\sigma^2 = \left(\sigma_{\text{intro}}\right)^2 + 2Dt_{\text{mig}} + \left(\sigma_{\text{det}}\right)^2 . \qquad [2.1]$$

In this multiprobe approach, where the gate and probe dimensions, as well as the analyte velocity (assuming the electrophoretic mobility of the analyte does not change on the time scale of the separation), are held constant throughout the experiment, the spatial variance of a peak is experimentally defined by

$$\sigma^2 = (v \cdot w_{1/2})^2 , \qquad [2.2]$$

where v is the analyte velocity and $w_{1/2}$ is the temporal full width at half maximum of the analyte peak. If diffusion is the only contributor to band broadening, the spatial variance of a peak (at the nth detection site) should be the sum of the spatial variance of the peak at the first probe site and the contribution from diffusional broadening:

$$\sigma^2_{n^{\text{th}}\text{peak}} = \sigma^2_{\text{peak 1}} + 2D\Delta t_{\text{mig}} . \qquad [2.3]$$

For the data shown in Fig. 2.8, the spatial variance of peak 1 (4 μm separation distance) was found to be 0.47 μm^2. Using the relationship in Equation 2.3, the spatial variance of peak 2 (8 μm separation distance) should be 0.50 μm^2 when theoretically

calculated using a diffusion coefficient for serotonin of $6.5 \times 10^{-6}\,\mathrm{cm^2 \cdot s^{-1}}$ [17]. For the purpose of these estimates, it was assumed that the photoproduct maintains the same diffusion coefficient as the parent species. However, when calculated directly from the data using Equation 2.2, the spatial variance for peak 2 was found to be 0.86 μm^2 - a value approximately 70% greater than would be expected if diffusion were the sole cause of spatial broadening. Following this analysis, the spatial variances found experimentally and theoretically for peaks 2, 3, and 4 and are shown in Figure 2.9. When the analyte plug reaches probe spot 4, the spatial variance is $\sim$ 3 times greater than would be expected if diffusion alone was the sole cause of band broadening.

To ensure that this unexpected increase in spatial variance was not to due differences in the physical dimensions of the focused probe beams, the probe sites were translated to the opposite side of the gate beam (upstream) and the electrodes were reversed such that when injected, the photoproducts migrated in the opposite direction towards the probe sites now placed on the opposite of the gate site. This resulted in spatial variances that were indistinguishable from previous experiments, thus eliminating differences in the shape of the probe spot as a contributor to this unexpected increase in spatial variance.
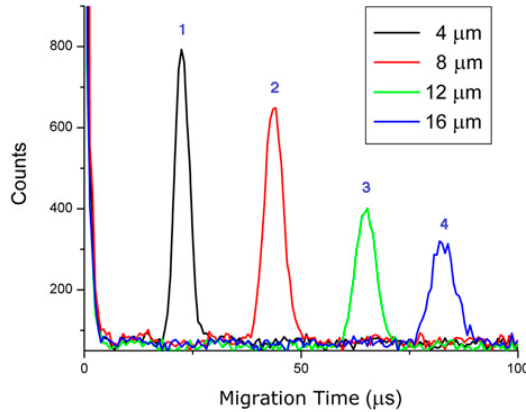
$$\sigma^2_{n^{th}\,peak} = \sigma^2_{peak1} + 2Dt_{mig}$$

Theoretical σ^2	Experimental σ^2
$\sigma^2_1 = 0.47\,\mu m^2$	$\sigma^2_1 = 0.47\,\mu m^2$
$\sigma^2_2 = 0.50\,\mu m^2$	$\sigma^2_2 = 0.86\,\mu m^2$
$\sigma^2_3 = 0.53\,\mu m^2$	$\sigma^2_3 = 1.35\,\mu m^2$
$\sigma^2_4 = 0.55\,\mu m^2$	$\sigma^2_4 = 1.65\,\mu m^2$

Figure 2.9: Theoretical and experimental spatial variances. The theoretical and experimental spatial variances (σ^2) for the data shown in Figure 2.9.

The Einstein equation [2.4] can be expressed graphically in a linear plot, where the spatial variance, σ^2, (y- axis) changes as a function of migration time, t, (x-axis) with the slope of that line equaling twice the diffusion coefficient (D).

$$\sigma^2 = 2Dt \qquad\qquad [2.4]$$

For the theoretical spatial variances shown in Fig. 2.9, the slope of that line was, by definition, found to be 6.5×10^{-6} cm^2·s^{-1} – the diffusion coefficient of serotonin used in the calculation. For the experimental variances shown in Figure 2.9, the apparent diffusion coefficient (D_{app}) was calculated to be 1.03×10^{-4} cm^2·s^{-1} – a value ~ 16 times greater than the known diffusion coefficient for serotonin. This relationship between the calculated and experimental spatial variances is represented graphically in Figure 2.10.
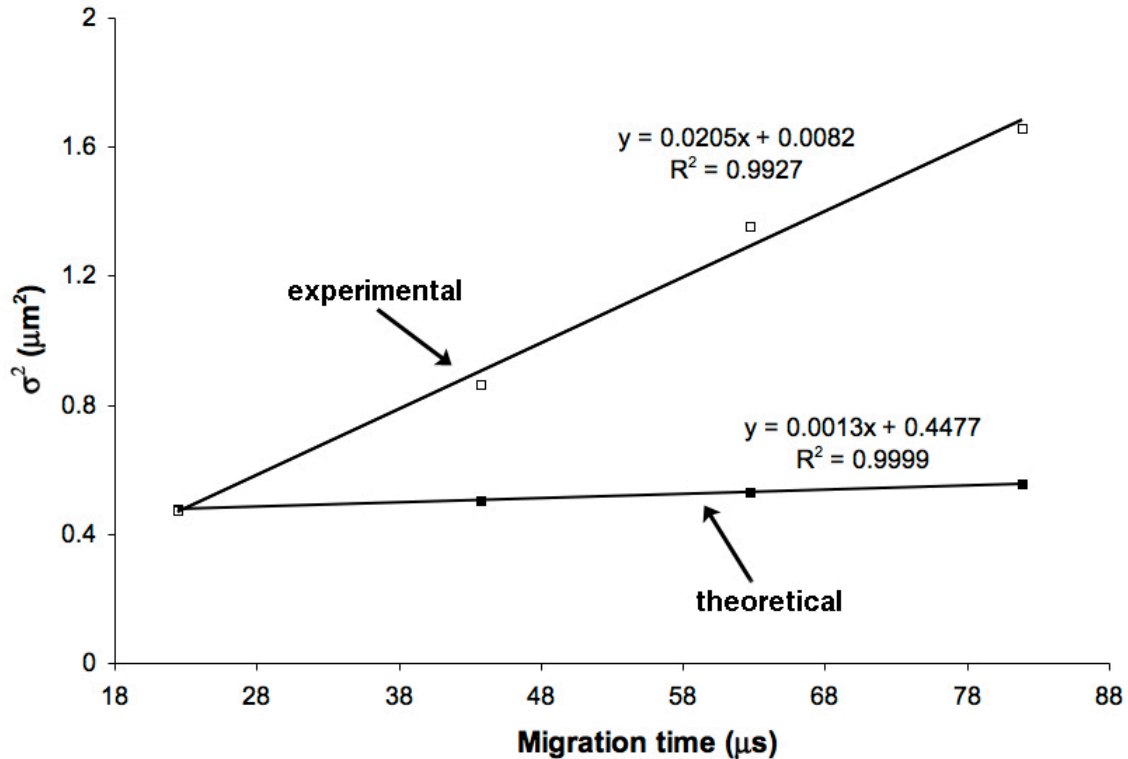
Figure 2.10: Experimental versus theoretical spatial variances. Graphical analysis of the spatial variance as a function of migration time for the data shown in Fig. 2.9, where the slope of the linear regression is equal to twice the diffusion coefficient, as shown by the Einstein equation (2.2).

In a CE experiment, there is no equilibrium between a stationary and mobile phases and the sole contribution to band broadening is molecular diffusion. Because of this, a dramatic increase in the D_{app} is usually due to Joule heating of the buffer, which occurs when current is passed through a conductive medium, such as an electrolyte buffer. This heating effect is often mitigated in CE through the use of low conductivity buffers, narrow-bore channels, and cooling systems. Experimental observation of a nonlinear relationship between the analyte velocity and the applied potential, as determined by a voltage-scaling experiment, is a strong indication of Joule heating.

Figure 2.11 shows the results of a voltage scaling experiment in this system (20 mM Hepes, pH 7.4) performed by monitoring the velocity at peak 1 (4 μm separation distance) at applied potentials of 5, 10, 15, and 20 kV.
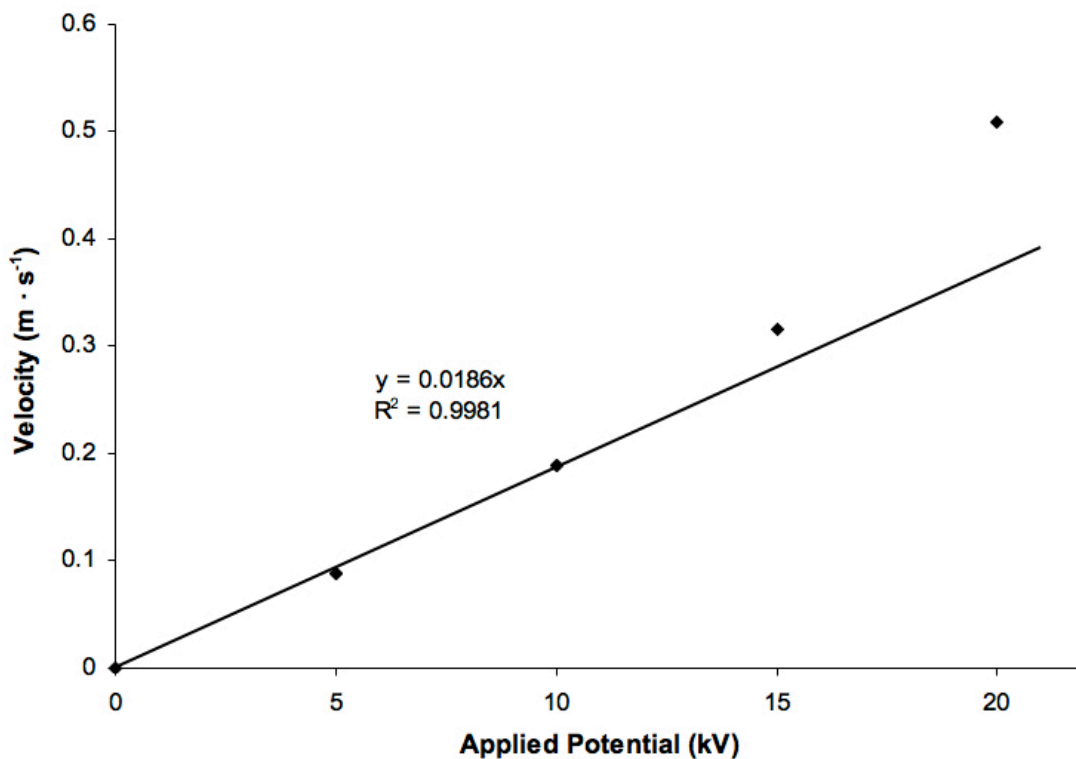
Figure 2.11: Voltage scaling. Plot of 5HT photoproduct velocity as a function of applied potential for a separation distance of 4 μm. A linear best-fit is placed through the first three points to emphasize nonlinearity at 15 and 20 kV.

A linear best fit was placed through the first three points (0, 5, and 10 kV) to demonstrate the nonlinearity that occurs at potentials higher than 10 kV. This rapid increase in velocity is most likely attributed to a decrease in the solution viscosity as a result of Joule heating. An increase in temperature (and a decrease in viscosity) causes an

46

increase in the buffer conductivity, the electroosmotic velocity, the current, and the linear analyte migration velocity.

A modified version of the Stokes-Einstein equation (Equation 2.5) can be used to estimate the temperature of a solution as a function of its diffusion coefficient and viscosity, where it relates the diffusion coefficient at 25°C ($D_{25°C}$), the temperature ($T_{25°C}$), and the viscosity ($\eta_{25°C}$) to the diffusion coefficient, temperature, and viscosity at some temperature, X [28, 29].

$$D_{25°C} = D_{X°C} \frac{T_{25°C}\eta_{X°C}}{T_{X°C}\eta_{25°C}} \qquad [2.5]$$

For the experiment described above, where the diffusion coefficient of serotonin is known ($6.5 \times 10\text{-}6 \ cm^2 \cdot s^{-1}$) and a D_{app} was found to be $1.03 \times 10^{-4} \ cm^2 \cdot s^{-1}$ at an applied potential of 10 kV, a buffer temperature was calculated to be approximately 120°C using Equation 2.5 (viscosity of water at 25°C of 0.89 $kg \ m^{-1} \cdot s^{-1}$) [30]. While only an estimate, a buffer temperature of greater than 100°C could be visualized by the boiling of the electrolyte buffer, yet this phenomenon was not observed. However, at 10 kV, Figure 2.11 shows approximate linear velocity scaling versus applied potential – an indication that heating is not occurring.

Due to the high electric fields, axial temperature gradients may also exist within the capillary. In addition, convective currents, as a result of these temperature gradients, may increase the apparent diffusion of the analyte plug. Such high instances of band

47

broadening could also be attributed to a change in the molecular structure, yet this would be indicated by asymmetrical peaks. It has been shown that hydroxyindole photoproducts maintain their charge up to low millisecond timescales [10], indicating that structural changes are not occurring that could result in a change in its charge-to-drag ratio or its molecular diffusion coefficient. Consequently, the exact cause of this large increase in band broadening has yet to be determined.

2.4 CONCLUSION

These studies demonstrate new capabilities for characterizing transient photochemical intermediates using CE after their creation at a photoreaction site. With this strategy, the fluorescence signal generated at the two probe spots is detected by a single PMT even when analytes simultaneously arrive at the probe site. This was achieved by rapidly alternating the laser power, thus temporally isolating the fluorescence generated at each probe spot. This system allows for the detection of positively and negatively charged transient photoproducts under low EOF conditions within 6 μs – a time scale several folder faster than would be expected ($\sim 20 \mu$s) based on a previous demonstration of the separation between a positive and neutral species within 10 μs using an approach that relied on solution conditions to generate a high EOF component [10].

This multi-probe spot approach also allows for the tracking of a single analyte as it migrates through a capillary after creation at a photoreaction site. This was demonstrated by tracking 5HT photoproducts at four distinct probe locations downstream from a gate spot within a pulled capillary. This technique could be used to examine

48

structural changes of a macromolecule as it migrates through a capillary under an electric field. Although feasibility for implementing of this technique is clearly demonstrated, increases in spatial variances were observed at levels that exceed the possible contribution from diffusion alone. While it was determined that Joule heating was not shown to be significant, the determined spatial variances were at levels that theoretically would indicate solution boiling (~ 120 °C), which was not experimentally observed. To effectively use this technique for monitoring a transforming molecule, this unexpected increase in spatial variance must be understood.

2.5 REFERENCES

1.   Callender, R., Dyer, R., Gilmanshin, R. and Woodruff, W., *Fast events in protein folding: the time evolution of primary processes*. Annual review of physical chemistry, 1998. **49**: p. 173-202.

2.   Chen, E., Goldbeck, R. and Kliger, D., *Nanosecond time-resolved spectroscopy of biomolecular processes*. Annual review of biophysics and biomolecular structure, 1997. **26**: p. 327-355.

3.   Gilmanshin, R., Williams, S., Callender, R., Woodruff, W. and Dyer, R., *Fast events in protein folding: Relaxation dynamics of secondary and tertiary structure in native apomyoglobin*. Proceedings of the National Academy of Sciences, 1997. **94**: p. 3709-3713.

4.   Bellelli, A., Antonini, G., Brunori, M. and Springer, B., *Transient spectroscopy of the reaction of cyanide with ferrous myoglobin. Effect of distal side residues*. Journal of Biological Chemistry, 1990. **265**(31): p. 18898-18901.

5.   George, S., Ashby, G., Wharton, C. and Thorneley, R., *Time-resolved binding of carbon monoxide to nitrogenase monitored by stopped-flow infrared spectroscopy*. Journal of the American Chemical Society, 1997. **119**: p. 6450-6451.

6.   Jones, C., Henry, E., Hu, Y., Chan, C., Luck, S., Bhuyan, A., Roder, H., Hofrichter, J., and Eaton, W., *Fast events in protein folding initiated by nanosecond laser photolysis*. Proceedings of the National Academy of Sciences, 1993. **90**: p. 11860-11864.

7.   Vauthey, E. and Henseler, A., *Picosecond transient thermal phase grating study of a photoinduced electron transfer reaction in solution*. Journal of Physical Chemistry, 1995. **99**: p. 8652-8660.

8.   Monnig, C.A. and Jorgenson, J.W., *On-column sample gating for high-speed capillary zone electrophoresis*. Anal. Chem., 1991. **63**: p. 802-807.

9.   Allen, P., Doepker, B. and Chiu, D., *High-throughput capillary-electrophoresis analysis of the contents of a single mitochondria*. Analytical Chemisry, 2009. **81**: p. 3784-3791.

10.   Gordon, M., Okerberg, E., Gostkowski, M. and Shear, J., *Electrophoretic characterization of transient photochemical reaction products*. Journal of the American Chemical Society, 2001. **123**: p. 10780-10781.

11.   Hapuarachchi, S., Premeau, S. and Aspinwall, C., *High-speed capillary zone electrophoresis with online photolytic optical injection*. Analytical Chemistry, 2006. **78**: p. 3674-3680.

12. Jacobson, S.C., Culbertson, C.T., Daler, J.E. and Ramsey, J.M., *Microchip structures for submillisecond electrophoresis*. Analytical Chemisry, 1998. **70**: p. 3476-3480.

13. Kennedy, R., German, I., Thompson, J. and Witowski, S., *Fast analytical-scale separations by capillary electrophoresis and liquid chromatography*. Chemical Reviews, 1999. **99**: p. 3081-3131.

14. Lapos, J.A. and Ewing, A.G., *Injection of fluorescently labeled analytes into microfabricated chips using optically gated electrophoresis*. Analytical Chemisry, 2000. **72**: p. 4598-4602.

15. Mcclain, M.A., Culbertson, C.T., Jacobson, S.C., Allbritton, N.L., Sims, C.E. and Ramsey, J.M., *Microfluidic devices for the high-throughput chemical analysis of cells*. Analytical Chemistry, 2003. **75**(21): p. 5646-5655.

16. Tao, L., Thompson, J.E. and Kennedy, R.T., *Optically gated capillary electrophoresis of o-phthalaldehyde/β-mercaptoethanol derivatives of amino acids for chemical monitoring* Analytical Chemisry, 1998. **70**: p. 4015-4022.

17. Plenert, M. and Shear, J., *Microsecond electrophoresis*. Proceedings of the National Academy of Sciences, 2003. **100**(7): p. 3853-3857.

18. Ritschdorff, E.T., Plenert, M. and Shear, J.B., *Microsecond analysis of transient molecules using bi-directional capillary electrophoresis*. Analytical Chemistry, 2009. **81**: p. 8790-8796.

19. Gostkowski, M.L., Allen, R., Plenert, M.L., Okerberg, E., Gordon, M.J. and Shear, J.B., *Multiphoton-excited serotonin photochemistry*. Biophysical Journal, 2004. **86**: p. 3223-3229.

20. Shear, J., Xu, C. and Webb, W., *Multiphoton-excited visible emission by serotonin solutions*. Photochemistry and Photobiology, 1997. **65**: p. 931-936.

21. Kuroda, D., Zhang, Y., Wang, J., Kaji, N., Tokeshi, M. and Baba, Y., *A viscosity-tunable polymer for DNA separation by microchip electrophoresis*. Analytical Bioanalytical Chemistry, 2008. **391**(7): p. 2543-2549.

22. Wu, C., Liu, T., Chu, B., Schneider, D.K. and Graziano, V., *Characterization of the PEO-PPO-PEO triblock copolymer and its application as a separation medium in capillary electrophoresis*. Macromolecules, 1997. **30**(16): p. 4574-4583.

23. Wu, C., Liu, T., White, H. and Chu, B., *Atomic force microscopy study of $E_{99}P_{69}E_{99}$ triblock copolymer chains on silicon surface*. Langmuir, 2000. **16**(2): p. 656-661.

24. Jorgenson, J.W. and Lukacs, K.D., *Capillary zone electrophoresis*. Science, 1983. **222**: p. 266-272.

25.   Volk, M., *Fast initiation of peptide and protein folding processes*. European Journal of Organic Chemistry, 2001.

26.   Hansen, K., Rock, R., Larsen, R. and Chan, S., *A method for photoinitating protein folding in a nondenaturing environment*. Journal of the American Chemical Society, 2000. **122**: p. 11567-11568.

27.   Rock, R., Hansen, K., Larsen, R. and Chan, S., *Rapid photochemical triggering of protein unfolding in a nondenaturing environment*. Chemical Physics, 2004.

28.   Miller, C.C., *The Stokes-Einstein law for diffusion in solution*. Proceedings of the Royal Society of London. Series A, Containing Papers of a Mathematical and Physical Character, 1924. **106**: p. 724-749.

29.   Giddings, J.C., *Unified Separation Science*. 1991, New York: Wiley-Interscience. 77.

30.   Kestin, J., Sokolov, M. and Wakeham, W.A., *Viscosity of liquid water in the range -50°C to 150°C*. Journal of Physical and Chemical Reference Data, 1978. **7**: p. 941-948.

Chapter 3: Multiphoton Lithography Using a High-Repetition Rate Microchip Laser*

3.1 INTRODUCTION

As discussed in Chapter 1, multiphoton lithography (MPL) is a powerful, three-dimensional (3D) photofabrication technique with applications in the fields of micro-optics [1, 2], micromachines [3-5], microfluidics [6-8], and cellular culture [9-11]. The 3D capabilities of this direct-write fabrication approach are derived from a nonlinear dependence on excitation intensity, where the photochemistry is restricted to the focal volume formed by focusing a high peak power laser with high numerical aperture (NA) optics. Microforms are created by scanning the femtoliter-sized fabrication voxel through a solution of monomer and photoinitiator (or photosensitizer), resulting in the photopolymerization (or photocrosslinking) of synthetic or biological micromaterials with feature sizes of tens to hundreds of nanometers [12-14].

Developing strategies for high-speed, high-resolution MPL requires pulsed laser sources capable of achieving high peak intensities with low average powers, which can prevent the thermal breakdown of the fabrication solution and photodamage to the fabricated material. The most common laser source used for MPL is the ubiquitous, "turn-key" femtosecond-pulsed titanium:sapphire (Ti:S) laser system. Well regarded for their ease-of-use and broad spectral tunability through the near-infrared region, Ti:S laser systems can be prohibitively expensive for many researchers, costing in excess of $150K, and this initial investment has placed a limit on the spread of this technology.

---

* Adapted from Ritschdorff and Shear, *Anal Chem*, **2010** (submitted)

The development of low-cost, microchip laser systems with relatively high repetition rates have presented an interesting alternative to the Ti:S as a laser source for MPL. These laser systems would increase the dissemination of this technology into laboratories whose primary area of research is not optically related, such as biology laboratories. Recently, inexpensive frequency-double Nd:YAG microchip lasers have demonstrated the ability to efficiently fabricate synthetic and protein-based micromaterials [13, 15]. For example, with a laser system costing ~30X less, the Shear lab has shown that biocompatible microforms with feature sizes of less than 500 nm can be created using a low-cost, frequency-doubled (532 nm) Q-switched microchip Nd:YAG laser, similar to those created using a more expensive Ti:S laser [13]. This source produces 500 picosecond pulses (μJ), compared to 200 femtosecond pulses (nJ) that are output from a Ti:S. With a relatively high photon energy (2.3 eV), materials can be fabricated in the absence of photosensitizers, compounds that are often toxic to biological systems [13]. Even though the pulses are ~1000 times longer from the Nd:YAG, the duty cycle (~10^{-6}) and peak power (~ 7 kW) are similar to those produced by the Ti:S. However, due to an ~ 10^4 difference in repetition rate (8.24 kHz vs. 76 MHz), the laser focus of the Nd:YAG must be translated at relatively slow velocities compared to the Ti:S to create microforms of high-integrity.

This chapter describes studies performed to evaluate the MPL capabilities of an existing (8.24 kHz) Nd:YAG laser versus a new, higher-repetition rate (36.6 kHz) version with similar specifications. To evaluate the lasers, bovine serum albumin (BSA) micropads were fabricated in a layer-by-layer basis using a galvo-scanner that allows for

54

user-controlled scan rate, amplitude, phase, and waveform. The integrity of the protein micropads were examined after scanning the laser focus at varying velocities, and it was found that the higher repetition rate laser system allows for a significant decrease in fabrication time. The capabilities of this laser system were further demonstrated by employing a dynamic mask-based 3D multiphoton-lithography technique to create 3D microarchitectures.

3.2 EXPERIMENTAL

3.2.1 Reagents and Solutions

BSA was obtained from Equitech-Bio (Kerrville, TX). Sodium HEPES and FAD were purchased from Sigma-Aldrich (St. Louis, MO). The acrylic-based resin components were obtained from Sartomer (Warrington, PA), and consisted of a fast-curing monomer (SR499; ethoxylated trimethylolpropane triacrylate), a hardness promoter (SR368; tris(2-hydroxyethyl)isocyanurate triacrylate), and a bi-molecular photoinitiator (Esacure TZT; 2,4,6-trimethylbenzophenone and 4-methylbenzophenone). To prepare the resin, SR368 first was heated to 53 ℃ then was mixed with SR499 to prepare a solution that was 1:1 in each component by weight. Esacure TZT was then brought to room temperature from -20 ℃ and added to the mixture of SR499 and SR368 to 3% of the total solution by weight. All reagents were used as received without purification.

3.2.2 Optical Configurations

3.2.2.1 Laser Comparison for Multiphoton Lithography

Two frequency-doubled (532-nm) diode-pumped Q-switched Nd:YAG lasers were used in this work: a lower repetition rate laser (3.5-μJ, 530-ps pulses at 8.24 kHz; NG10320-110, JDS Uniphase, San Jose, CA) and a new, higher-repetition-rate laser (1.5-μJ, 530-ps pulses at 36.6 kHz; Teem Photonics, Meylan, France). Each laser output was aligned through a telescoping lens set (TLS; fl = 5 cm) to establish equal beam diameters, passed through a half-wave plate, and directed into a single optical path using a polarizing beamsplitter (Figure 3.1). This arrangement provided a means to independently vary laser-beam intensities.

The beams were aligned into a scanbox containing a two-axis, galvonometer-driven scan mirror obtained from a dismantled confocal microscope (Leica TCS-4D, Bensheim, Germany). The mirror was controlled by software written in LabView™ (National Instruments, Austin, TX) that allows for the independent control of the scan frequency, amplitude, phase, and waveform. After the scan mirror, the beams were passed through lenses L1 (fl = 3.2 cm) and L2 (fl = 15.2 cm) for expansion and collimation, respectively. Before reaching the microscope, two additional lenses (L3 and L4; fl = 15.2 cm) were placed in the optical train to focus and re-collimate the beam, which was then directed into the back aperture of a Zeiss Fluar, 100x/1.3 NA, oil-immersion objective situated on a Zeiss Axiovert microscope. The orthogonal polarization of the two beams produced by this optical arrangement did not affect fabrication results.
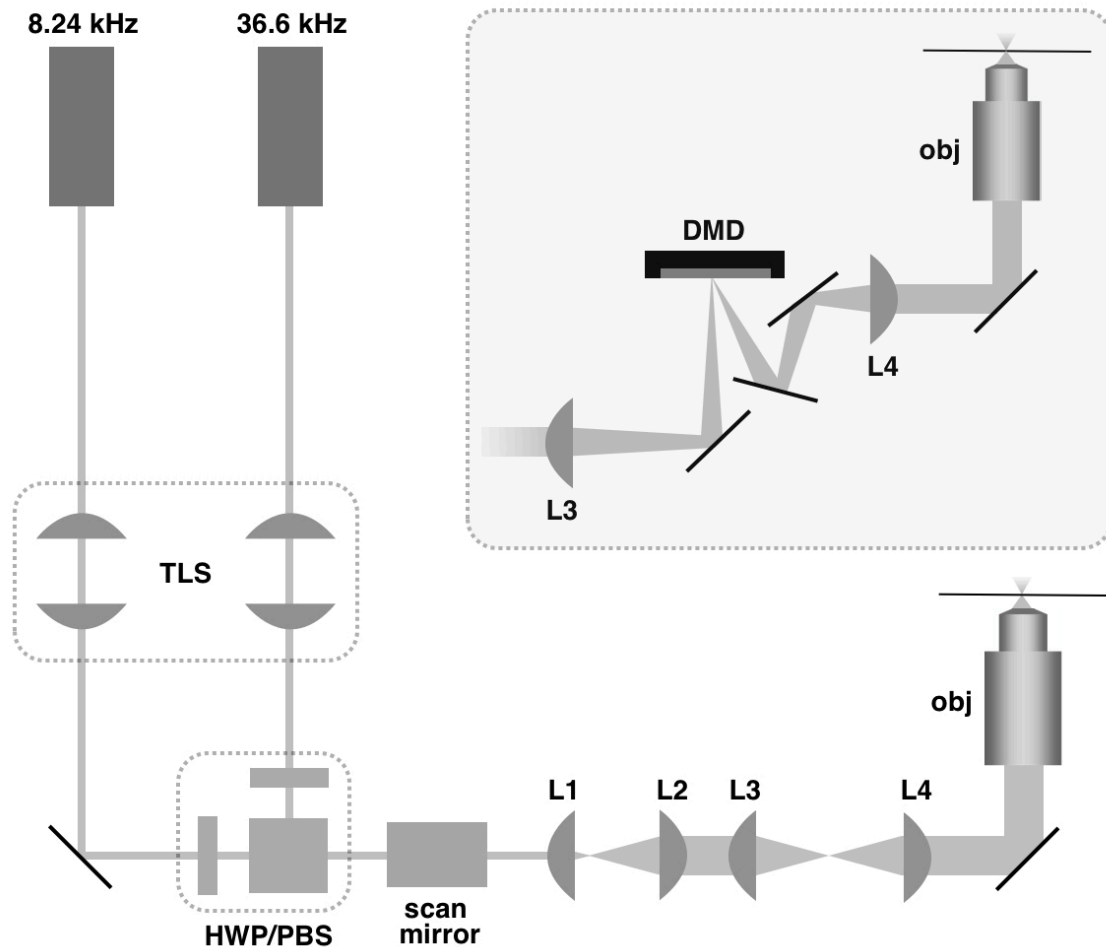
Figure 3.1. Microchip MPL. Schematic showing the optical configuration for MPL in which two 532-nm Nd:YAG microchip lasers (8.24 and 36.6 kHz) were compared. The outputs from the lasers were sent through individual telescoping lens sets (TLS) to collimate and equalize their respective beam diameters. The beams then were passed through half waveplates (HWP) into the same polarizing beam-splitter (PBS), then aligned into a dual-axis, single-mirror galvo-scanner that provided independent control over scan amplitude, frequency, phase, and waveform for each axis. The scanned beams were passed through lenses L1 (fl = 3.2 cm) and L2 (fl = 15.2 cm) for beam expansion and collimation, then focused using L3 (fl = 15.2 cm) to create a plane in which amplitude masking using a digital micromirror device (DMD) could be performed. Lens L4 (fl = 15.2 cm) re-collimated the beam into the microscope. *Inset:* Placement of the DMD in the L3 focal plane provided a means to dynamically mask the fabrication plane created by the microscope objective.

3.2.2.2 Dynamic Mask-Based Multiphoton Lithography

For fabrication of complex 3D microforms, a digital micromirror device (DMD) was inserted into the focal plane between lenses L3 and L4 (Figure 3.1, inset). Because coordinates in this plane mapped in a one-to-one fashion to positions within the fabrication plane, the DMD acted as an array of dynamic (amplitude) masking elements. This instrument has been described in detail previously[16]. Briefly, a DLP® DMD projector (BenQ, MP510) was partially dismantled, exposing an 800 x 600 array of 16μm x 16μm individually addressable mirrors. Micromirrors could be switched to "on" and "off" states based on the input of binary image data from a PC. White pixels in an image directed DMD pixels to be in "on" states and thus angled to reflect a laser beam through the remainder of the optical system into the microscope.

Each binary image sent to the DMD represented a desired fabrication pattern for a single horizontal slice of the desired microform. For complex 3D microstructures, presentation of a sequence of binary images was synchronized to stage movements in the optical axis, resulting in the photofabrication of 3D microarchitectures from stacks of 2D image data. The 2D binary image data used in this study were prepared from in-house designs created using Adobe Photoshop and from processed stacks of x-ray computed tomography (CT) images (digimorph.org).

3.2.3 Microfabrication

3.2.3.1 Laser Comparison Studies

All microstructures were fabricated on an inverted microscope from the ceiling of a reagent chamber downward, with fabrication solution sandwiched between two #1

coverslips separated by 30-μm glass microspheres (Duke Scientific Corp., cat. #9030, Palo Alto, CA). By fabricating structures using this inverted approach, we reduced exposure of the nascent microstructures to high-intensity laser light, thus limiting scattering of the beam and possible photodamage to the microforms.

The reagent solution was composed of bovine serum albumin (BSA) at 400 mg mL^{-1} with 10 mM flavin adenine dinucleotide (FAD) as a photosensitizer in 20 mM HEPES buffer (pH 7.4). BSA micropads were created by scanning a 10 μm x 16.5 μm rectangular area in twelve sequential fabrication planes, each separated by 0.25 μm z-axis (optical axis) steps. Mirrors were controlled using a triangular amplitude-versus-time function (i.e., mirrors were scanned along both axes at constant rates with essentially no pause when switching directions). After completion of a single cycle of the triangular function in the slow scan dimension, steps in the z-axis were performed using a three-axis translational stage (model 562, Newport Corp., Irvine, CA) driven by motorized actuators (model LTA-HS, Newport Corp., Irvine, CA) that were controlled using a motion controller/driver (model ESP300, Newport Corp., Irvine, CA).

The power of each laser beam was adjusted based on a qualitative assessment of the photofabrication quality, and was selected to create micropads having high integrity while preventing catastrophic break-down of the fabrication solution within the laser focus. Laser powers at the back aperture of the microscope objective were 1.8 mW and 6.9 mW for the 8.24-kHz and 36.6-kHz lasers, respectively. These powers yielded similar peak focal intensities for the two lasers and were close to the maxima that could be used without causing damage to nascent protein micropads during fabrication.

3.2.3.2 DMD-Directed Microfabrication

For all DMD-based MPL studies, the 36.6 kHz laser supplied powers of 2 mW and 6.5 mW (measured at the objective back aperture) for fabrication of the acrylic resin and BSA microstructures, respectively. All structures were fabricated using 0.2-μm z-axis stage increments, with the galvo-scanner operated at 0.5 Hz and 80 Hz in the slow and fast dimensions, respectively. Triangular amplitude-versus-time waveforms were applied to each scan axis. As in the laser comparison studies, microstructures were fabricated in an inverted fashion with the fabrication solution sandwiched between two #1 coverglass separated using 30-μm glass microspheres.

3.2.4 Scanning Electron Microscope (SEM) Sample Preparation

Microstructures composed of BSA were fixed in 5% gluteraldehyde (v/v) for 15 min, then sequentially washed in HEPES buffer (20 mM, pH 7.4), H_2O, 1:1 EtOH:H_2O, 100% EtOH, 1:1 EtOH:MeOH, and 100% MeOH (2 times), each for 15 min. Samples then were left to dry overnight in a desiccator. Structures composed of acrylic resin were washed with 100% EtOH (8 times) then 100% MeOH (2 times) and left to air-dry overnight in a desiccator. After fixation and drying, BSA and acrylic resin samples were sputter coated with Pt/Pd to a nominal thickness of 12 nm and imaged using a Zeiss Supra 40VP scanning electron microscope.

3.2.5 Bacterial Cell Culture

E. coli strain RP9535 (smooth swimming, ΔcheA) were streaked on 1.5% agar (Becton Dickinson, 214050) containing 1% tryptone broth (Becton Dickinson, 2116505)

and 0.05% w/v NaCl, then grown at room temperature. Single colonies were used to inoculate 4 mL of tryptone broth and grown to saturation on a rotary shaker (200 rpm) overnight at 32°C. An aliquot was diluted and grown to mid-exponential phase for experiments. Cells collected in BSA microstructures were grown at 32ºC in tryptone broth.

3.3 RESULTS AND DISCUSSION

3.3.1 Laser Comparison Study

Protein microfabrication has shown be a useful tool with interesting applications in tissue microreplication [16] and cell culture [6, 10, 11] and cell guidance [9, 11]. Numerous proteins are capable of photocrosslinking through multiphoton excitation and these fabricated protein matrices have attractive attributes, including high-resolution spatial features [13, 14], environmental and chemical responsivity [10], and biocompatibility [17]. To this end, BSA was chosen as a model crosslinkable protein for comparing the two microchip lasers.

For this study, BSA micropads were fabricated to a nominal height of 3 μm (12 planes separated by 0.25-μm increments) using the optical configuration shown in Figure 3.1. However, due to the z-axis component of the fabrication voxel, the actual height of the structures was slightly greater than the sum of the prescribed optical steps. For the remainder of this dissertation, the multiphoton fabrication microstructure height will be referred to as the 'nominal height', which is the sum of the fraction of the fabrication voxel that creates the initial fabrication layer and the total distance the voxel is translated into the solution as dictated by the optical axis stage motion. The laser-scanning

parameters were varied to determine the conditions that demonstrated the fabrication of high-integrity BSA micropads in the minimum amount of time.

Structures were fabricated with a triangle waveshape applied to both segments of the raster scanning mirror, with the scan period for a single fabrication layer (plane) defined by the time required to complete a single cycle of the slow dimension (SD). SD scan frequencies of 0.1, 0.25, 0.5, and 1 Hz were used in the short axis of the BSA micropad. At each slow dimension frequency, a fast dimension (FD, long axis of the micropad) frequency of 20, 40, 80, and 120 Hz was examined. This resulted in the photofabrication of an array of 32 BSA micropads used to evaluate the two lasers.
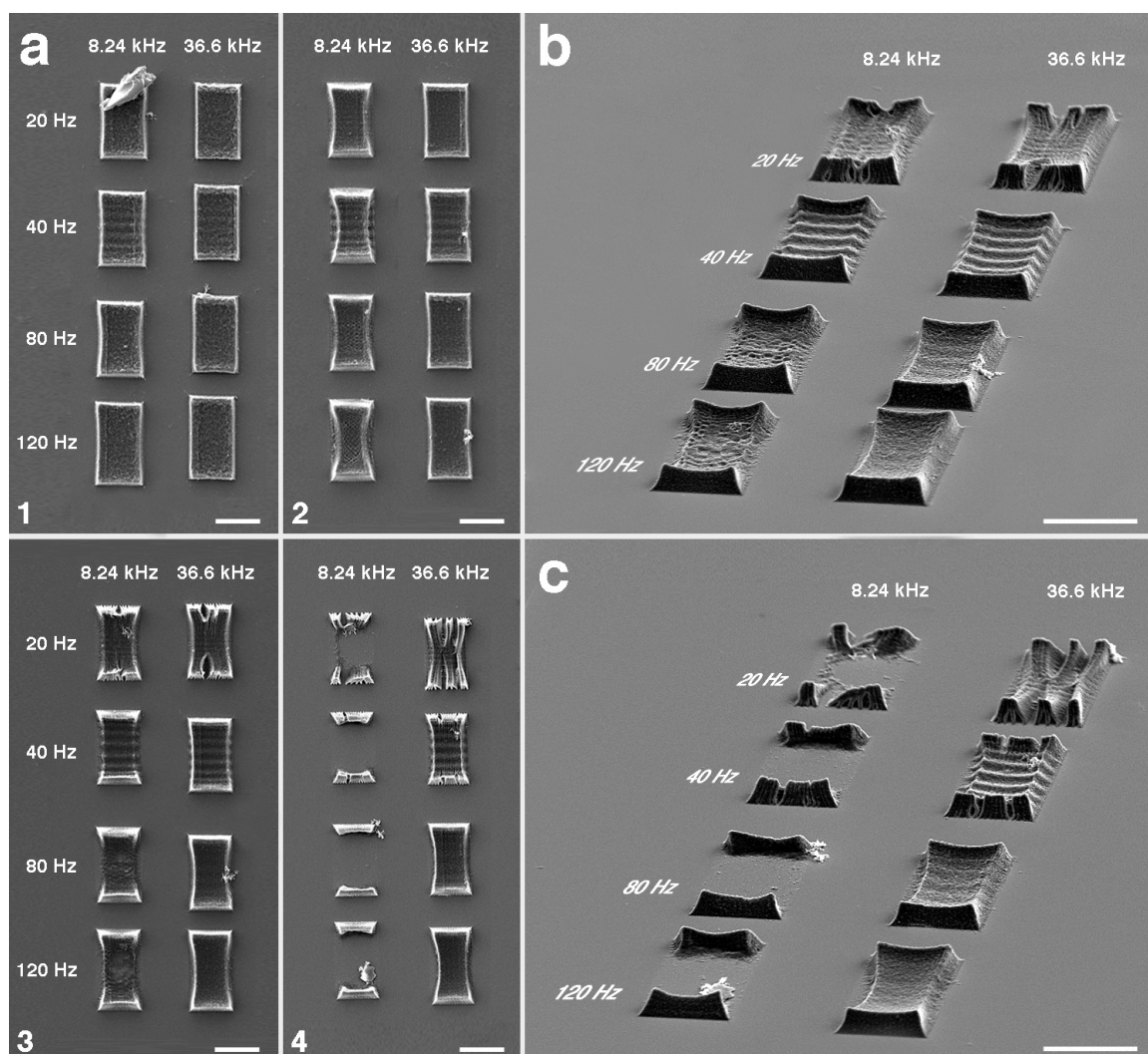
Figure 3.2: Comparison of MPL fabrication using 8.24-kHz and 36.6-kHz microchip lasers. (a) Over-head view of BSA micropads fabricated using slow dimension scan rates of 0.10 Hz (1), 0.25 Hz (2), 0.50 Hz (3), and 1.00 Hz (4). (b) Views of BSA micropads from an angled perspectives at a scan rate of 0.50 Hz in the slow dimension and 20, 40, 80, and 120 Hz in the fast dimension. (c) Analogous studies to those in part (b) with the scan rate in the slow dimension increased to 1.00 Hz. Scale bars, 10 μm.

Figure 3.2 shows scanning electron micrographs of the laser comparison study. At the lowest SD scan frequency examined (0.1 Hz), there was no discernible difference between BSA micropads fabricated by the two lasers. With a SD scan frequency of

63

0.1 Hz, 120 s were required to fabricate these 12-layer structures. At a SD scan frequency of 0.25 Hz (48 s fabrication time), the microstructures fabricated using the 36.6 kHz laser maintained high integrity at all examined fast-segment scan speeds (through 120 Hz), while the 8.24 kHz laser fabricated micropads at the highest FD frequency of uneven quality (Figure 3.2a, panel 2). At higher FD scan frequencies (Figure 3.2a, panels 2 – 4) where the fabricated protein matrix is less dense due to decreased laser fluence for each fabrication layer, the BSA micropads have the appearance of an hourglass morphology. This shape was not seen during the fabrication of micropads, nor when the fabrication solution (400 mg mL-1 BSA and 10 mM FAD) was replaced with aqueous buffer (20 mM HEPES, pH 7.4), and is an artifact of the dehydration and drying steps used in the preparation for electron microscopy (Figure 3.3).
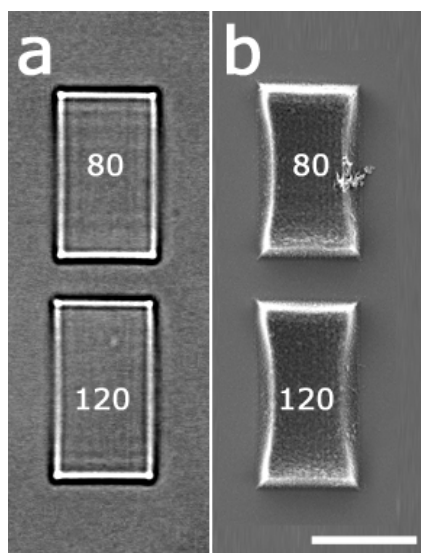
Figure 3.3:   BSA microstructure dehydration. (a) Brightfield and (b) SEM images of the same BSA micropads fabricated using the 36.6 kHz laser at an SD scan rate of 0.5 Hz at FD scan rates of 80 and 120 Hz (seen in Figure 3a; panel 3). The hourglass shape of the micropads in the SEM images is an artifact of the dehydration steps used in the preparation of samples for electron microscopy. Scale bar, 10 μm.

At a SD scan rate of 0.5 Hz (Figure 3.2a, panel 3; Figure 3.2b), structures were fabricated by both lasers with similar results at 20 Hz, with visible "rips" in the structures due to the relatively slow fast-segment scan. These rips are the result of under-scanning each fabrication layer as a result of inadequate FD scan rate coverage for an SD scan rate of 0.5 Hz (2.0 s per layer). With FD scan rates of 80 Hz and 120 Hz, BSA micropads of high integrity were formed using the 36.6 kHz laser at a total fabrication time of 24 s. However, the 8.24 kHz was unable to fabricate micropads of even quality at these conditions, with increased material thickness at the "top" and "bottom" edges of the micropad. This uneven thickness is due to triangle waveform and is the result of an increase in laser dwell-time at the turn-around points of the scan. This effect is also seen in micropads formed using the 36.6 kHz laser, to a lesser extent, and could be eliminated by synchronizing the scan with a shutter to block the laser beam as it is approaching the turn-around segment of the waveform.

For the fastest scan segment examined (1 Hz), the total fabrication time was reduced to 12 s, and at all FD scan rates, the 8.24 kHz laser was unable to successfully fabricate BSA micropads (Figure 3.2a, panel 4; Figure 3.2c). Conversely, the 36.6 kHz laser demonstrated the ability to fabricate micropads at FD scan rates of 80 and 120 Hz. A comparison of these micropads fabricated with the 36.6 kHz laser at an FD scan rate of 80 Hz to those fabricated with the 8.24 kHz laser at an SD frequency of 0.25 Hz (FD = 80 Hz) reveals similarities, indicating the 36.6 kHz laser allows structures to be at

a rate 4 times faster, a value approximately equally to the difference in laser repetition rate.

A number of factors simultaneously influence the fabrication of BSA micropads, including the SD and FD scan frequencies (individually and in relation to each other), the laser repetition rate, and the focal dimensions of the focused laser spot. Photofabricating an even, unbroken protein layer requires that the laser beam is translated at a fast dimension rate such that the laser pulses are not separated by more than the radial extent of the two dimensional focal spot. To this end, the maximum FD frequency that results in even fabrication can be calculated by considering the laser spot size and the inter-pulse period. For the 8.24 kHz laser, the maximum velocity that allows for radial coverage of the focused laser spot is ~2000 μm s^{-1} (0.25 μm/120 μs; beam waist divided by the inter-pulse period). Thus, for the long axis of the test structures in Figure 3.2 (16.5 μm), the maximum FD frequency applied via a triangle waveform that results in even coverage across the scan is ~60 Hz. At higher FD scan rates the fabrication along a single axis will be undersampled, resulting in a protein matrix of poor integrity. Although, this effect can be diminished through the use of low SD frequencies, which allows for multiple FD passes to occur across the same coordinates.

While it is sufficient to use low SD frequencies to mitigate the degradation of the protein matrix at the expense of total scan time, using very slow FD frequencies can be counterproductive and may result in structures of low integrity. It is crucial to complete, at a minimum, one entire scan line from the FD cycle before the focal position is translated in the orthogonal direction (slow dimension) by more than the size of the beam

66

waist (beam radius). This effect is seen as rips in the micropads in Figure 3.2a, panels 3 and 4 at an FD rate of 20 Hz, and Figure 3.2b (20Hz) and 2c (20 and 40 Hz). Thus, using FD rates that are too slow can result in microstructures of low structural integrity, especially when mated with high SD scan rates.

3.3.2 Fabrication of 3D Polymer and Protein Microstructures

Combining MPL with electronic optical masking allows for the rapid creation of arbitrary microarchitectures with the possibility of on-the-fly iterations. This approach, described in Chapter 1, allows for the creation of 3D arbitary microforms with high resolution[16]. By scanning a focused laser across the face of a digital micromirror device (DMD) aligned in an optical plane conjugate to the microscope objective image plane, the 2D binary images presented on the DMD are rendered as 2D photofabricated material on the coverglass substrate by the high-numerical objective, with the magnification of the fabricated material being determined by the lens system and the microscope objective. 3D objects can be created by synchronizing the presentation of 2D binary image slices derived from 3D objects (tomographic data), or computer-illustrated designs, on the DMD with incremental optical-axis stage movements. Here, the capabilities of the 36.6 kHz laser were examined to create complex 3D microforms using the approach described above. Moderately high scan frequencies of 0.5 Hz and 80 Hz were used in the slow dimension and fast dimension, respectively. While it is possible to fabricate using a higher SD scan rate, these parameters allowed for the fabrication of high-quality microforms in short amount of time.
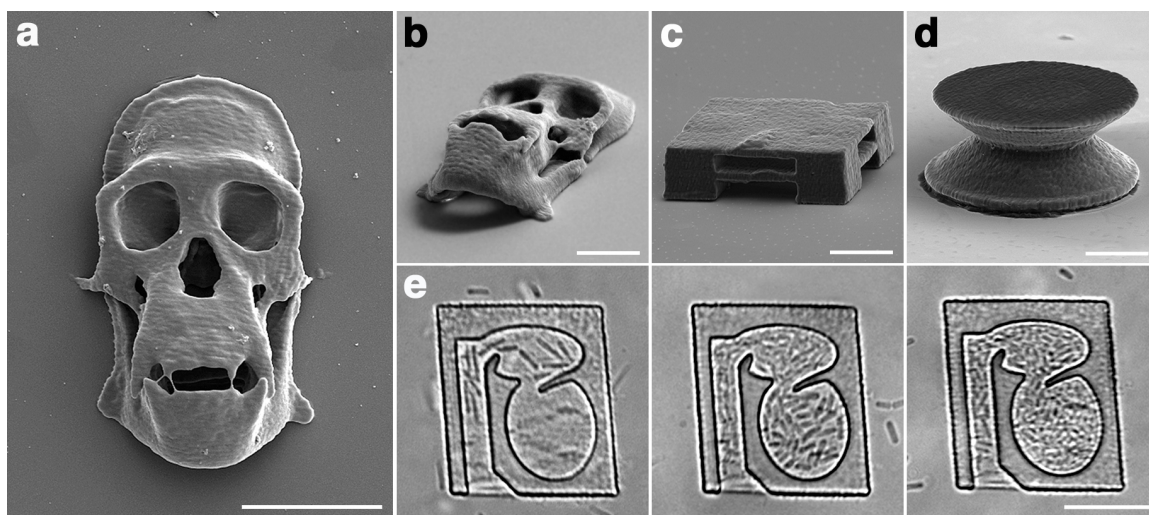
Figure 3.4: Three-dimensional acrylic-based resin polymer and BSA microstructures fabricated using the high-repetition-rate microchip laser. Microforms were fabricated using the dynamic mask technique (Figure 1, *inset*), with the presentation of the two-dimensional binary images on the DMD synchronized to 0.2-μm stage movements along the optical axis. (a) and (b) Microreplication of *Pan troglodytes* (common chimpanzee) from a stack of X-ray CT images. (c) Two-tiered coffee table fabricated from four designed masks. (d) An hourglass created using a sequence of 30 masks of progressively smaller circles followed by an inversion of this sequence. (e) A sequence showing the initial trapping of small numbers of *E. coli* in a biocompatible BSA microstructure and subsequent cell division that fills the structure (time points, left-to-right: 0 h, 15 h, 24 h). Scale bars: a, e, 10 μm; b – d, 5 μm.

Figure 3.4 shows scanning electron micrographs of microforms composed of acrylic-based resin or BSA created using the 36.6 kHz microchip laser. Figures 4a and 4b show tissue replicas of a common chimpanzee (*Pan troglodytes*) skull that were fabricated using a sequence of ~ 50 modified binary images obtained from X-ray computed tomographic (CT) data (digimorph.org) with optical axis steps of 0.2 μm between each presented image, a process requiring 100 s.

Graphic design using photoillustrative software can also be used to create a sequence of binary images that can be combined to create a 3D microform. Figure 3.4c and Figure 3.4d show a two-tiered table and an hourglass, respectively, that were created using illustrated binary designs. Each structure was created using optical steps of 0.2 μm between fabrication layers. The two-tiered table was created from four binary images, with each image being used for multiple fabrication planes. The hourglass was fabricated from a set of 30 individual of incrementally smaller circles, with the set of images presented in reverse order once the fabrication reach the waist of the hourglass.

The 36.6 kHz laser was also used to fabricated 3D biocompatible BSA microcontainers using DMD-directed MPL. Shown in Figure 3.4e, a simple microstructure was created using two photomask images, one used to define the microstructure internal geometry, which was fabricated using 16 optical steps of 0.25-μm steps, and a fully reflective mask, which was used in the final 4 optical steps to create the roof of the microcontainer. The simple microstructure, which contains a long entrance canal leading to two sequential cavities, was inoculated with *E. coli* and incubated at 32ºC for a 24-h period. The bacteria were observed entering the structure (Figure 3.4e, left panel), creating a "log-jam" within the long entrance that plugged the chamber and prevented cells from within the two chambers from escaping. Over the 24-hour observation period, the cells continued to divide, filling both chambers with bacteria (Figure 3.4e – middle and right panels).

3.4 CONCLUSION

This chapter demonstrated the use of a low-cost, 36.6 kHz repetition rate microchip laser for the formation of protein and polymer-based microarchitectures using multiphoton lithography. This laser system was found to be capable of creating multilayered protein micropads in one quarter the time compared to lower-repetition-rate microchip source. This four-fold decrease in minimum fabrication time enables complex 3D microarchitectures to be rapidly created. This source demonstrated 3D MPL capabilities similar to a Ti:S at a much-reduced cost, thus creating opportunities for the widespread dissemination of this technology to be applied to the creation of microarchitectures for applications in cell culture and analysis.

3.5 REFERENCES

1. Ledermann, A., Cademartiri, L. and Hermatschweiler, M., *Three-dimensional silicon inverse photonic quasicrystals for infrared wavelengths*. Nature Materials, 2006. **5**: p. 942-945.

2. Sun, H., Matsuo, S. and Misawa, H., *Three-dimensional photonic crystal structures achieved with two-photon-absorption photopolymerization of resin*. Applied Physics Letters, 1999. **74**: p. 786-788.

3. Bayindir, Z., Sun, Y., Naughton, M.J., Lafratta, C.N., Baldacchini, T., Fourkas, J.T., Stewart, J., Saleh, B.E.A., and Teich, M.C., *Polymer microcantilevers fabricated via multiphoton absorption polymerization*. Applied Physics Letters, 2005. **86**(6): p. 064105.

4. Galajda, P. and Ormos, P., *Complex micromachines produced and driven by light*. Applied Physics Letters, 2001. **78**: p. 249-251.

5. Kawata, S., Sun, H., Tanaka, T. and Takada, K., *Finer features for functional microdevices*. Nature, 2001. **412**: p. 697-698.

6. Kaehr, B. and Shear, J., *High-throughput design of microfluidics based on directed bacterial motility*. Lab Chip, 2009. **9**: p. 2632-2637.

7. Kumi, G., Yanez, C.O., Belfield, K.D. and Fourkas, J.T., *High-speed multiphoton absorption polymerization: fabrication of microfluidic channels with arbitrary cross-sections and high aspect ratios*. Lab Chip, 2010. **10**(8): p. 1057-1060.

8. Maruo, S. and Inoue, H., *Optically driven micropump produced by three-dimensional two-photon microfabrication*. Applied Physics Letters, 2006. **89**: p. 144101.

9. Kaehr, B., Allen, R., Javier, D., Currie, J. and Shear, J., *Guiding neuronal development with in situ microfabrication*. Proceedings of the National Academy of Sciences, 2004. **101**: p. 16104-16108.

10. Kaehr, B. and Shear, J.B., *Multiphoton fabrication of chemically responsive protein hydrogels for microactuation*. Proceedings of the National Academy of Sciences, 2008. **105**: p. 8850-8854.

11. Seidlits, S.K., Schmidt, C.E. and Shear, J.B., *High-resolution patterning of hydrogels in three dimensions using direct-write photofabrication for cell guidance*. Advanced Functional Materials, 2009. **19**: p. 3543-3551.

12. Basu, S., Wolgemuth, C. and Campagnola, P., *Measurement of normal and anomalous diffusion of dyes within protein structures fabricated via multiphoton excited cross-linking*. Biomacromolecules, 2004. **5**: p. 2347-2357.

13.   Kaehr, B., Ertas, N., Nielson, R., Allen, R., Hill, R.T., Plenert, M. and Shear, J.B., *Direct-write fabrication of functional protein matrixes using a low-cost Q-switched laser*. Analytical Chemistry, 2006. **78**: p. 3198-3202.

14.   Li, L., Gattass, R., Gershgoren, E., Hwang, H. and Fourkas, J., *Achieving {lambda}/20 resolution by one-color initiation and deactivation of polymerization*. Science, 2009. **324**: p. 910-913.

15.   Wang, I., Bouriau, M., Baldeck, P., Martineau, C. and Andraud, C., *Three-dimensional microfabrication by two-photon-initiated polymerization with a low-cost microlaser*. Optics Letters, 2002. **27**(15): p. 1348-1350.

16.   Nielson, R., Kaehr, B. and Shear, J., *Microreplication and design of biological architectures using dynamic-mask multiphoton lithography*. Small, 2009. **5**: p. 120-125.

17.   Basu, S., Cunningham, L., Pins, G., Bush, K., Taboada, R., Howell, A.R., Wang, J. and Campagnola, P.J., *Multiphoton excited fabrication of collagen matrixes cross-linked by a modified benzophenone dimer: bioactivity and enzymatic degredation*. Biomacromolecules, 2005. **6**: p. 1465-1474.

Chapter 4: Thermally Responsive Multiphoton-Fabricated Protein Hydrogels

4.1 INTRODUCTION

Materials that conformationally respond to external stimuli have current and potential applications in numerous fields, including microfluidics [1], biosensors [2], drug delivery [3, 4], and cell culture [5]. These materials, commonly referred to as "smart materials", respond to changes in their local environment, with stimuli such as pH [6], temperature [7], ionic strength [8], light [9], humidity [10], and electric fields [11] providing a possible means of actuation. Stimuli-responsive materials are often composed of polymers, either synthetic or natural. Of these polymeric materials, hydrogels have demonstrated good biocompatibility, versatile chemistry, and conformational responsiveness that have brought them to the forefront of "smart materials" for use in bio-related applications.

Hydrogels consist of a hydrated network of interconnected polymeric chains. Hydrogel-based materials, composed of either natural polymers, such as hyaluronic acid (HA), or synthetic polymers, such as poly(ethylene glycol)-poly(lactic acid)-poly(ethylene glycol) (PEG-PLA-PEG), have been used extensively for three-dimensional (3D) cell culture because they can be prepared with similar elastic properties to biological tissue with good control over the chemistry that is presented to the cell system [4, 5, 12]. Hydrogels can be selectively hydrated and dehydrated using stimuli such as changes in pH or ionic strength that causes the gel to expand or contract. These

73

materials have been adopted for use as microfluidic valves [1], optical components [6], and actuators [11, 13].

Temperature changes can also be used as a stimulus for responsive hydrogel materials. One of the most commonly used thermoresponsive hydrogels, poly(N-isopropylacrylamide) (PNIPAm), demonstrates a sharp transition between swollen and contracted states at 32 °C [14, 15]. PNIPAm hydrogels have been used in a wide variety of applications, including drug delivery [16], microfluidic actuators [17], microlens arrays [18], and as photonic crystals [19].

Some researches have turned their interests from large-scale, bulk hydrogels to micro or nano-sized hydrogel-based materials. Responsive hydrogels have been demonstrated with feature sizes ranging from hundreds of nanometers to tens of microns [10, 20, 21], yet they are generally prepared by techniques that lack the ability to form arbitary 3D features, such as etching (e.g., Bosch process followed by chemical treatment) or two-dimensional photolithographic techniques (soft or hard lithography). A photofabrication technique capable of creating responsive hydrogel materials with intricate 3D spatial features would of great interest and could have potential uses as microfluidic valves [1], micro-optics, such as adaptive microlenses [6], or for 3D cell culture on the micro scale.

Multiphoton lithography (MPL) presents an alterative to traditional photolithographic techniques for preparing stimuli-responsive hydrogels by localizing the photochemistry to high-resolution 3D coordinates. Watanabe *et al*. initially reported the preparation of an acrylic-based hydrogel by MPL that responded to UV illumination;

however, the slow responsiveness of the material, due to the kinetics of the photoreaction, and relatively low resolution (>50 μm), leave much to be improved on [22].

As an alternative to acrylic-based materials, protein matrices can be patterned using MPL to create functional biocompatible materials, as discussed in Chapter 1 [23-27]. Proteins have a native responsiveness to changes in their local environment. A protein's secondary and tertiary structure are maintained by a number of noncovalent interactions (ionic interactions, hydrogen bonding, van der Walls forces, etc.) that can be altered through changes in pH, ionic strength, or temperature. Changes in the protein's local environment can result in the unfolding or denaturing of the native conformation. Kaehr and Shear presented the development of chemically responsive protein hydrogels prepared by MPL [28]. By altering the pH or ionic strength, these materials provided a means for microactuation by rapidly swelling or contracting and presented a novel mode of capturing and releasing small numbers of microorganisms. However, to capture or release small numbers of cells, large shifts in pH or ionic strength were required, both of which could negatively influence the metabolic state of the microorganism under study. Therefore, understanding the effects of other stimuli, such as thermal changes, on protein hydrogels could have profound impacts the development of novel smart materials and on the study of small populations of microorganisms.

This chapter describes the development of stimuli-responsive, tunable, multiphoton fabricated protein hydrogels that undergo defined, irreversible volume changes (swelling or contracting) when exposed to elevated temperatures. The swelling response of a number of protein microstructures (BSA, avidin, ovalbumin, lysozyme)

fabricated using different photosensitizers (rose bengal (RB) and methylene blue (MB)) is demonstrated. By altering the fabrication parameters, the swelling response of these hydrogels can be tuned. Chemical effects due to changes in pH and salt concentration were also investigated in conjunction with thermal changes. Using these thermally responsive materials, microcavities were created that provide a means to trap and release small populations of microorganisms.

4.2 EXPERIMENTAL

4.2.1 Reagents and Solutions

BSA was obtained from Equitech-Bio (Kerrville, TX). Avidin and biotin-tetramethylrhodamine (biotin-TMR) were purchased from Invitrogen (Carlsbad, CA). Lysozyme, ovalbumin, sodium HEPES, Triton-X, rose bengal, methylene blue, and sodium sulfate were purchased from Sigma-Aldrich (St. Louis, MO). All reagents were used as received without purification.

4.2.1 Hydrogel Fabrication

Protein hydrogels were fabricated on untreated No. 1 coverslips housed in thermally conductive aluminum wells. These wells maintain a solution void volume of ~ 2.5 mL and were coated with epoxy (Epoxy 907 Adhesive System, Miller-Stephenson, Danbury, CT) to prevent aluminum oxide formation. All structures were created using mask-directed MPL, as previously described in Chapter 3 and elsewhere [29]. Briefly, the output from a mode-locked titanium:sapphire laser (Tsunami; Spectra Physics) operated at 740 nm was first sent through a half-wave plate/polarizing beam-splitter pair for laser

power attenuation. The beam was then aligned into commercial confocal scanner (Bio-Rad MRC600) that raster scanned the focused beam across the face of a dynamic reflective mask (digital micromirror device (DMD)) placed in an optical plane conjugate to the microscope objective image plane. The DMD consists of an array of micromirrors that can be individually addressed to "on" or "off" states based on input binary image data. The presentation of white image data on the DMD resulted in the reflection of the laser beam through the remainder of the optical system and into the microscope. The 2D binary image presented on the DMD was rendered as a 2D fabrication plane of finite thickness due to the axial component of the multiphoton fabrication voxel on the coverglass substrate. The laser beam reflected by the DMD was expanded and collimated to overfill the back aperture of a Zeiss Fluar, 100x/1.3 NA, oil-immersion objective situated on a Zeiss Axiovert microscope. 3D protein microforms were created from 2D binary image stacks by incrementally translating the laser focal point deeper into the fabrication solution using a motorized focus driver (Prior, H122) for each 2D binary image displayed on the DMD.

4.2.2 Hydrogel Characterization

A number of factors involved in the fabrication process can influence the thermal and chemical response of multiphoton fabricated protein hydrogels, including protein type, protein concentration, photosensitizer concentration, laser wavelength, average laser power, and the incremental optical steps between photofabrication layers. For all hydrogel characterization experiments the laser was operated at 740 nm. All microstructures of photocrosslinked protein were fabricated from a solution containing

protein at a concentration of 400 mg mL^{-1} in 20 mM HEPES, 0.1 M NaCl buffer (pH 7.4), which insured the fabrication of microstructures at various photosensitizer concentrations. The laser power was adjusted to 50 mW at the back aperture of the microscope objective, a power that insured quality fabrication without catastrophic breakdown of the fabrication solution or damage to the nascent fabricated protein material.

The thermal response of photocrosslinked protein hydrogels was investigated for a variety of proteins (BSA, avidin, lysozyme, and ovalbumin) using different photosensitizers at different concentrations (RB (3.5 mM – 11.5 mM) and MB (1mM – 3 mM)) with some hydrogels fabricated using different z-axis optical step sizes between fabrication layers (0.1 – 1 μm). The chemical response of protein hydrogels was also investigated in conjunction with the thermal response for a number of stimuli, including increasing salt concentration (up to 1 M Na$_2$SO$_4$) and changes in pH (20 mM phosphate buffer, pH 2 and pH 12). The solution temperature within the aluminum fabrication well was controlled using a microscope stage heater (Brook Industries) and monitored using a thermocouple (Omega) placed near the surface of the coverglass adjacent to the microstructures. All temperature experiments were initiated at 23 °C, a stable temperature above a room temperature that ranges daily between 16 °C and 21 °C. Each temperature step was reached in 5 min and temperature points were held for 5 min prior to imaging. Within 5 min., the thermal response was demonstrated and did not change with longer incubation (up to 2 –3 h) at that given temperature. All given temperatures are ± 0.2 °C.

All hydrogel test structures were fabricated to nominal dimensions of 10 μm x 10 μm x 8 μm (length x width x height) and imaged under brightfield illumination on a Zeiss Axiovert 135 inverted microscope with a 12-bit CCD (Hamamatsu). Square areas (A) of the microstructures were measured from the top of the microstructure for all test structures and the swelling ratio was defined by the ratio A/A°, where A° is the area of the structure at the start of the experiment.

4.2.3 Cell Culture

Pseudomonas aeruginosa PA01 carrying the pMRP9-1 *gfp* plasmid was used in all cellular experiments. Planktonic cultures were grown aerobically overnight at 37°C in tryptic soy broth (TSB) and incubated with carbenicillin (300 μg mL^{-1}) for plasmid selection. TSB is a commonly used growth medium for microorganisms that contains proteins (e.g., casein) and sugar (e.g., dextrose) at a phosphate buffered pH of 7.3. Cells were diluted in TSB, grown to mid-logarithmic phase at 37°C, allowed to reach room temperature, and introduced to the microchambers under sterile conditions via pipette.

4.3 RESULTS AND DISCUSSION

Multiphoton-fabricated protein hydrogels have attributes attractive to cell culture and materials science, most notably good biocompatibility [25, 26, 29], chemical functionality [23, 24], and chemical responsivity [28]. As demonstrated by Kaehr and Shear, multiphoton fabricated protein hydrogels rapidly swell or contract in response to changes in pH or ionic strength likely as a result of disruptions in the native conformation

of the protein [28]. This disruption causes an increase or decrease in the solvent space that water molecules can occupy producing a volume change. To expand of the characterization of these materials, this study examines the effects of increased temperature on multiphoton fabricated protein hydrogels and demonstrates further tunability and usefulness of these materials.

4.3.1 Thermally Responsive BSA Hydrogels

To characterize the swelling response of BSA hydrogels to changes in temperature, test structures were fabricated using RB (5.5 mM) and MB (2 mM) as photosensitizers. RB and MB are both well-characterized Type II photosensitizers commonly used in protein microfabrication [23, 25-27, 30]. The BSA hydrogels were heated to 43 °C from 23 °C in approximately 15 min. and maintained at 43 °C for 5 min. The temperature increase was halted at 43 °C because these materials are commonly used to capture and study microorganisms and understanding the behavior of these materials at near physiological conditions is important. It was observed that structures fabricated with MB as the photosensitizer did not swell while those fabricated using RB underwent a volume expansion, with a swelling ratio (A/A˚) of ~ 1.10. The lack of observed swelling of BSA hydrogels fabricated with MB in response to increased temperatures may be due to a number of factors and is discussed in greater detail in an section 4.3.3.

To test the reversibility of the swelling response of BSA hydrogels fabricated with RB (5.5 mM), the temperature was increased from 23 °C to four incrementally higher temperatures and returned to 23 °C after each temperature step (e.g., 23 → 27 → 23 → 32 → 23 → 37 → 23 → 43 → 23 °C). The results of this experiment are shown in Figure

80

4.1. At all temperature steps examined, the thermal response of BSA hydrogels fabricated with RB was found to be irreversible. Slight increases and decreases are observed in the swelling ratio when the temperature was returned to 23 °C from a higher temperatures in Figure 4.1. However, these changes in the swelling ratio are small ($\sim \pm 0.001 - 0.002$) and are due to measurement error.
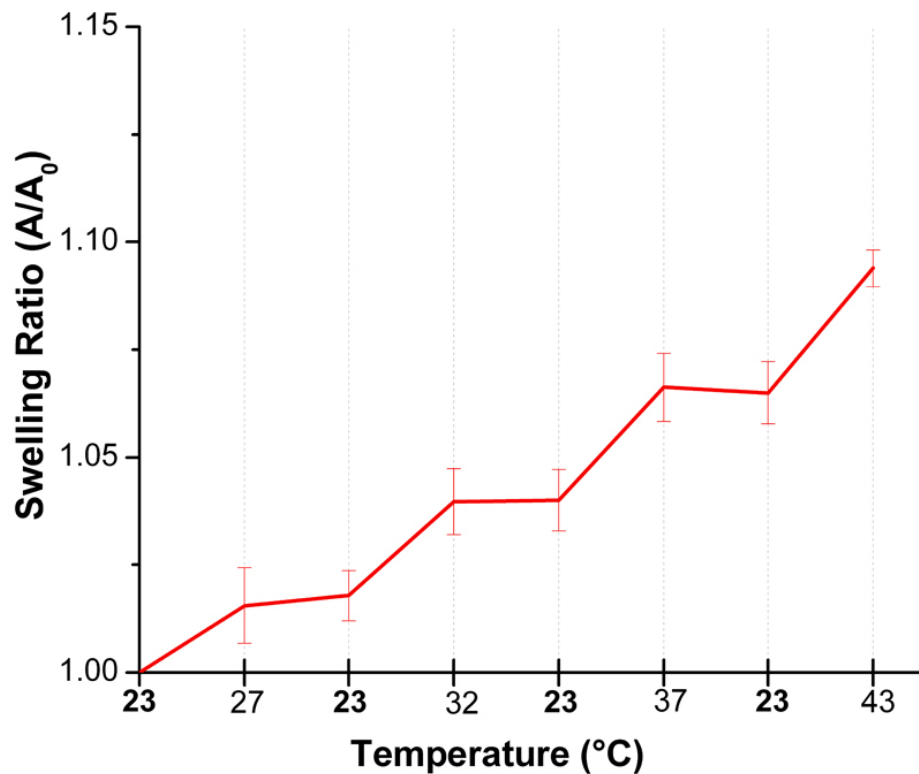
Figure 4.1: Irreversibility of the thermal response of multiphoton fabricated BSA hydrogels. BSA hydrogels fabricated with 5.5 mM RB using 0.5-μm incremental optical steps between fabrication layers were exposed to a cycling of increasingly greater temperatures. Error bars represent the standard deviation (N=4), where N is the number of microstructures examined.

Exposing proteins to elevated temperatures can disrupt the non-covalent interactions that maintain the native secondary and tertiary structures. At temperatures of less than 45 °C, this process is typically reversible for mammalian proteins [31]. However, at temperatures greater than 45 °C, irreversible denaturation processes such as protein aggregation and gelation can occur [31, 32]. BSA has been shown to have two denaturation temperatures: ~ 30 °C and 65 – 70 °C [31-33]. The lower denaturation temperature (30 °C) was experimentally observed by Takeda *et al.* using circular dichroism from a marked decrease in the α-helical proportion of the protein [32]. Importantly, this structural change was found to be reversible if the temperature remained below 45 °C [32].

As shown in Figure 4.1, the thermal swelling response of BSA hydrogels is irreversible. Even though the thermal denaturation of the individual protein moieties is likely occurring over the examined temperature range (up to 43 °C), the irreversible responsive behavior of the protein hydrogels cannot be fully explained simply by thermal denaturation. Rather, it could be attributed to a disruption in the entanglement of the crosslinked polymers within the protein hydrogel.

The protein hydrogels are most likely an arrangement of crosslinked polymer chains that are randomly interwoven with each other forming a porous solid matrix. As the temperature is increased (e.g., 23 °C → 37 °C) the intermolecular interactions between the polymer chains can be disrupted. In this expanded state, the entangled polymer chains could be caught in a kinetic energy trap and are unable to return to their

previous confirmation as the temperature is decreased (e.g., 37 °C → 23 °C), resulting in an irreversible response.

4.3.2 Tuning the Thermal Response of BSA Hydrogels

The responsive behavior of BSA hydrogels to changes in pH and ionic strength has been shown to be modulated by a change in the crosslinking density as function of the laser exposure [28]. As discussed in the previous section, the irreversible thermal response of BSA hydrogels could likely be attributed to a disruption in the entanglement of the polymer chains that make up the hydrogel matrix. By increasing the crosslinking density between the entangled polymer chains, the matrix should be less likely to undergo a transition that would result in hydrogel expansion.

Towards developing multiphoton-fabricated BSA hydrogels with a tunable, predictable thermal response, two factors involved in the photofabrication process that would alter the crosslinking density of the protein matrix were independently varied: photosensitizer concentration (RB) and the incremental optical step-size between fabrication layers.

Figure 4.2 shows the thermal response of BSA hydrogels fabricated with four different concentrations of RB: 3.5 mM, 5.5 mM, 8.8 mM, and 11.5 mM using 0.5-μm incremental optical steps between fabrication layers for all test structures. This RB concentration range was chosen to produce BSA structures of slightly different crosslinking densities. At the lowest RB concentration (3.5 mM), the structures did not appear as solid as those fabricated at higher concentrations. At a RB concentration of 5.5 mM and above, all structures were of good structural integrity. The thermal

83

experiments were initiated at 23 °C and hydrogel response was observed at four increasingly higher temperatures, $27 \rightarrow 32 \rightarrow 37 \rightarrow 43$ °C.
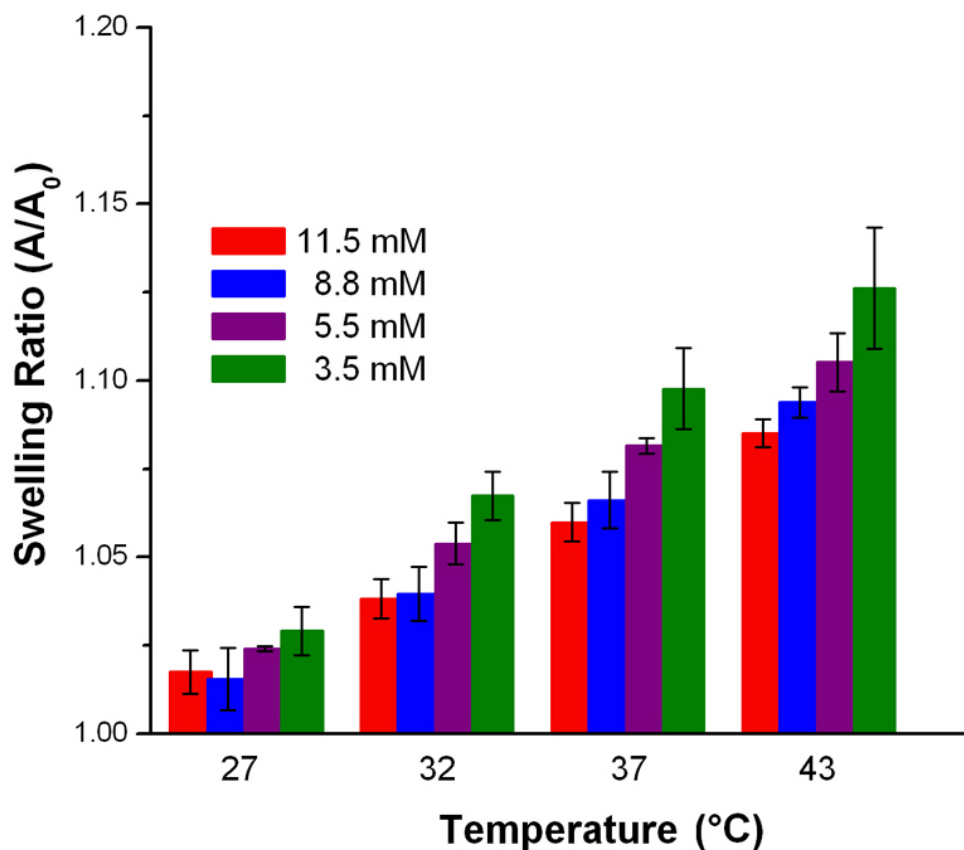
Figure 4.2: The thermal response of BSA hydrogels as a function of RB concentration. All structures were fabricated using 0.5-μm incremental steps between fabrication layers. Error bars represent the standard deviation (N=4).

As the photosensitizer concentration was increased, a reduction in the thermal swelling response of BSA hydrogels was observed (Figure 4.2). For example, when the solution temperature was raised from 23 °C to 43 °C, swelling ratios of ~1.12 and 1.07 were observed for hydrogels fabricated with 3.5 mM and 11.5 mM RB, respectively. The

decrease in swelling response as a function of RB concentration is attributed to the creation of a hydrogel matrix with a greater crosslink density due to the greater availability of photosensitizing molecules participating in the photochemical reaction. At higher crosslink densities, there are fewer possible stimuli-induced polymer chain disruptions that can occur, resulting in a more temperature-stable hydrogel material.

Toward further developing the tunability of BSA hydrogels, the effect of increasing the incremental distance between fabrication layers was also investigated and the results of these experiments are shown in Figure 4.3.
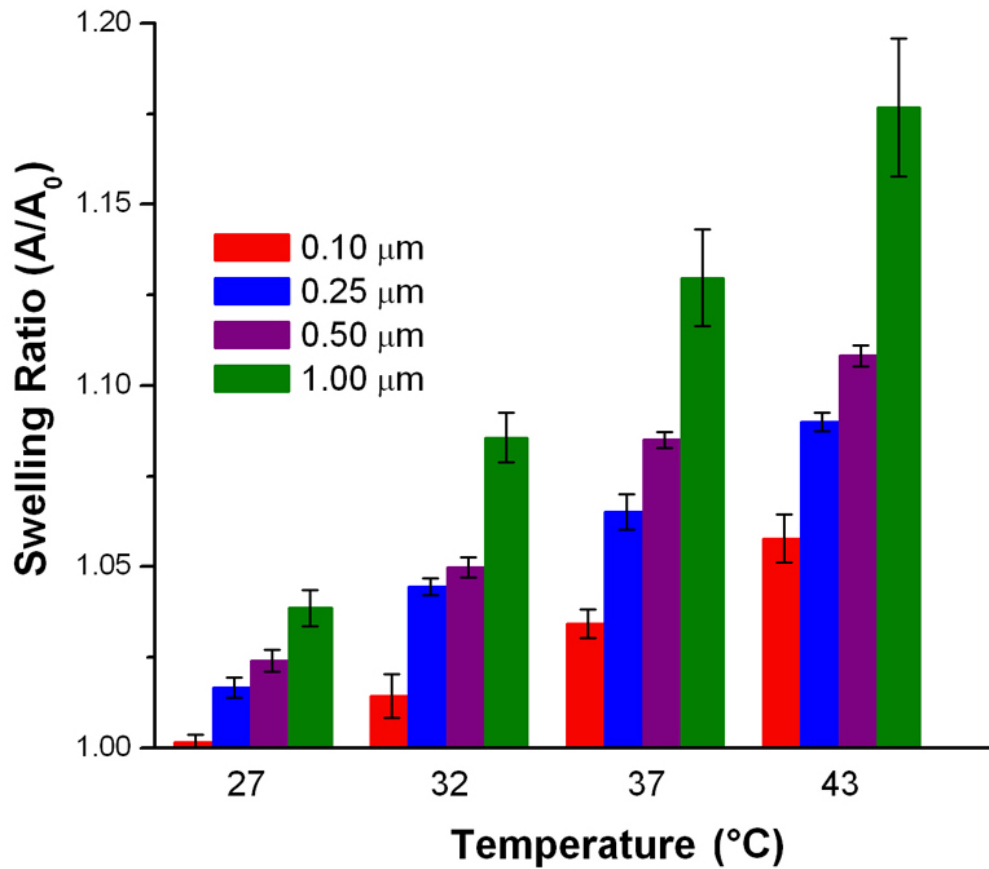
Figure 4.3: The thermal response of BSA hydrogels as a function of the incremental distance between fabrication layers. All structures were fabricated using 5.5 mM RB. Error bars represent the standard deviation (N=4).

Test structures were fabricated from a solution containing 400 mg mL^{-1} BSA with 5.5 mM RB at increasing optical axis incremental steps (0.10 μm, 0.25 μm, 0.50 μm, and 1.00 μm). An RB concentration of 5.5 mM was chosen because the structures could be fabricated with good structural integrity while demonstrating a thermal response. All test structures were fabricated to the same nominal height of 8 μm as prescribed by number of incremental optical steps. For example, structures fabricated using 1.0 μm optical steps were created with 8 fabrication layers, whereas structures fabricated with 0.10 μm optical

steps were created with 80 fabrication layers. An increase in the swelling ratio was observed as the distance between photofabrication layers was increased. Specifically, when the solution temperature was raised from 23 °C to 43 °C, swelling ratios of ~1.17 and 1.06 were observed for hydrogels fabricated using 1.0 μm and 0.10 μm, respectively.

At smaller distances between optical steps, the photofabrication layers are increasingly overlapped as a result of the nominal thickness of the multiphoton fabrication voxel, which is expected to be in the low micron range using a 1.3 NA microscope objective [34]. Therefore, as the distance between the incremental optical steps was decreased, the BSA hydrogels were fabricated with a higher crosslink density because of the greater laser exposure. When heated, the higher crosslinked hydrogels swell less, similarly to structures fabricated using higher concentration of RB (Figure 4.3). Finally, it should be possible to fabricate BSA hydrogels such that their response to increased temperatures is greater than those demonstrated in Figures 4.2 or 4.3. For example, a BSA hydrogel fabricated using 3.5 mM RB with 1.00 μm optical steps would be expected to swell to a greater extent than in any test structure used to prepare either Figure 4.2 or 4. 3.

4.3.3 BSA Hydrogels and Methylene Blue

As mentioned in section 4.3.1, BSA microstructures fabricated using MB as the photosensitizer did not swell when exposed to elevated temperatures. BSA hydrogels fabricated with MB appear dark blue in color when observed under a microscope, indicating that MB is retained within the microstructure even after rinsing with a large volume (20 mL) of HEPES buffer (pH 7.4) following by an incubation of 2.5 mL of

HEPES buffer for > 24 hr. Initially, numerous unsuccessful steps were taken to chemically remove MB from the BSA microstructures. These include (1) a cycled exposure to large changes in pH (pH 7.4 to pH 2.0 and pH 7.4 to pH 12) to disrupt noncovalent interactions between MB and BSA. This was performed by exchanging pH 7.4 HEPES buffer with multiple volumes (2.5 mL) of either pH 2.0 or pH 12 followed by incubation for 1 h.; (2) incubation with a nonionic surfactant (1% (w/v) Triton X-100), which forms a 1:1 complex with MB [35, 36]; and (3) incubation with 2.5 mL of 400 mg mL^{-1} BSA solution in an attempt to competitively remove MB from the fabricated protein matrix.

To further investigate this thermal response, BSA microstructures were fabricated using RB (5.5 mM) as the photosensitizer and subsequently rinsed with multiple volumes of 20 mM HEPES, 0.1 M NaCl buffer (pH 7.4) to remove the fabrication solution from the sample well. This buffer was used as both the solvent for BSA fabrication solutions and for all rinsing to maintain the solution in a physiologically relevant state. The structures were then exposed to varying concentrations of MB (1.0, 2.0, 3.5, and 4.5 mM in 20 mM HEPES, 0.1 M NaCl buffer (pH 7.4)). The structures were incubated in a MB solution for 15 min and then rinsed with multiple volumes HEPES buffer to remove residual MB. Thermal experiments were initiated at 23 °C and the microstructure response was observed at four increasingly higher temperatures, 27 → 32 → 37 → 43 °C. The results of this study are shown in Figure 4.4.
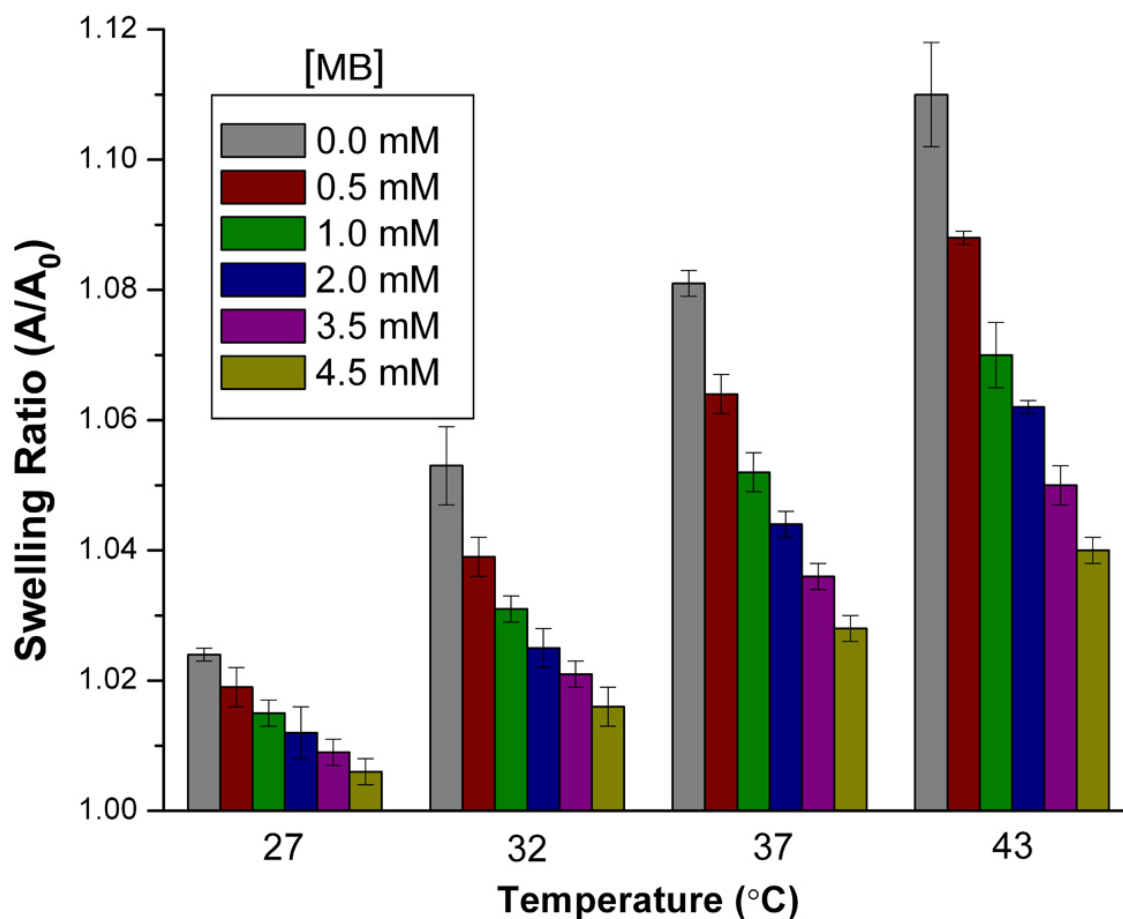
Figure 4.4:   Attenuating the thermal response of BSA hydrogels with MB. The effect of
increasing MB incubation concentration on the thermal response of BSA
hydrogels fabricated with RB. Error bars represent the standard deviation
(N=4).

The data in Figure 4.4 show that as the concentration of incubated MB was

increased, the thermally induced swelling response of the BSA hydrogels decreased. For

example, when heated to 37 ℃, a change in the swelling ratio of BSA hydrogels was

noted from 1.08 to 1.03 when incubated in 0.0 mM and 4.5 mM MB, respectively.

While the mechanism for the attenuation of the thermal response of BSA

hydrogels is unknown, it may be due to ionic interactions between MB and BSA. At pH

7.4, BSA (pI ≈ 4.7) is a negatively charged protein that interacts electrostatically with positively charged MB molecules [37]. The interaction of MB and BSA may inhibit the disruption of the interwoven constituent polymer chains of the protein matrix. Interestingly, this presents another alternate mode of tuning the thermal swelling properties of BSA hydrogels.

4.3.4 Thermal Responsive Protein Hydrogels: Avidin, Lysozyme, Ovalbumin

BSA is considered the "work-horse" of protein microfabrication for its low-cost and ease of fabrication. However, other proteins with interesting functionalities can also be photofabricated to form protein hydrogels. Therefore, test structures consisting of avidin, lysozyme, and ovalbumin were fabricated and their response to increasing temperature was investigated.

Lysozyme acts naturally to enzymatically break down polysaccharide components found in bacterial cell walls and has been shown to respond differently from BSA to stimuli such as pH and ionic strength when crosslinked as a constituent protein in a multiphoton fabricated hydrogel [28]. Test structures of lysozyme were fabricated with MB (2.5 mM) at a solution concentration of 400 mg mL^{-1} and exposed to increased temperatures similarly to BSA hydrogels shown in Figure 4.3. Lysozyme structures could only be fabricated using MB, as RB interacts with lysozyme [38] and formed insoluble precipitates [39]. Similarly to BSA, lysozyme structures fabricated using MB showed no thermal response at all examined temperatures (23 °C to 43 °C).

Ovalbumin is a globular glycoprotein that specifically binds to several lectin proteins (e.g., concanavalin A [40]) and can be fabricated using multiphoton excitation to

90

form solid hydrogels using either RB or MB as photosensitizers. Combining MPL with ligand binding could enable the creation of high-resolution 3D "smart" microsensors, such as lectin-binding ovalbumin protein hydrogels. Test structures were fabricated using both MB and RB as photosensitizers and subsequently exposed to increased temperatures (23 °C to 43 °C). Similar to lysozyme, no thermal response was observed at all temperatures examined. Attempts to create thermally responsive hybrid protein hydrogels of BSA and ovalbumin (1:1 w/v) fabricated with RB as the photosensitizer were unsuccessful, as no thermal response was noted from these materials at elevated temperatures (up or 43 °C).

Avidin is a well-characterized protein the Shear group has previously photocrosslinked in hydrogels. In earlier work, Kaehr and Shear showed that avidin retains specific biotin-binding capacity and undergoes volume changes in response to changes in pH and ionic strength [28]. To probe the thermal response of avidin hydrogels, multiple sets of avidin test structures were fabricated from a solution of 400 mg mL^{-1} avidin with 2.5 mM MB or 5.5 mM RB and were subsequently incubated overnight in either buffer or 5 μM biotin-TMR (TMR was used to confirm biotin binding by increased red-channel fluorescence). The thermal experiments were initiated at 23 °C and hydrogel response was observed at four increasingly higher temperatures, $27 \rightarrow 32 \rightarrow 37 \rightarrow 43$ °C, with the results of these experiments shown in Figure 4.5.
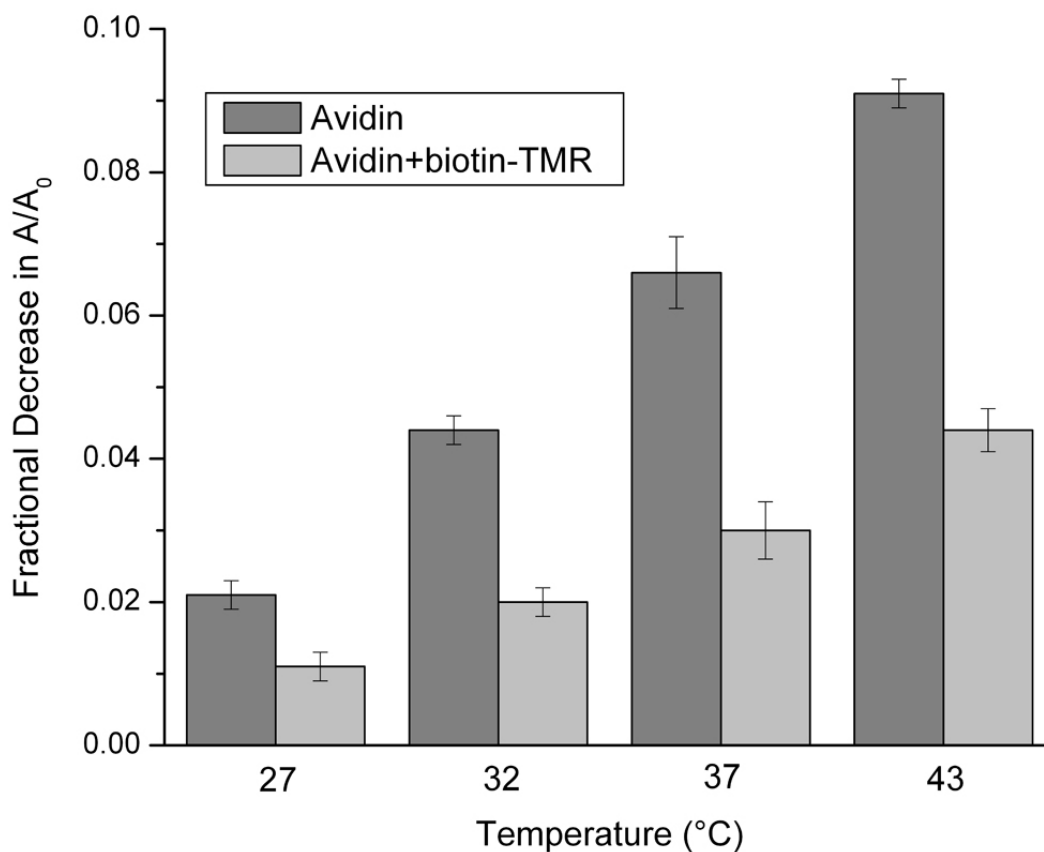
Figure 4.5: Thermal response of avidin and avidin+biotin-TMR hydrogels. The y-axis represents the fractional decrease in the swelling ratio (A/A_0). Error bars represent the standard deviation (N=4).

Surprisingly, in contrast to hydrogels fabricated from BSA, avidin hydrogels demonstrate a volume contraction at elevated temperatures, with a fractional decrease in the swelling ratio of ~ 0.07 at 37 °C. When in a TMR-biotin-bound state, the thermal response (volume contraction) of avidin is attenuated by ~ 50% at each temperature. For example, hydrogel contractions of ~ 7 % and ~ 3% are seen at 37°C for avidin and avidin+biotin-TMR, respectively. Similar structures were created using RB and no thermal response was noted from avidin or TMR-biotin-avidin.

92

The thermally induced contraction of the avidin hydrogels cannot be due to thermal denaturation of avidin over the temperatures examined (up to 43 °C), as avidin is known to thermally denature at 84 °C [41]. In addition, when biotin is bound to avidin, the denaturation temperature increases to 117 °C [41]. In contrast to BSA hydrogels, the thermal response of avidin hydrogels may be due to a collapse of the interconnected polymer chains as the temperature is increased, which would cause a decrease in the amount of water present in the matrix resulting in a contracted state. This process may be interrupted when biotin is bound to avidin, which resulted in less contraction with increased temperature. Kaehr and Shear demonstrated the swelling attenuation of multiphoton fabricated avidin hydrogels that were bound to biotin when exposed to a low pH solution [28]. When in the bound state (avidin+biotin-TMR), avidin hydrogels were found to respond to a pH change from pH 7.4 to pH 2 by swelling ~ 20% less compared to unbound avidin hydrogels [28].

Tuning the thermal response of avidin hydrogels by altering photofabrication parameters such as optical axis step size or photosensitizer concentration proved to be challenging due to the difficulty in fabricating high-integrity microstructures at conditions different from those used to create the test structures for Figure 4.5, which were 400 mg mL^{-1} avidin with 2.5 mM MB using 0.25-μm incremental optical steps. To examine other means of tuning the thermal response of avidin-based hydrogels, protein mixtures containing different mass percent amounts of avidin and BSA (% avidin; 50%, 67%, 75%, and 100%) were prepared and photofabricated using 2.5 mM MB as the photosensitizer. The structures were thermally probed at four increasingly higher

temperatures, 27 → 32 → 37 → 43 °C, and the results of this experiment are shown in Figure 4.6. When avidin is photofabricated in the presence of increasing amounts of BSA, the volumetric contraction of the avidin:BSA hydrogels in response to increasing temperatures is attenuated as a function of BSA concentration. This attenuation further demonstrates the utility of these materials to be able to precisely tune the volume change of 3D microtopographical features. Also, due to the high cost of avidin, "cutting" the avidin fabrication solution with BSA provides a means to reduce the overall cost of producing these materials.
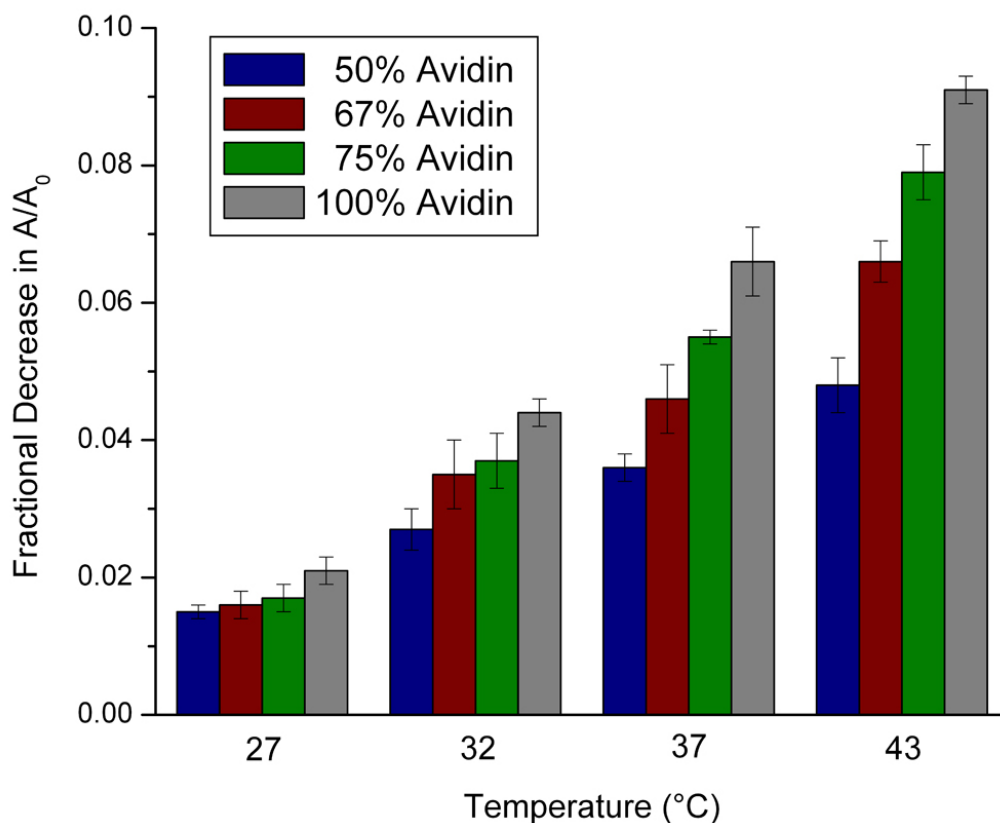
Figure 4.6: Tuning the thermal response of avidin hydrogels. A total protein concentration of 400 mg mL^{-1} was used for all experiments. BSA was used to reduce the percent avidin composition. The y-axis represents the fractional decrease in the swelling ratio (A/A$_0$). Error bars represent the standard deviation (N=4).

Avidin hydrogels were successfully fabricated using RB as the photosensitizer, however, the structures did not respond to increasing temperatures. The results shown here are reproducible and present an interesting mode of tunable actuation for high-resolution 3D "smart" materials that respond oppositely from those created from BSA.

4.3.5 Chemical and Thermal Response of BSA Hydrogels

To further characterize the responsive properties of BSA hydrogels, experiments were performed that examined the stimuli effects of both thermal and chemical changes acting independently and concurrently. Specifically, changes in ionic strength (Na$_2$SO$_4$)

and pH (high (pH 12) and low (pH 2)) were investigated in conjunction with thermal changes.

As demonstrated by Kaehr and Shear, multiphoton fabricated BSA hydrogels in a pH-induced (pH 2.2 or pH 11.9) swollen state underwent a volume contraction when exposed to non-chaotropic salts (salts that do not act directly on the protein and do not disrupt its native confirmation) such as NaCl, Na_2SO_4, and Na_2PO_4, with the greatest response noted for Na_2SO_4 [28]. This volume contraction was consistent with the "salting out" effect commonly used for protein purification purposes that results in the precipitation of the protein from solution [42].

The effect of a non-chaotropic salt (Na_2SO_4) on the thermal response of RB-fabricated (5.5 mM) BSA hydrogels was investigated and the results of this study are shown in Figure 4.7. The motivation for this work was an attempt to reverse the irreversible swelling response of BSA hydrogels to increased temperatures by chemically inducing hydrogel contraction. In this study, BSA hydrogels were initially expanded by heating from 23 °C to 37 °C and then returned to 23 °C and subsequently exposed to increasing concentrations of Na_2SO_4 (0.01 to 0.10 to 1.00 M) in pH 7.4 HEPES buffer for 15 min at each concentration (Figure 4.7a). With the addition of increasingly concentrated Na_2SO_4 solutions, the hydrogels contracted to a size less than their original size observed at 23 °C ($A/A_0 \approx 0.83$ at 1.00 M). With the exchange of 1 M Na_2SO_4 for HEPES buffer, the hydrogels returned to a size equivalent to that observed when initially heated to 37 °C, demonstrating a reversibility in the chemical effects while maintaining the thermally swollen state, indicating that the proteins could be "salted out" while in the

polymer matrix. Additionally, the entanglement of the polymer chains was irreversibly altered by increased temperatures and could not be returned to its pre-heated state. The structures were then heated to 37 °C and further thermal expansion was not observed. The structures maintained their size when returned to 23 °C and were subsequently contracted when again exposed to 1 M Na_2SO_4. When finally heated to 37 °C in the presence 1 M Na_2SO_4, a volume change was not observed.

Next, BSA hydrogels were pre-treated in 1 M Na_2SO_4 (in pH 7.4 HEPES buffer) for 15 min, which induced a volume contraction resulting in a swelling ration of ~ 0.83 (Figure 4.7b). The 1 M Na_2SO_4 solution was then exchanged for HEPES buffer and the hydrogels returned to their original size. When heated to 37 °C, the hydrogels expanded to a swelling ratio of ~ 1.08 – a value consistent with previous experiments without exposure to high salt concentrations (Figures 4.2 and 4.3), indicating that 1 M Na_2SO_4 does not irreversibly disrupt the protein conformation, as expected due its non-chaotropic nature.
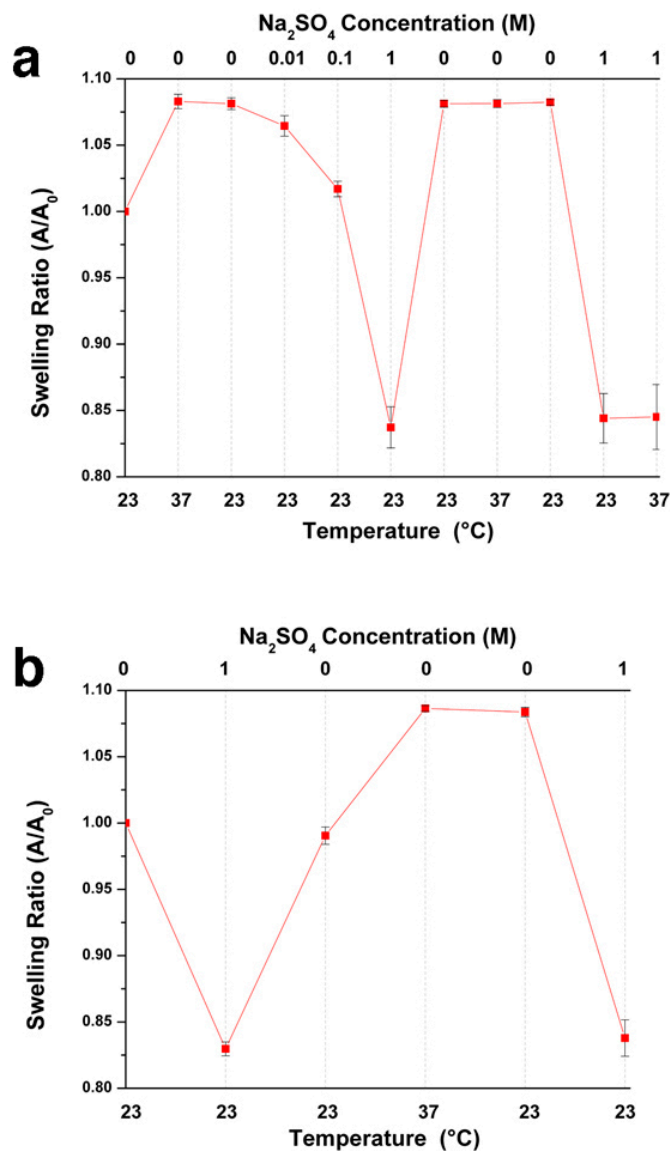
Figure 4.7: BSA hydrogel response to changes in temperature and ionic strength. (a) BSA microstructures were first heated to 37 °C then treated with increasing amounts of Na_2SO_4 (up to 1 M). The Na_2SO_4/HEPES solution was exchanged for HEPES buffer and the temperature was cycled once between 23 °C and 37 °C. Finally, the structures were bathed in 1 M Na_2SO_4 and heated again to 37 °C (b) BSA microstructures were first bathed in 1 M Na_2SO_4, which was then replaced with HEPES buffer and the structures were exposed to a 37 °C solution. After cooling back to 23 °C, the structures were again incubated in 1 M Na_2SO_4. Error bars represent the standard deviation (N=4).

The response of BSA hydrogels exposed to large changes in pH (pH 7.4 to pH 2 and pH 7.4 to pH 12) and elevated temperatures was investigated and is shown in Figure 4.8. When exposed 20 mM phosphate buffer prepared to either pH 12 or pH 2 for 15 min, BSA hydrogels expanded considerably, with swelling ratios of ~ 1.92 and 1.55 observed for each for pH, respectively. The trend observed in these results were consistent with work demonstrated by Kaehr and Shear in which BSA hydrogels expanded to a greater extent at pH 12 compared to pH 2 [28]. When returned to pH 7.4 (HEPES), the hydrogels bathed in pH 12 contracted to a swelling ratio of ~ 1.14 and were unresponsive when the temperature was subsequently increased to 37 °C (Figure 4.8, *inset*). The BSA hydrogels exposed to pH 2 contracted to ~ 1.02 when returned to pH 7.4 and expanded to ~ 1.05 when heated to 37 °C, a value ~ 30% less than would be observed without low pH treatment (Figure 4.8, *inset)*. BSA is known to expand in both acidic (below pH 3.5) and alkaline (above pH 10.5) conditions [43]. Interestingly, this process is reversible at both pH 12 and pH 2 [44]. The altered thermal response of BSA hydrogels exposed to large changes in pH may be due to irrervible changes in the polymer entanglement as a result of protein denaturation that render the hydrogel either less responsive or completely irresponsive to increases in temperature over the range examined.
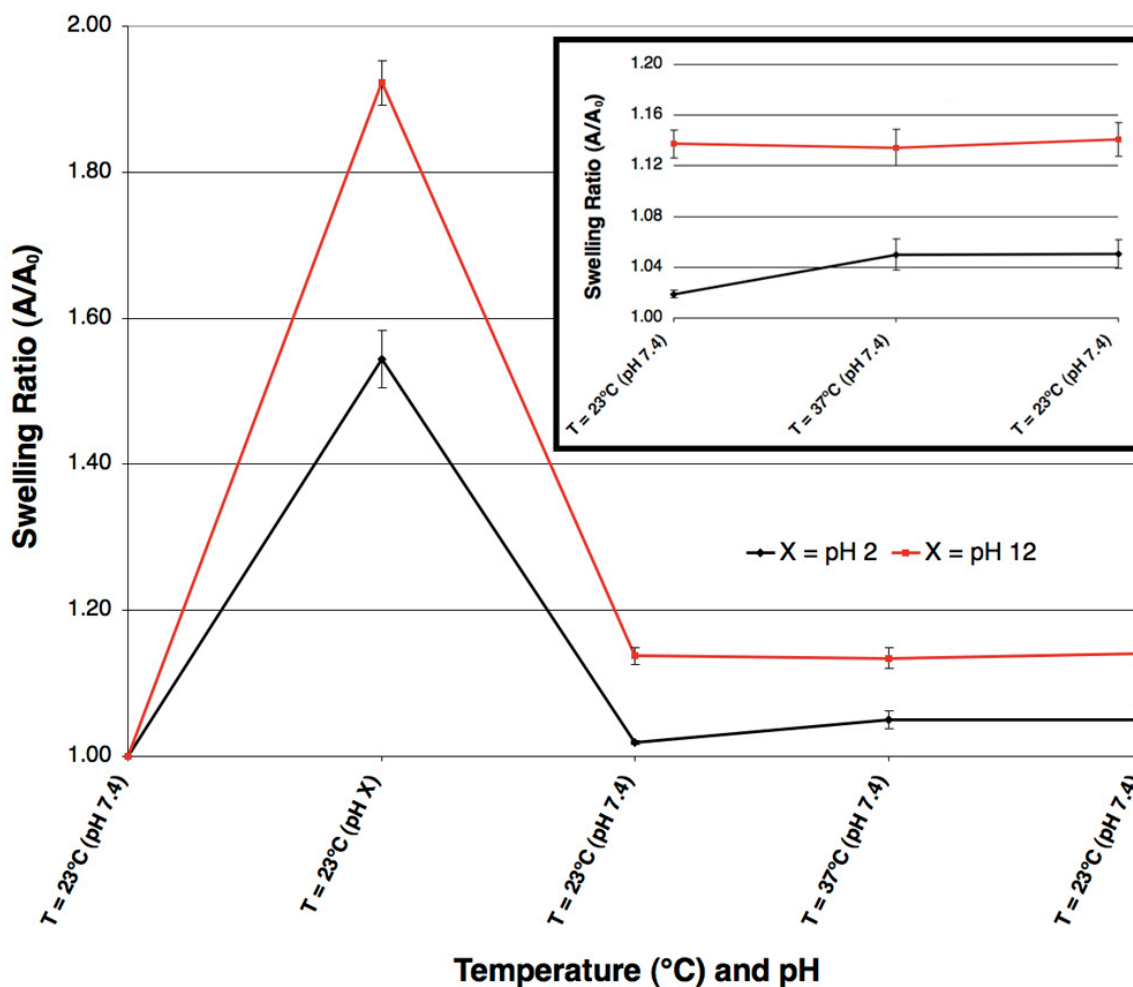
Figure 4.8: Thermal response of BSA hydrogels after exposure to pH 2 and pH 12 (20 mM phosphate). Microstructures were cycled between pH 7.4 and either high pH (12) or low pH (12) then heated to 37 °C and finally cooled to 23 °C. *Inset*: zoomed-in view of the temperature cycling. Error bars represent the standard deviation (N=4).

4.3.6 Interfacing Thermally Responsive Protein Hydrogels with Motile Cells for Bacterial Trap and Release

Bacteria are social organisms that display behaviors such as biofilm formation [45] and specific motility [46] when initiated by a cell-to-cell signaling

pathway called quorum sensing [47]. Quorum sensing is a process in which small signaling molecules are produced and sensed by the bacteria, resulting in the regulation of gene expression and the control of the group behavior [47]. Understanding the mechanism of this process for small populations of cells has been an area of great interest to microbiologists [47-50], yet the methods used to study small numbers of cells are often in environments where normal cell growth and metabolism are impeded [47, 49, 51].

Multiphoton fabricated protein microstructures have demonstrated significant utility for the study of small populations of microorganisms due to attributes such as a porous crosslinked matrix that allows for the movement of waste and nutrients in and out of the structure [26, 27, 29, 52], highly definable 3D features capable of corralling motile cells [26, 29, 52], and environmental responsivity [28]. Therefore, the application of tunable, thermally responsive multiphoton fabricated protein hydrogels could present interesting utility for the capture and release of motile microorganisms for cell culture studies for understanding the behaviors of small populations of cells.

Figure 4.9 shows a BSA microstructure in which different regions of a bacterial trap were created using varied fabrication parameters that allowed for the differential closure of external and internal apertures based on temperature, where the internal aperture separated two subsections within the structure. Specifically, the distance between fabrication layers was altered such that one section thermally responded to a greater extent at lower temperatures, as described in Figure 4.3. The external square-shaped section was fabricated using 0.50-μm incremental steps between fabrication layers while the two oval-shaped inner sections were fabricated using 0.30-μm

incremental steps. Finally, a BSA roof was fabricated to prevent cells from entering or exiting from the top.
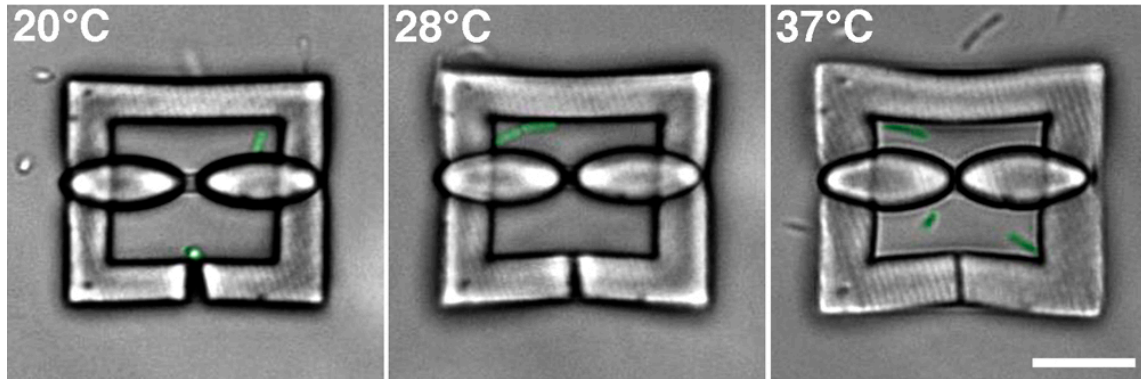
Figure 4.9: Thermally responsive cell enclosure. The exterior square section and the oval-shaped sections were fabricated using 0.50 μm and 0.30 μm incremental steps, respectively. At 20 ℃, both apertures were open, which allowed motile *P. aeruginosa* in the surrounding media to freely swim between the two subsections within the structure. The temperature was raised to 28 ℃, which caused the exterior section (square) to swell resulting in the closure of the exterior aperture that trapped a single cell. The cell was observed dividing at 28 ℃ in the top section. At 37 ℃, the interior aperture (ovals) closed creating two isolated microcavities. The cells are false-colored green for visualization. Scale bar, 10 μm.

At 20 ℃, both apertures were open, which allowed the motile bacteria (*P. aeruginosa*) in the surrounding growth medium to freely enter the structure and move throughout both subsections. Once a bacterium entered the trap, the temperature was raised to 28℃, which caused the exterior aperture to swell closed, resulting in the capture of a single cell that could continue to move throughout both subsections. The cell then divided, as seen by the formation of a septum that is present prior to the cell splitting into two daughter cells (Figure 4.9, 28℃). The temperature was raised to 37℃, which caused the closure of the inner aperture (ovals) resulting in the creation of two isolated

subsections within the microtrap. This demonstration could be used to isolate two clonal populations of cells to study their behavior. Researchers have proposed that cell population and/or density affect bacterial quorum sensing [45-47]. Using the approach described in Figure 4.9, the cell density and population was rapidly changed through the closure of the intra-structure aperture at 37°C. This technology may prove useful for the study of bacterial quorum sensing by tuning the swelling properties of the BSA hydrogels to respond at specific temperature and time points that corresponds to a cell population or density.

Similarly, Figure 4.10 shows a hybrid structure that was created using both BSA and avidin matrices to trap and release motile bacteria. Specifically, the oval-shaped sections at the top of the image were fabricated from 400 mg mL^{-1} avidin with 2.5 mM MB and the L-shaped sides and bottom were fabricated from 400 mg mL^{-1} BSA with 5.5 mM RB. Both sections were fabricated using 0.50 μm steps between photofabrication layers. Because MB rinsing attenuated the thermal response of BSA hydrogels (Figure 4.4), the avidin section was fabricated first, followed by copious rinsing with HEPES buffer. Finally the BSA sections were fabricated, followed by the creation of a BSA roof that covered both the avidin and BSA sections. At 20 °C, the BSA aperture (L-shaped structure) was open and the avidin aperture (ovals) was closed, which allowed a bacterium (*P. aeruginosa*) to enter the structure as shown at the bottom of the image (Figure 4.10, 20°C). The temperature was then increased to 28 °C, which caused the BSA aperture to close, resulting in the capture of a single bacterium. The cell was observed dividing, as can be seen by the formation of a septum between daughter cells (Figure

4.10, 28 ℃), which resulted in the doubling of the cell density. The temperature was raised to 37℃ causing the avidin aperture to open as the oval-shaped avidin microstructures contracted. This opening initially allowed one cell to escape into the surrounding media (Figure 4.10 at 37 ℃), demonstrating a reduction in the cell density and the cell population by half. This could be used to probe bacterial group behavior by initiating a rapid reduction in both the cell population and density, which may influence quorum sensing, as previously discussed.
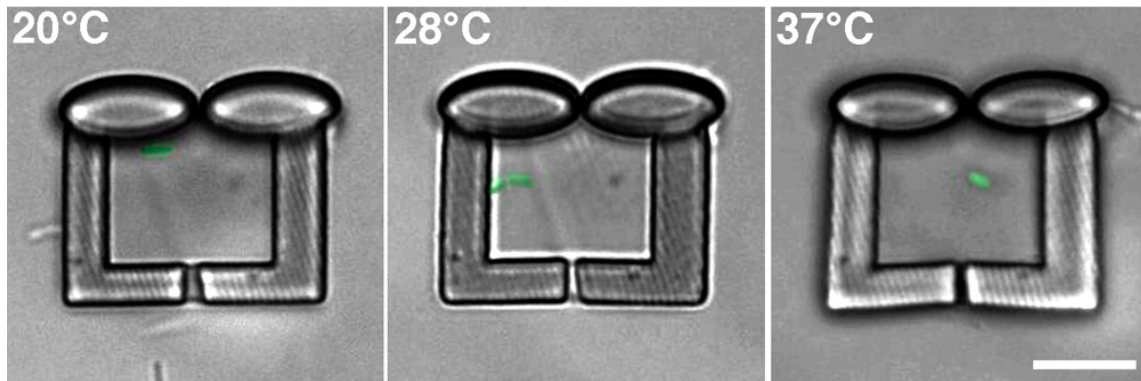
Figure 4.10: Hybrid BSA and avidin microstructure for trapping and releasing *P. aeruginosa*. The oval-shaped structures at the top were composed of avidin and the L-shaped walls were composed of BSA. At 20 ℃, the avidin aperture is closed and the BSA aperture is open, which permitted the cells to enter the structure through only the BSA section (L-shaped). The temperature was raised to 28 ℃, which resulted in the closure of the BSA aperture and the capture of a single cell, which then divided to create two daughter cells. The temperature was then raised to 37 ℃, which caused the avidin section to contract and opened the cavity to the surrounding medium. One cell was observed to rapidly exit the structure through the avidin aperture. The cells are false-colored green for visualization. Scale bar, 10 μm.

4.4 CONCLUSION

This chapter described the development and characterization of thermally responsive, tunable multiphoton-fabricated protein hydrogels. Hydrogels fabricated from BSA and RB were found to swell when exposed to elevated temperatures. While the mechanism for this behavior was not fully understood, it may be due to reduction in the entanglement of the polymer chains that make up the protein matrix. By altering the photofabrication parameters to influence the crosslinking density, the thermal response of BSA hydrogels could be tuned to a wide range of swelling ratios. Avidin hydrogels were created and found to undergo a volume contraction when exposed to elevated temperatures. The chemical influences of pH and ionic strength on the thermal response of BSA hydrogels were examined. Furthermore, novel strategies for interacting with small populations of microorganisms were demonstrated by thermally trapping and releasing cells "on command" without the need for harsh chemicals to initiate aperture opening (hydrogel contraction). Using this technology, single cells can be captured and grown to clonal populations by increasing the temperature to a value favorable for cell growth. The protein microstructure geometries could be altered such that phenotypic differences, such as motility, within a cell population could be distinguished and studied using these materials.

4.5 REFERENCES

1.   Beebe, D.J., Moore, J.S., Bauer, J.M., Yu, Q., Liu, R.H., Devadoss, C. and Jo, B.-H., *Functional hydrogel structures for autonomous flow control inside microfluidic channels*. Nature, 2000. **404**: p. 588-590.

2.   Tokarev, I. and Minko, S., *Multiresponsive, hierarchically structured membranes: new, challenging, biomimetic materials for biosensors, controlled release, biochemical gates, and nanoreactors*. Advanced Materials, 2009. **21**: p. 241-247.

3.   Park, K., *Environment-sensitive hydrogels for drug delivery*. Advanced Drug Delivery Reviews, 2001. **53**: p. 321-339.

4.   Hoffman, A.S., *Hydrogels for biomedical applications*. Advanced Drug Delivery Reviews, 2002. **43**: p. 3-12.

5.   Cushing, M. and Anseth, K., *Hydrogel cell cultures*. Science, 2007. **316**: p. 1133-1134.

6.   Dong, L., Agarwal, A., Beebe, D. and Jiang, H., *Adaptive liquid microlenses activated by stimuli-responsive hydrogels*. Nature, 2006. **442**: p. 551-554.

7.   Kiyonaka, S., Sugiyasu, K., Shinkai, S. and Hamachi, I., *First thermally responsive supramolecular polymer based on glycosylated amino acid*. J. Am. Chem. Soc., 2002. **124**: p. 10954-10955.

8.   Zhao, B. and Moore, J., *Fast pH-and ionic strength-responsive hydrogels in microchannels*. Langmuir, 2001. **17**: p. 4758-4763.

9.   Li, M., Keller, P., Li, B., Wang, X. and Brunet, M., *Light-driven side-on nematic elastomer actuators*. Advanced Materials, 2003. **15**: p. 569-572.

10.   Sidorenko, A., Krupenkin, T., Taylor, A., Fratzl, P. and Aizenberg, J., *Reversible switching of hydrogel-actuated nanostructures into complex micropatterns*. Science, 2007. **315**: p. 487 - 490.

11.   Liu, Z. and Calvert, P., *Multilayer hydrogels as muscle-like actuators*. Advanced Materials, 2000. **12**(4): p. 288-291.

12.   Leach, J., Bivens, K., Patrick, C. and Schmidt, C.E., *Photocrosslinked hyaluronic acid hydrogels: natural, biodegradable tissue engineering scaffolds*. Biotechnology and Bioengineering, 2003. **82**: p. 578-589.

13.   Knoblauch, M., Noll, G., Müller, T., Prüfer, D., Schneider-Huther, I., Scharner, D., Van Bel, A.J.E., and Peters, W.S., *ATP-independent contractile proteins from plants*. Nature Materials, 2003. **2**: p. 600-603.

14.   Gil, E. and Hudson, S., *Stimuli-reponsive polymers and their bioconjugates*. Progress in Polymer Science, 2004. **29**: p. 1173-1222.

15. Schild, H.G., *Poly (N-Isopropylacrylamide) - Experiment, Theory and Application*. Progress in Polymer Science, 1992. **17**: p. 163-249.

16. Huang, X. and Lowe, T.L., *Biodegradable thermoresponsive hydrogels for aqueous encapsulation and controlled release of hydrophilic model drugs*. Biomacromolecules, 2005. **6**: p. 2131-2139.

17. Harmon, M., Tang, M. and Frank, C., *A microfluidic actuator based on thermoresponsive hydrogels*. Polymer, 2003. **44**: p. 4547-4556.

18. Dong, L., Agarwal, A.K., Beebe, D.J. and Jiang, H., *Variable-focus liquid microlenses and microlens arrays actuated by thermoresponsive hydrogels*. Advanced Materials, 2007. **19**: p. 401-405.

19. Kang, J.-H., Moon, J.H., Lee, S.-K., Park, S.-G., Jang, S.G., Yang, S. and Yang, S.-M., *Thermoresponsive hydrogel photonic crystals by three-dimensional holographic lithography*. Advanced Materials, 2008. **20**(16): p. 3061-3065.

20. Sidorenko, A., Krupenkinb, T. and Aizenberg, J., *Controlled switching of the wetting behavior of biomimetic surfaces with hydrogel-supported nanostructures*. Journal of Materials Chemistry, 2008. **18**: p. 3841-3846.

21. Tirumala, V., Divan, R., Ocola, L. and Mancini, D.C., *Direct-write e-beam patterning of stimuli-responsive hydrogel nanostructures*. Journal of Vacuum Technology, 2005. **23**: p. 3124-3128.

22. Watanabe, T., Akiyama, M., Totani, K., Kuebler, S.M., Stellacci, F., Wenseleers, W., Braun, K., Marder, S.R., and Perry, J.W., *Photoresponsive hydrogel microstructure fabricated by two-photon initiated polymerization*. Advanced Functional Materials, 2002. **12**(9): p. 611-614.

23. Allen, R., Nielson, R., Wise, D. and Shear, J., *Catalytic three-dimensional protein architectures*. Analytical Chemistry, 2005. **77**: p. 5089-5095.

24. Hill, R. and Shear, J., *Enzyme−nanoparticle functionalization of three-dimensional protein scaffolds*. Analytical Chemistry, 2006. **19**: p. 7022-7026.

25. Kaehr, B., Allen, R., Javier, D., Currie, J. and Shear, J., *Guiding neuronal development with in situ microfabrication*. Proceedings of the National Academy of Sciences, 2004. **101**: p. 16104-16108.

26. Kaehr, B. and Shear, J., *Mask-directed multiphoton lithography*. Journal of the American Chemical Society, 2007. **129**: p. 1904-1905.

27. Kaehr, B. and Shear, J., *High-throughput design of microfluidics based on directed bacterial motility*. Lab Chip, 2009. **9**: p. 2632-2637.

28. Kaehr, B. and Shear, J.B., *Multiphoton fabrication of chemically responsive protein hydrogels for microactuation*. Proceedings of the National Academy of Sciences, 2008. **105**: p. 8850-8854.

29.   Nielson, R., Kaehr, B. and Shear, J., *Microreplication and design of biological architectures using dynamic-mask multiphoton lithography*. Small, 2009. **5**: p. 120-125.

30.   Basu, S., Wolgemuth, C. and Campagnola, P., *Measurement of normal and anomalous diffusion of dyes within protein structures fabricated via multiphoton excited cross-linking*. Biomacromolecules, 2004. **5**: p. 2347-2357.

31.   Bischof, J.C. and He, X., *Thermal stability of proteins*. Annals New York Academy of Sciences, 2006. **1066**: p. 12-33.

32.   Takeda, K., Wada, A., Yamamoto, K., Moriyama, Y. and Aoki, K., *Conformational change of bovine serum albumin by heat treatment*. Journal of Protein Chemistry, 1989. **8**(5): p. 653-659.

33.   Kosa, T., Maruyama, T. and Otagiri, M., *Species differences of serum albumins: II. chemical and thermal stability*. Pharmaceutical Research, 1998. **15**(3): p. 449-454.

34.   Sun, H., Tanaka, T. and Kawata, S., *Three-dimensional focal spots related to two-photon excitation*. Appl. Phys. Lett., 2002. **80**: p. 3673-3675.

35.   Bhowmik, B.B. and Mukhopadhyay, M., *Spectral and photophysical studies of thiazine dyes in Triton X-100*. Colloid & Polymer Science, 1988. **266**: p. 672-676.

36.   Pramanick, D. and Mukherjee, D., *Molecular interaction of methylene blue with Triton X-100 in reverse micellar media*. Journal of Colloid and Interface Science, 1993. **157**: p. 131-134.

37.   Hu, Y., Liu, Y., Zhao, R., Dong, J. and Qu, S., *Spectroscopic studies on the interaction between methylene blue and bovine serum albumin*. Journal of Photochemistry and Photobiology A: Chemistry, 2006. **179**: p. 324-329.

38.   Zhang, Y. and Gorner, H., *Photoprocesses of xanthene dyes bound to lysozyme or serum albumin*. Photochemistry and Photobiology, 2009. **85**: p. 677-685.

39.   Tseng, S.C.G. and Zhang, S.H., *Interaction between rose bengal and different protein components*. Cornea, 1995. **14**(4): p. 427-435.

40.   Pilobello, K., Krishnamoorthy, L., Slawek, D. and Mahal, L.K., *Development of a lectin microarray for the rapid analysis of protein glycopatterns*. ChemBioChem, 2005. **6**: p. 985-989.

41.   González, M., Argarana, C. and Fidelio, G., *Extremely high thermal stability of streptavidin and avidin upon biotin binding*. Biomolecular engineering, 1999. **16**: p. 67-72.

42.   Arakawa, T. and Timasheff, S., *Mechanism of protein salting in and salting out by divalent cation salts: balance between hydration and salt binding*. Biochemistry, 1984. **23**: p. 5912-5923.

43.   Yamasaki, M. and Yano, H., *Differential scanning calorimetric studies on bovine serum albumin: I. Effects of pH and ionic strength*. International Journal of Biological Macromolecules, 1990. **12**: p. 263-268.

44.   Peters, T., *Serum albumin*. Advances in Protein Chemistry, 1985. **37**: p. 161-245.

45.   Parsek, M. and Greenberg, E., *Sociomicrobiology: the connections between quorum sensing and biofilms*. Trends in Microbiology, 2005. **13**: p. 27-33.

46.   Redfield, R.J., *Is quorum sensing a side effect of diffusion sensing?* Trends in Microbiology, 2002. **10**: p. 365-370.

47.   Carnes, E.C., Lopez, D.M., Donegan, N.P., Cheung, A., Gresham, H., Timmins, G.S. and Brinker, C.J., *Confinement-induced quorum sensing of individual Staphylococcus aureus bacteria*. Nature Chemical Biology, 2018. **6**(1): p. 41-45.

48.   Horswill, A.R., Stoodley, P., Stewart, P.S. and Parsek, M.R., *The effect of the chemical, biological, and physical environment on quorum sensing in structured microbial communities*. Analytical Bioanalytical Chemistry, 2007. **387**: p. 371-380.

49.   Boedicker, J.Q., Vincent, M.E. and Ismagilov, R.F., *Microfluidic confinement of single cells of bacteria in small volumes initiates high-density behavior of quorum sensing and growth and reveals Its variability*. Angew. Chem. Int. Ed., 2009. **121**(32): p. 6022-6025.

50.   Hense, B.A., Kuttler, C., Muller, J., Rothballer, M., Hartmann, A. and Kreft, J.-U., *Does efficiency sensing unify diffusion and quorum sensing*. Nature Reviews Microbiology, 2007. **5**: p. 230-239.

51.   Baca, H.K., Ashley, C., Carnes, E., Lopez, D., Flemming, J., Dunphy, D., Singh, S., Chen, Z., Nanguo, L., Fan, H., Lopez, G.P., Brozik, S.M., Werner-Washburne, M., and Brinker, C.J., *Cell-directed assembly of lipid-silica*. Science, 2006. **313**: p. 337-341.

52.   Khripin, C.Y., Brinker, C.J. and Kaehr, B., *Mechanically tunable multiphoton fabricated protein hydrogels investigated using atomic force microscopy*. Soft Matter, 2010. **6**(12): p. 2842-2848.

Chapter 5: Multifocal Multiphoton Lithography

5.1 INTRODUCTION

As discussed in previous chapters, multiphoton lithography (MPL) is a true three-dimensional (3D) lithographic technique in which photocrosslinking or polymerization occurs within a femtoliter-sized fabrication voxel that is formed by tightly focusing a high peak power laser into a reagent solution with high numerical aperture (NA) optics. While the 3D fabrication capabilities of MPL are appealing for many applications such as micromachines [1, 2] and cell culture [3, 4], a major drawback MPL is that it is an inherently serial technique in which microstructures are created in a voxel-by-voxel approach. Depending on the complexity of the desired microform, this process can require minutes to hours to complete using vector-based stage movements. Alternatively, the Shear lab has developed mask-directed laser-scanning MPL technology that allows for the 3D rapid prototyping of iterative designs [5, 6]. However, using either vector-based or mask-directed scanning methods, MPL remains a serial process and creating complex 3D microforms in parallel remains challenging.

One approach for creating 3D microforms in parallel relies on a traditional soft lithographic technique, microtranser molding (μTM), in which liquid polydimethylsiloxane (PDMS) is poured over a master structure(s) that are fabricated using vector-based stage movements [7, 8]. The PDMS is then cured, resulting in the formation of a mold that can then be filled with monomer and photoinitiator and cured on a separate substrate [7, 8]. However, this approach is not truly parallel since it still relies

on the serial fabrication of the master structure(s) prior to molding. Also, structures with small openings leading to a microcavity enclosed by walls and a roof, such as those commonly used in the Shear lab for capturing small numbers of microorganisms [6, 9, 10], can be difficult to replicate using this approach depending on the complexity.

Another approach for performing MPL in parallel relies on the vector-based translation of multiple laser foci through a reagent solution to rapidly create identical microstructures over large areas [11, 12]. In this approach, the output from a regeneratively amplified titanium:sapphire (Ti:S) laser is passed through a microlens array (MLA), creating hundreds of redundant parallel laser beams separated by 5.5 μm (center-to-center) when brought to focus within a sample using a microscope objective. While this permits the parallel fabrication of hundreds of structures, the small interfocal distance between the laser spots limited the absolute size of any individual microform. In addition, due to the redundancy of each laser foci, creating structures with different topographical features or crosslinking densities in parallel would be impossible.

This chapter presents the development of a multifocal approach to MPL that overcomes these limitations. In this work, two laser beams are used in conjunction with dynamic reflectance masking to improve both the speed and versatility of this technique. The focused laser beams are aligned slightly off-axis and raster-scanned in a rectangular pattern across the mirrored-face of a digital micromirror device (DMD) placed in a plane conjugate to the microscope image plane formed by a high NA microscope objective. The binary image pattern displayed on the DMD directs the laser beams to the microscope objective, which reproduces the pattern as a two-dimensional (2D) fabrication plane with

the magnification factor of the fabricated pattern being roughly equal to the power of the microscope objective. In this proof-of-concept, the focused beams are aligned such that their interfocal distance is ~ 40 μm to perform parallel fabrication when identical masks are displayed on the DMD and scanned with each laser beam. By displaying a pattern on the DMD that is scanned by two beams across different regions simultaneously, the entire mask can be rapidly transferred. In addition, the scan areas of the individually attenuated laser beams can be overlapped to achieve multiple laser exposure zones to fabricate topographies of varying crosslinking densities.

5.2 EXPERIMENTAL

5.2.1 Reagents and Solutions

Bovine serum albumin (BSA) was obtained from Equitech-Bio (Kerrville, TX). HEPES sodium salt and rose bengal were purchased from Sigma-Aldrich (St. Louis, MO). All reagents were used as received without purification.

5.2.2 Multifocal Optical Configuration

The optical configuration for multifocal MPL is shown in Figure 5.1. The 740-nm output from mode-locked Ti:S oscillator (Coherent Mira 900F) pumped by a 532 nm 10 W frequency-doubled neodymium-vanadate laser (Coherent Verdi) was first passed through a telescoping lens set (TLS; fl = 5 cm) to establish a collimated beam. The laser beam was then sent through a half-wave plate (HWP) and polarizing beamsplitter (PBS) to create two beams. The reflected beam from the PBS was then sent through a second HWP/PBS pair, which permitted the power of each beam to be attenuated individually. Both beams are then aligned slightly off-axis (~ 2°) into a scanbox containing a two-axis,

galvanometer-driven scan mirror obtained from a dismantled confocal microscope (Leica TCS-4D, Bensheim, Germany). The mirror was controlled by software written in LabView™ (National Instruments, Austin, TX) that provides independent control of the scan frequency, amplitude, phase, and waveform. The scanning beams were passed through lenses L1 (fl = 3.2 cm) and L2 (fl = 15.2 cm), then to L3 (fl = 15.2 cm), which focused the beams onto the DMD. The interfocal distance between the laser spots on the DMD was dictated by the beam's convergence angle before the scan mirror and the lenses L1 – L3. Using the aforementioned lens system with an ~ 2° convergence angle before entering the scanbox, the focused laser spots on the DMD were separated by ~ 4 mm with axis that are parallel to each other. The laser beams are reflected down the optical path by the DMD and through a tube lens (L4, fl = 15.4 cm) for final laser beam collimation before being directed via a dichroic mirror into a Zeiss Fluar, 100X/1.3 NA microscope objective situated on a Zeiss Axiovert 135 inverted microscope. With the 100X objective, the focused beam separation in the specimen plane was ~ 40 μm. The overlap of the raster scanning beams was visually insured to be 1 μm. With a higher quality scanning system, the minimum scan overlap could be reduced to tens of nanometers. With an interfocal distance of ~ 40 μm, the total scan area of the two beams with minimal overlap (~ 1 μm) was ~ 80 μm x 50 μm. This corresponded to approximately 40% laser scan coverage of the DMD chip. A partially dismantled DLP® DMD projector (BenQ, MP510) was used for all experiments. The DMD consists of an 800 x 600 array of individually addressable 16 μm x 16 μm aluminum mirrors (17 μm

pixel pitch with a 1 μm intermirror distance), corresponding to a total chip area of 13.6 mm x 10.2 mm.
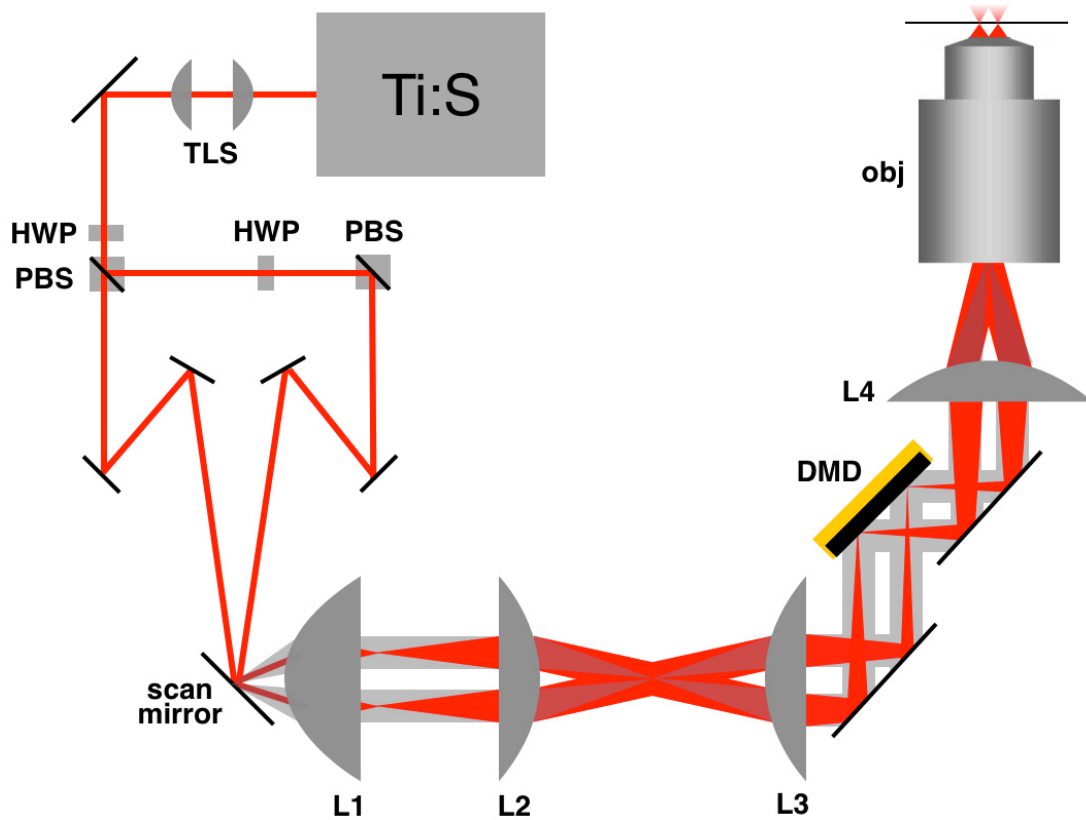
Figure 5.1. Optical configuration for Multifocal MPL. The output from a mode-locked Ti:S was passed through a 1:1 telescoping lens set (TLS) and directed to a half-wave plate (HWP) and polarizing beam splitter (PBS) to create two beams. The beam reflected by the PBS was passed through a second HWP/PBS, which permitted the power of each beam to be attenuated individually. Both beams were aligned slightly off-axis onto the galvanometer-driven scan mirror. After the scan mirror, the beam focus and scan translation are represented by the red beam and gray beam, respectively. The beams were relayed to the DMD using L1 (fl = 3.2 cm), L2 (fl = 15.2 cm), and L3 (fl = 15.2). The interfocal distance between the focused beams on the DMD was dictated by the convergence angle ($\sim$ 2°) between the beams prior to the scan mirror. The focused beams on the DMD have axis that are parallel to each other. After being reflected by the DMD, the beams were passed through L4 to collimate the beam before being directed into the back aperture of the microscope objective.

5.2.3 Microfabrication

BSA microstructures were fabricated on untreated No. 1 coverslips (Fisher Scientific). All microstructures were fabricated from a solution containing 400 mg mL^{-1} BSA and 8.5 mM rose bengal in 20 mM sodium HEPES buffer with 0.1 mM NaCl (pH 7.4) using either 0.50 μm or 0.75 μm incremental steps between fabrication layers with each horizontal fabrication plane requiring 5 s to complete. Microstructures were created by synchronizing the sequence of binary images displayed on the DMD with stage movements in the optical axis, which were controlled using a three-axis translational stage (model 562, Newport Corp., Irvine, CA) driven by motorized actuators (model LTA-HS, Newport Corp., Irvine, CA) that were controlled using a motion controller/driver (model ESP300, Newport Corp., Irvine, CA). The binary image data used for DMD patterns were prepared using Adobe Photoshop.

5.2.4 Scanning Electron Microscope Sample Preparation

BSA microstructures were fixed in 5% gluteraldehyde (v/v) for 15 min, then sequentially washed in HEPES buffer (20 mM with 0.1 M NaCl, pH 7.4), H$_2$O, 1:1 EtOH:H$_2$O, 100% EtOH, 1:1 EtOH:MeOH, and 100% MeOH (2 times), each for 15 min. Samples then were left to dry overnight in a desiccator. After fixation and drying, the samples were sputter coated with Pt/Pd to a nominal thickness of 10 nm and imaged using a Zeiss Supra 40VP scanning electron microscope.

5.2.5 Cell Culture

Pseudomonas aeruginosa PA01 wildtype was used in all cellular experiments. Planktonic cultures were grown aerobically overnight at 37°C in tryptic soy broth (TSB. Cells were diluted in TSB, grown to mid-logarithmic phase at 37°C, cooled to room temperature, and introduced to the microchambers under sterile conditions via pipette.

5.3 RESULTS AND DISCUSSION

5.3.1 Large-format structures

Creating large microforms with non-repeating features is time consuming with MPL when directed by vector-based stage movements. Mask-directed MPL allows the creation of arbitrary 3D patterns with the absolute size of the microform determined by the scan area and the magnification of the optical system. Highly defined microstructures extending over large areas can be formed by stitching the fabricated patterns with coordinated x,y stage movements that coincide with the sequential display of DMD masks. By performing mask-directed MPL with two laser beams, microforms could be fabricated, in principle, at twice the rate.

Figure 5.2(b and c) shows a scanning electron micrograph of a stitched multiphoton fabricated BSA maze created using the optical configuration shown in Figure 5.1. A binary maze pattern (Figure 5.2a) was sectioned into 12 individual masks (Figure 5.2a, solid red lines) that were individually scanned by each laser beam simultaneously with a scan overlap of ~ 1 μm (Figure 5.2a, dashed red lines). For example, Figure 5.2d shows a single BSA subsection (subsection #1). The slight angle of

116

the scan overlap seen in Figure 5.2a (dashed red lines) was due to the reflection geometry

of the DMD chip.
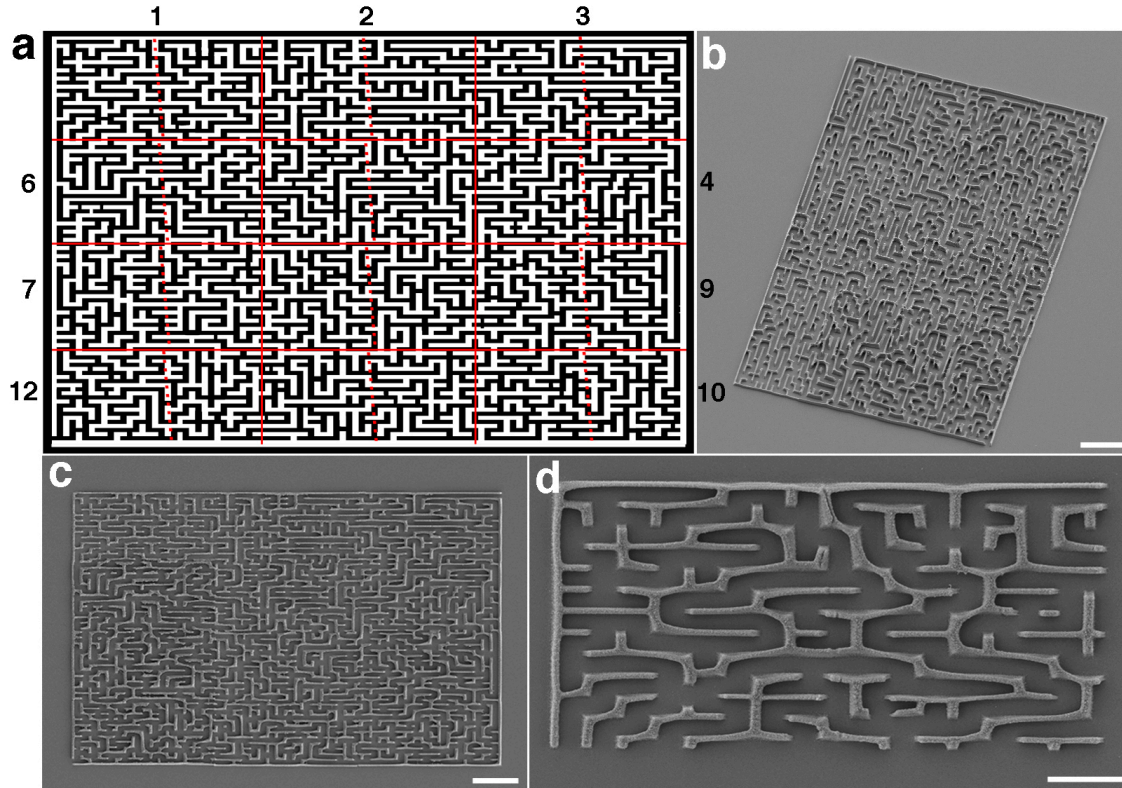
Figure 5.2: Stitched maze structure fabricated from BSA. (a) Binary maze pattern showing the 12-segmented images used for the stitched structure (solid red lines) and the order in which they were fabricated (numbers, lower left corner). The dashed red lines show the overlap zone of the two laser scans used for fabrication. (b) SEM image of the large 3-μm tall BSA maze structure. (c) Top-down SEM image of the same BSA maze in (b). (d) SEM image of subsection #1 fabricated from BSA. Total fabrication time: 4 min. Scale bars: b and c, 20 μm; d 10 μm.

The stitched BSA maze was fabricated to lateral dimensions of 210 μm x 135 μm

at a nominal height of 3 μm using four 0.75-μm incremental optical axis steps, a process

requiring 4 min. Slight imperfections can be seen in the BSA maze at the stitched joints

and were due to inaccurate positioning of the scan areas. Also, slight curvature and rounding of the corners can be seen in the SEM image (Figure 5.2 (b – d)) and were to due to the dehydration steps used in preparation for electron microscopy.

The creation of extended structures of a repeating pattern in parallel could have potential applications in numerous fields, including cell culture, microfluidics, and micro-optics. To investigate this, the multifocal approach was applied to the creation of a large structure of a repeating pattern; the results of this are shown in Figure 5.3. Here, a binary pattern of an array of repeating circles was displayed on the DMD and scanned using two laser beams with slightly overlapping raster scan areas. The final pattern was fabricated from BSA on a glass substrate using a stitching procedure to create a 245 μm x 425 μm structure from 36 individual fabricated subsections to a nominal height of 2 μm using four 0.5-μm incremental optical axis steps. With each fabrication segment in a plane requiring 5 s to complete, the total fabrication time for this procedure was 12 min.
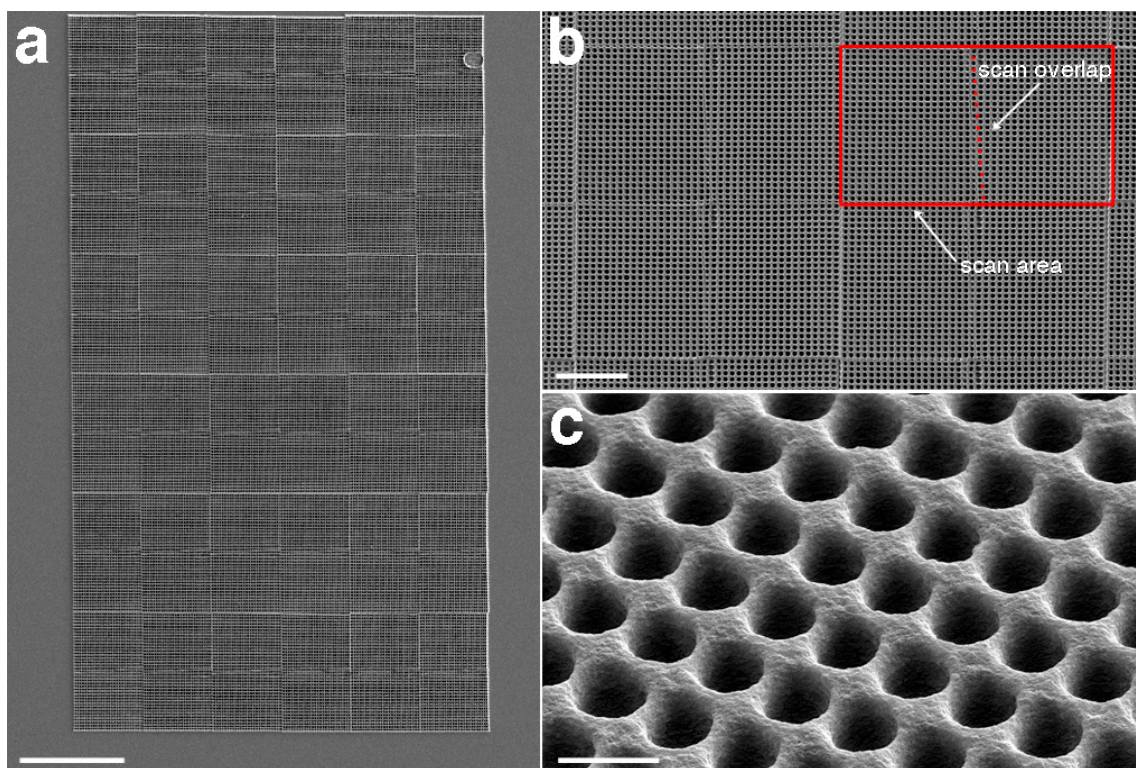
Figure 5.3: SEM images of stitched repeating pattern fabricated from BSA. (a) Top view of the large scale BSA structure of repeating microholes stitched from 36 individual fabricated subsections. (b) A view of the same structure in (a) showing four fabricated subsections. The overlaid solid red box shows the total scan area for an individual subsection and the dashed red line shows the overlap of the individual laser beam scan areas. (c) A high magnification view of the fabricated microholes. Scale bars: a, 60 μm; b, 20 μm; c, 2 μm.

The pattern of fabricated micro-holes in the stitched BSA pad was highly reproducible, with an average hole size of 1.27 μm ± 0.07 μm (average ± standard deviation). This value was obtained by averaging the measured diameter of 200 holes selected from different segments of the final stitched structure. While the total area of the final structure was truncated at 245 μm x 425 μm, it is feasible to extend the stitching of this pattern over even larger areas. Additionally, the pattern displayed on the DMD could be rapidly manipulated using photoillustrative illustrative (e.g., Adobe Photoshop) to

prototype structures of similar patterns with different sized holes and/or different inter-hole spacing.

The fabrication stitching seams in the final pattern are due to both the slightly overlapping scan areas (~ 1 μm) and inaccuracies in stage positioning. Reducing the appearance of these seams could be achieved through a combination of limiting the amount of scan overlap and using a stage with more accurate positioning capabilities. Also, a blemish is seen in the top right corner of the structure (Figure 5.3a), which was caused by laser damage to the nascent fabricated protein material as a result of an impurity in the protein solution.

5.3.2 Multifocal exposure zones

As discussed in Chapter 4, structures fabricated from BSA behave as responsive hydrogels and undergo a volume change (swelling or contracting) to stimuli such as pH, ionic strength, and temperature. Kaehr and Shear demonstrated that the crosslinking density of BSA structures could be altered to reduce or increase the swelling response to changes in pH [10]. The crosslinking density of the fabricated BSA matrix can be altered through a modification of various fabrication parameters, including laser power, laser dwell time, laser exposure, protein and photosensitizer concentration, and the incremental distance between fabrication layers.

With the multifocal optical configuration shown in Figure 5.1, each laser beam can be individually attenuated using the two HWP/PBS pairs. By increasing the amplitude of the function that defines the raster scan area, the individual laser scans can be spatially overlapped, thus creating multiple laser exposure zones (summed average

power per scan period). While overlapping scan areas could be accomplished by reducing the interfocal distance of the laser beams through mirror adjustments on the optical table, it is more straightforward to use software to control the raster scan size. Specifically, two or three exposure zones can be created using the following approaches when spatially overlapping scan areas.

By using equal laser powers for each scanning beam, two exposure zones are created in three spatially distinct areas in which the center scan area of higher exposure is sandwiched by two areas of half the exposure. To demonstrate this approach, nominally 8-μm tall BSA cylinders were created using multiple exposure zones and subsequently exposed to a pH step to induce a volume increase in the structure. The results of this study are shown in Figure 5.4. The scan areas of lasers beams of equal power (20 mW) were expanded to create an overlap zone of ~ 12 μm, thus generating three exposure zones as described above – a center zone of 40 mW (20 mW + 20mW per scan period) sandwiched by two 20 mW zones per scan period (Figure 5.4a). BSA microcylinders were fabricated and washed with buffer solution (1 mM phosphate, pH 7.4) (Figure 5.4a, top) and exposed to high pH (1 mM phosphate buffer, pH 11), which induced a swelling response (Figure 5.4a, bottom). To characterizer the swelling response, the swelling ratio was determined as the ratio of the area of the image of the structure at pH 11 to the area at pH 7.4 ($A_{(pH\ 11)}/A_{(pH\ 7.4)}$) that was determined by measuring the diameter of the structure at the top of the structure. The swelling ratios (average ± standard deviation for three structures) for the left, right, and center exposure zones were found to be $1.4_2 \pm 0.0_2$, $1.1_9 \pm 0.0_2$, and $1.4_4 \pm 0.0_3$, respectively (Figure 5.4a, bottom).

The structures fabricated within the center exposure zone were of higher crosslinking density and, as expected, their swelling response was reduced when exposed to large changes in pH.

By repeating this protocol using laser beams of different powers, three distinct exposure zones can be created (Figure 5.4b): a center zone (Figure 5.4b, top, center cylinder) of 40 mW (16 mW + 24 mW) per scan period sandwiched by a 16 mW zone (Figure 5.4b, top, left cylinder) and 24 mW zone (Figure 5.4b, top, right cylinder). In this demonstration, microcylinders were created in each scan area, rinsed with buffer solution (1 mM phosphate, pH 7.4) (Figure 5,4b, top) and exposed to high pH (1 mM phosphate buffer, pH 11) (Figure 5,4b, bottom). This high pH exposure caused the structures to swell, with swelling ratios of $1.6_2 \pm 0.0_3$, $1.1_8 \pm 0.0_1$, and $1.3_0 \pm 0.0_3$ for the center (40 mW per scan period), left (16 mW per scan period), and right (24 mW per scan period) exposure zones, respectively. As expected, the microcylinders fabricated at the lower exposure underwent the greatest volume expansion at high pH. The center exposure zone (40 mW per scan period) displayed a swelling ratio of 1.1_8, which roughly equivalent to that of the center zone of the same exposure in Figure 5.4a (bottom).

These results further demonstrate the tunable response of multiphoton fabricated BSA structures to changes in pH. When combined with multifocal scanning, this response can be spatially tuned to rapidly create, for instance, valves for microfluidic devices or biocompatible micromachines.
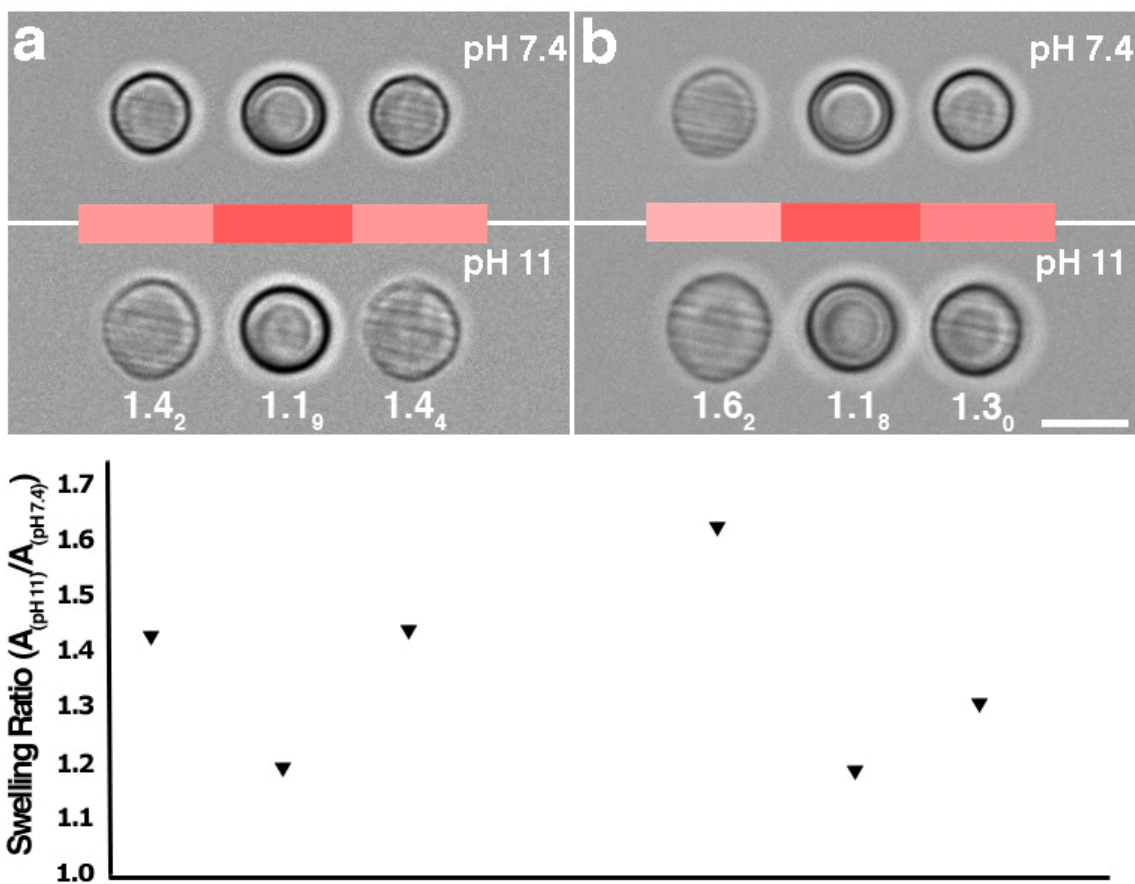
Figure 5.4: Multiple exposure zones formed by overlapping rectangular laser scan areas. (a) Three nominally 8-μm tall BSA cylinders were fabricated using two overlapping scan areas of equal power (20 mW). Top: the left and right cylinders were each fabricated with one scan area (light red) and the center cylinder was fabricated by overlapping both scan areas (dark red) and bathed in a pH 7.4 buffer. Bottom: Replacement of buffer with a pH 11 buffer induced swelling of the three BSA cylinders. (b) Top: Three nominally 8-μm tall cylinders were fabricated using three laser exposure zones: a center zone of 40 mW (16 mW + 24 mW) per scan period sandwiched by a 16 mW zone (left) and 24 mW zone (right). Here, microstructures were bathed in pH 7.4 buffer. Bottom: Replacement of the pH 7.4 buffer with a pH 11 buffer induced swelling of three BSA cylinders. The values given below the structures in the bottom images represent the swelling ratio, given by the ratio of the area of the structure at pH 11 to the area at pH 7.4 ($A_{(pH\ 11)}/A_{(pH7.4)}$). *Bottom:* Graphical representation of the swelling ratios. Scale bar, 10 μm.

5.3.3 Multifocal fabricated structures for cell culture

The Shear lab has pioneered the use of BSA microcavities created using MPL for studying small populations of microorganisms [5, 6, 9, 10] and multifocal MPL improves on this technique through the ability to create multiple structures in parallel or large structures more rapidly to study even larger populations of cells. To demonstrate the creation of structures capable of cell capture using multifocal MPL, a microcavity was fabricated using a mask that covered the areas of the slightly overlapping scanning laser beams (Figure 5.5a). This structure was created using two masks, one to define the cavity geometry and a fully reflective mask for the roof. The cavity was created using 12 0.75-μm incremental optical steps followed by a nominal 1.5-μm roof (2 optical steps) in 70 s. A visible seam was observed in the structure (Figure 5.5a, 1) due to the overlapping scan areas of ~ 1 μm. The structure was inoculated with *P. aeruginosa* at room temperature (~ 18° C) and cells were observed migrating in and out of the structure (Figure 5.5a, 1). The sample was placed in an incubator at 37° C, which caused the structure to swell as shown in Chapter 4 where BSA structures fabricated using rose bengal as the photosensitizer undergo a volume increase with increased temperature. This swelling response resulted in the closure of the entrance aperture and the capture of a small number of cells. The structure was then incubated at 37° C for 2 h, over which time the cells divided considerably (Figure 5.5a, 2). The incubation was then continued for 12 h. The cells divided and densely packed the cavity causing the roof to extend upward without breakage at the fabrication seam (Figure 5.5a, 3).
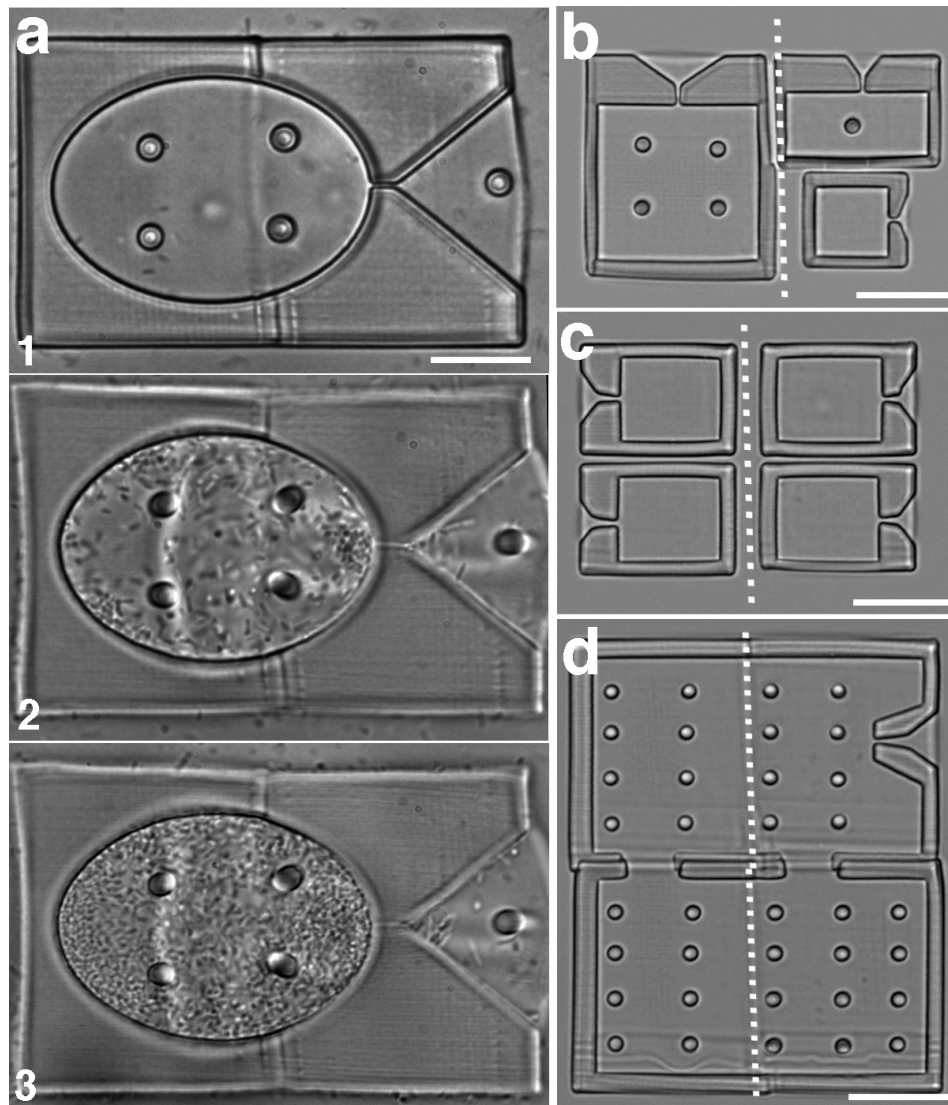
Figure 5.5:   Multifocal MPL fabricated microorganism traps. (a) Differential interference contrast (DIC) image of a cell trap fabricated using two scanning lasers with a seam visible through the center of the structure. (a-1): The structure was inoculated with *P. aeruginosa* at 18˚ C. (a-2): After incubating for 2 h at 37˚ C, the structure underwent a thermally-induced volume increase, causing the capture of a number of cells that subsequently divided. (a-3): After incubation at 37˚ C for 12 hours, the cells were densely packed causing the roof to expand upwards. (b) Three microcavity geometries of different internal volumes created simultaneously. (c) Four microcavities created in parallel. (d) A large stitched structure created from two fabricated subsections. The dashed white lines represent the placement of the overlapping scan areas. Scale bars: a-c, 15 μm; d, 30 μm.

125

Using a multifocal approach to MPL for the creation of structures for cell capture, cavity designs can be rapidly prototyped and created in parallel in several minutes. Figure 5.5b shows three microstructures of different cavity volumes created using two masks, one to define the cavity geometry and one to define the roof. The cavity was created using 12 0.75-μm incremental optical steps followed by a nominal 1.5-μm roof (2 optical steps) in 70 s. The structure of a larger volume (5.5b, left) was created with one laser scan area and the two smaller structures were created with the other laser scan area (5.5b, right). Figure 5.5c shows four identical microcavities fabricated in parallel using the same fabrication procedure for the structures in Figure 5.5b. By stitching two fabricated subsections together, a large volume microstructure was created (Figure 5.5d) using three masks to define the final structure, two to create the internal geometry, and one to create the roof. The posts in the center of the structure were needed to prevent the collapse of the roof into the cavity and also provided an optimal stitching location.

5.4 CONCLUSION

This chapter demonstrated the development of a multifocal approach to MPL that enabled the creation of arbitary microstructures in parallel and over large areas in a rapid fashion. Additionally, multiple laser beam exposure zones were generated by overlapping the raster-scan areas of each laser beam, which allowed the simultaneous creation of microstructures of varying crosslinking densities.

This proof-of-concept was presented with only two laser beams for a number of reasons. (1) The scanbox used in these experiments was obtained from a dismantled

confocal microscope. Because of this, the housing of the scan mirror prevented the alignment of laser beams with a convergence angle of more than 2˚. This ultimately limited the interfocal distance between the laser beams and thus, the total laser scan area. This limitation could be avoided by using a commercially available galvanometer-driven scan system that has unobstructed access to the scan mirrors, thereby allowing multiple beams to be aligned into the system with convergence angles of > 2˚. (2) All relay lenses used in this demonstration were 2.5 cm in diameter, which limits the total scan area due to aberrations and attenuation of the laser beam as it is translated closer to the edge of the lens. With larger diameter lenses, the total scan area could be increased, which would result in a larger scan area. (3) The Ti:S system used in this demonstration has maximum output of ~ 800 mW at 740 nm. With this system, up to three beams could potentially be aligned into the scanning system with sufficient power to promote photocrosslinking, when accounting for power losses due to optical interfaces such as polarizing optics, mirrors, the DMD chip, and the throughput of the microscope objective. With a regeneratively amplified Ti:S laser system, the number of laser beams that could be used would be drastically increased at the expense of laser repetition rate. However, as described in Chapter 3, pulsed lasers with relatively low repetition rates are capable of performing mask-directed MPL at relatively rapid scan times (1 – 5 s per fabrication plane).

To improve on this proof-of-concept, this technology could potentially be applied with the use many more laser beams. With many beams simultaneously promoting photocrosslinking, the fabrication speed for a large-scale structure would be rapidly

127

increased. In addition, with a sufficient number of parallel scanning laser beams, a near continuous power gradient could be achieved, which would permit the creation of a large-scale structure with a crosslinking density that could be continuous as well. Finally, the total area of the DMD microchip is what ultimately limits the total size of the available scan area. This demonstration used an XVGA resolution DMD chip, which has an array of 800 x 600 micromirros (pixels) with a total chip area of 13.6 mm x 10.2 mm. Higher resolution chips are available, such as the HDTV chip (1920 x 1080), which has a total mirrored area of 32.6 mm x 18.4 mm [13]. With an approximate 4-fold increase in total available scan area, by combining more scanning laser beams with this higher resolution HDTV DMD chip, a significant increase in the total fabrication area and a significant decease in fabrication time would be realized.

5.5 REFERENCES

1.   Bayindir, Z., Sun, Y., Naughton, M.J., Lafratta, C.N., Baldacchini, T., Fourkas, J.T., Stewart, J., Saleh, B.E.A., and Teich, M.C., *Polymer microcantilevers fabricated via multiphoton absorption polymerization*. Applied Physics Letters, 2005. **86**(6): p. 064105.

2.   Kawata, S., Sun, H., Tanaka, T. and Takada, K., *Finer features for functional microdevices*. Nature, 2001. **412**: p. 697-698.

3.   Kaehr, B., Allen, R., Javier, D., Currie, J. and Shear, J., *Guiding neuronal development with in situ microfabrication*. Proceedings of the National Academy of Sciences, 2004. **101**: p. 16104-16108.

4.   Kaehr, B., Ertas, N., Nielson, R., Allen, R., Hill, R.T., Plenert, M. and Shear, J.B., *Direct-write fabrication of functional protein matrixes using a low-cost Q-switched laser*. Analytical Chemistry, 2006. **78**: p. 3198-3202.

5.   Kaehr, B. and Shear, J., *Mask-directed multiphoton lithography*. Journal of the American Chemical Society, 2007. **129**: p. 1904-1905.

6.   Nielson, R., Kaehr, B. and Shear, J., *Microreplication and design of biological architectures using dynamic-mask multiphoton lithography*. Small, 2009. **5**: p. 120-125.

7.   Lafratta, C.N., Baldacchini, T., Farrer, R.A., Fourkas, J.T., Teich, M.C., Saleh, B.E.A. and Naughton, M.J., *Replication of two-photon-polymerized structures with extremely high aspect ratios and large overhangs*. Journal of Physical Chemistry B, 2004. **108**: p. 11256-11258.

8.   Lafratta, C.N., Li, L. and Fourkas, J.T., *Soft-lithographic replication of 3D microstructures with closed loops* Proceedings of the National Academy of Sciences, 2006. **103**(23): p. 8589-8594.

9.   Kaehr, B. and Shear, J., *High-throughput design of microfluidics based on directed bacterial motility*. Lab Chip, 2009. **9**: p. 2632-2637.

10.   Kaehr, B. and Shear, J.B., *Multiphoton fabrication of chemically responsive protein hydrogels for microactuation*. Proceedings of the National Academy of Sciences, 2008. **105**: p. 8850-8854.

11.   Kato, J., Takeyasu, N., Adachi, Y. and Sun, H., *Multiple-spot parallel processing for laser micronanofabrication*. Applied Physics Letters, 2005: p. 044102.

12.   Formanek, F., Takeyasu, N., Tanaka, T., Chiyoda, K., Ishikawa, A. and Kawata, S., *Three-dimensional fabrication of metallic nanostructures over large areas by two-photon polymerization*. Optics Express, 2006. **14**(2): p. 800-809.

13.   Younse, J., *Projection display systems based on the digital micromirror device (DMD)*. Proceedings of SPIE, 1995. **2641**: p. 64-75.

Bibliography

Allen, P., Doepker, B. and Chiu, D. (2009). "High-throughput capillary-electrophoresis analysis of the contents of a single mitochondria." <u>Analytical Chemisry</u> **81**: 3784-3791.

Allen, R., Nielson, R., Wise, D. and Shear, J. (2005). "Catalytic three-dimensional protein architectures." <u>Analytical Chemistry</u> **77**: 5089-5095.

Arakawa, T. and Timasheff, S. (1984). "Mechanism of protein salting in and salting out by divalent cation salts: balance between hydration and salt binding." <u>Biochemistry</u> **23**: 5912-5923.

Baca, H. K., Ashley, C., Carnes, E., Lopez, D., Flemming, J., Dunphy, D., Singh, S., Chen, Z., Nanguo, L., Fan, H., Lopez, G. P., Brozik, S. M., Werner-Washburne, M. and Brinker, C. J. (2006). "Cell-directed assembly of lipid-silica." <u>Science</u> **313**: 337-341.

Basu, S., Cunningham, L., Pins, G., Bush, K., Taboada, R., Howell, A. R., Wang, J. and Campagnola, P. J. (2005). "Multiphoton excited fabrication of collagen matrixes cross-linked by a modified benzophenone dimer: bioactivity and enzymatic degradation" <u>Biomacromolecules</u> **6**: 1465-1474.

Basu, S., Wolgemuth, C. and Campagnola, P. (2004). "Measurement of normal and anomalous diffusion of dyes within protein structures fabricated via multiphoton excited cross-linking." <u>Biomacromolecules</u> **5**: 2347-2357.

Bayindir, Z., Sun, Y., Naughton, M. J., Lafratta, C. N., Baldacchini, T., Fourkas, J. T., Stewart, J., Saleh, B. E. A. and Teich, M. C. (2005). "Polymer microcantilevers fabricated via multiphoton absorption polymerization." <u>Applied Physics Letters</u> **86**(6): 064105.

Beebe, D. J., Moore, J. S., Bauer, J. M., Yu, Q., Liu, R. H., Devadoss, C. and Jo, B.-H. (2000). "Functional hydrogel structures for autonomous flow control inside microfluidic channels." <u>Nature</u> **404**: 588-590.

Bellelli, A., Antonini, G., Brunori, M. and Springer, B. (1990). "Transient spectroscopy of the reaction of cyanide with ferrous myoglobin. Effect of distal side residues." <u>Journal of Biological Chemistry</u> **265**(31): 18898-18901.

Bhowmik, B. B. and Mukhopadhyay, M. (1988). "Spectral and photophysical studies of thiazine dyes in Triton X-100." <u>Colloid & Polymer Science</u> **266**: 672-676.

Bischof, J. C. and He, X. (2006). "Thermal stability of proteins." <u>Annals New York Academy of Sciences</u> **1066**: 12-33.

Boedicker, J. Q., Vincent, M. E. and Ismagilov, R. F. (2009). "Microfluidic confinement of single cells of bacteria in small volumes initiates high-density behavior of quorum sensing and growth and reveals Its variability." <u>Angew. Chem. Int. Ed.</u> **121**(32): 6022-6025.

Brown, E., Wu, E., Zipfel, W. and Webb, W. (1999). "Measurement of molecular diffusion in solution by multiphoton fluorescence photobleaching recovery." <u>Biophysical Journal</u> **77**: 2837-2849.

Brown, E. B., Shear, J. B., Adams, S. R., Tsien, R. Y. and Webb, W. W. (1999). "Photolysis of caged calcium in femtoliter volumes using two-photon excitation." <u>Biophysical Journal</u> **76**: 489-499.

Callender, R., Dyer, R., Gilmanshin, R. and Woodruff, W. (1998). "Fast events in protein folding: the time evolution of primary processes." <u>Annual review of physical chemistry</u> **49**: 173-202.

Carnes, E. C., Lopez, D. M., Donegan, N. P., Cheung, A., Gresham, H., Timmins, G. S. and Brinker, C. J. (2018). "Confinement-induced quorum sensing of individual Staphylococcus aureus bacteria." <u>Nature Chemical Biology</u> **6**(1): 41-45.

Chen, E., Goldbeck, R. and Kliger, D. (1997). "Nanosecond time-resolved spectroscopy of biomolecular processes." <u>Annual review of biophysics and biomolecular structure</u> **26**: 327-355.

Correa, D. S., Tayalia, P., Cosendey, G., Santos, D. S. d., Aroca, R. F., Mazur, E. and Mendonca, C. R. (2009). "Two-photon polymerization for fabricating structures containing the biopolymer chitosan." <u>Journal of Nanoscience and Nanotechnology</u> **9**: 5845-5849.

Cushing, M. and Anseth, K. (2007). "Hydrogel cell cultures." <u>Science</u> **316**: 1133-1134.

Daviesa, M. J. and Truscottb, R. J. (2001). "Photo-oxidation of proteins and its role in cataractogenesis." <u>Journal of Photochemistry and Photobiology B: Biology</u> **63**: 114-125.

Denk, W. (1994). "Two-photon scanning photochemical microscopy: mapping ligand-gated ion channel distributions." <u>Proceedings of the National Academy of Sciences</u> **91**: 6629-6633.

Denk, W., Strickler, J. H. and Webb, W. W. (1990). "Two-photon laser scanning fluorescence microscopy." <u>Science</u> **248**: 73-76.

Dong, L., Agarwal, A., Beebe, D. and Jiang, H. (2006). "Adaptive liquid microlenses activated by stimuli-responsive hydrogels." <u>Nature</u> **442**: 551-554.

Dong, L., Agarwal, A. K., Beebe, D. J. and Jiang, H. (2007). "Variable-focus liquid microlenses and microlens arrays actuated by thermoresponsive hydrogels." <u>Advanced Materials</u> **19**: 401-405.

Evans, C. L., Potma, E. O., Puorishaag, M., Cote, D., Lin, C. P. and Xie, X. S. (2005). "Chemical imaging of tissue in vivo with video-rate coherent anti-Stokes Raman scattering microscopy." Proceedings of the National Academy of Sciences **102**(46): 16807-16812.

Fisher, G. J., Dutta, S. C., Talwar, H. S., Wang, Z., Varani, J., Kang, S. and Voorhees, J. J. (1996). "Molecular bases of sun-induced premature sking ageing and retinoid antoagonism." Nature **379**: 335-339.

Formanek, F., Takeyasu, N., Tanaka, T., Chiyoda, K., Ishikawa, A. and Kawata, S. (2006). "Three-dimensional fabrication of metallic nanostructures over large areas by two-photon polymerization." Optics Express **14**(2): 800-809.

Galajda, P. and Ormos, P. (2001). "Complex micromachines produced and driven by light." Applied Physics Letters **78**: 249-251.

George, S., Ashby, G., Wharton, C. and Thorneley, R. (1997). "Time-resolved binding of carbon monoxide to nitrogenase monitored by stopped-flow infrared spectroscopy." Journal of the American Chemical Society **119**: 6450-6451.

Giddings, J. C. (1991). Unified Separation Science. New York, Wiley-Interscience.

Gil, E. and Hudson, S. (2004). "Stimuli-reponsive polymers and their bioconjugates." Progress in Polymer Science **29**: 1173-1222.

Gilmanshin, R., Williams, S., Callender, R., Woodruff, W. and Dyer, R. (1997). "Fast events in protein folding: Relaxation dynamics of secondary and tertiary structure in native apomyoglobin." Proceedings of the National Academy of Sciences **94**: 3709-3713.

González, M., Argarana, C. and Fidelio, G. (1999). "Extremely high thermal stability of streptavidin and avidin upon biotin binding." Biomolecular Engineering **16**: 67-72.

Göppert-Mayer, M. (2009). "Elementary processes with two quantum transitions." Annalen der Physik **18**: 466-479.

Gordon, M., Okerberg, E., Gostkowski, M. and Shear, J. (2001). "Electrophoretic characterization of transient photochemical reaction products." Journal of the American Chemical Society **123**: 10780-10781.

Gostkowski, M. L., Allen, R., Plenert, M. L., Okerberg, E., Gordon, M. J. and Shear, J. B. (2004). "Multiphoton-excited serotonin photochemistry." Biophysical Journal **86**: 3223-3229.

Grossman, P. D. and Colburn, J. C. (1992). Capillary Electrophoresis: Theory and Pracitce. San Diego, Academic Press, Inc.

Hansen, K., Rock, R., Larsen, R. and Chan, S. (2000). "A method for photoinitating protein folding in a nondenaturing environment." Journal of the American Chemical Society **122**: 11567-11568.

Hapuarachchi, S., Premeau, S. and Aspinwall, C. (2006). "High-speed capillary zone electrophoresis with online photolytic optical injection." <u>Analytical Chemistry</u> **78**: 3674-3680.

Harmon, M., Tang, M. and Frank, C. (2003). "A microfluidic actuator based on thermoresponsive hydrogels." <u>Polymer</u> **44**: 4547-4556.

Hell, S., Booth, M., Wilms, S., Schnetter, C., Kirsch, A. K., Arndt-Jovin, D. J. and Jovin, T. M. (1998). "Two-photon near-and far-field fluorescence microscopy with continuous-wave excitation." <u>Optics Letters</u> **23**: 1238-1240.

Hense, B. A., Kuttler, C., Muller, J., Rothballer, M., Hartmann, A. and Kreft, J.-U. (2007). "Does efficiency sensing unify diffusion and quorum sensing." <u>Nature Reviews Microbiology</u> **5**: 230-239.

Hill, R. and Shear, J. (2006). "Enzyme–nanoparticle functionalization of three-dimensional protein scaffolds." <u>Analytical Chemistry</u> **19**: 7022-7026.

Hoffman, A. S. (2002). "Hydrogels for biomedical applications." <u>Advanced Drug Delivery Reviews</u> **43**: 3-12.

Horswill, A. R., Stoodley, P., Stewart, P. S. and Parsek, M. R. (2007). "The effect of the chemical, biological, and physical environment on quorum sensing in structured microbial communities." <u>Analytical Bioanalytical Chemistry</u> **387**: 371-380.

Hu, Y., Liu, Y., Zhao, R., Dong, J. and Qu, S. (2006). "Spectroscopic studies on the interaction between methylene blue and bovine serum albumin." <u>Journal of Photochemistry and Photobiology A: Chemistry</u> **179**: 324-329.

Huang, X. and Lowe, T. L. (2005). "Biodegradable thermoresponsive hydrogels for aqueous encapsulation and controlled release of hydrophilic model drugs." <u>Biomacromolecules</u> **6**: 2131-2139.

Jacobson, S. C., Culbertson, C. T., Daler, J. E. and Ramsey, J. M. (1998). "Microchip structures for submillisecond electrophoresis." <u>Analytical Chemisry</u> **70**: 3476-3480.

Jones, C., Henry, E., Hu, Y., Chan, C., Luck, S., Bhuyan, A., Roder, H., Hofrichter, J. and Eaton, W. (1993). "Fast events in protein folding initiated by nanosecond laser photolysis." <u>Proceedings of the National Academy of Sciences</u> **90**: 11860-11864.

Jorgenson, J. W. and Lukacs, K. D. (1983). "Capillary zone electrophoresis." <u>Science</u> **222**: 266-272.

Kaehr, B., Allen, R., Javier, D., Currie, J. and Shear, J. (2004). "Guiding neuronal development with in situ microfabrication." <u>Proceedings of the National Academy of Sciences</u> **101**: 16104-16108.

Kaehr, B., Ertas, N., Nielson, R., Allen, R., Hill, R. T., Plenert, M. and Shear, J. B. (2006). "Direct-write fabrication of functional protein matrixes using a low-cost Q-switched laser." Analytical Chemistry **78**: 3198-3202.

Kaehr, B. and Shear, J. (2007). "Mask-directed multiphoton lithography." Journal of the American Chemical Society **129**: 1904-1905.

Kaehr, B. and Shear, J. (2009). "High-throughput design of microfluidics based on directed bacterial motility." Lab Chip **9**: 2632-2637.

Kaehr, B. and Shear, J. B. (2008). "Multiphoton fabrication of chemically responsive protein hydrogels for microactuation." Proceedings of the National Academy of Sciences **105**: 8850-8854.

Kaiser, W. and Garrett, C. G. B. (1961). "Two-photon excitation in $CaF_2:Eu^{2+}$." Physical Review Letters **7**: 229-231.

Kang, J.-H., Moon, J. H., Lee, S.-K., Park, S.-G., Jang, S. G., Yang, S. and Yang, S.-M. (2008). "Thermoresponsive hydrogel photonic crystals by three-dimensional holographic lithography." Advanced Materials **20**(16): 3061-3065.

Kato, J., Takeyasu, N., Adachi, Y. and Sun, H. (2005). "Multiple-spot parallel processing for laser micronanofabrication." Applied Physics Letters: 044102.

Kawata, S., Sun, H., Tanaka, T. and Takada, K. (2001). "Finer features for functional microdevices." Nature **412**: 697-698.

Kennedy, R., German, I., Thompson, J. and Witowski, S. (1999). "Fast analytical-scale separations by capillary electrophoresis and liquid chromatography." Chemical Reviews **99**: 3081-3131.

Kestin, J., Sokolov, M. and Wakeham, W. A. (1978). " Viscosity of liquid water in the range -50°C to 150°C." Journal of Physical and Chemical Reference Data **7**: 941-948.

Khripin, C. Y., Brinker, C. J. and Kaehr, B. (2010). "Mechanically tunable multiphoton fabricated protein hydrogels investigated using atomic force microscopy." Soft Matter **6**(12): 2842-2848.

Kiyonaka, S., Sugiyasu, K., Shinkai, S. and Hamachi, I. (2002). "First thermally responsive supramolecular polymer based on glycosylated amino acid." J. Am. Chem. Soc. **124**: 10954-10955.

Klein, J. and Kafka, J. D. (2010). "The Ti:Sapphire laser: The flexible research tool." Nature Photonics **4**(5): 289-289.

Knoblauch, M., Noll, G., Müller, T., Prüfer, D., Schneider-Huther, I., Scharner, D., Van Bel, A.J.E., and Peters, W. S. (2003). "ATP-independent contractile proteins from plants." Nature Materials **2**: 600-603.

Korlach, J., Schwille, P. and Webb, W. (1999). "Characterization of lipid bilayer phases by confocal microscopy and fluorescence correlation spectroscopy." <u>Proceedings of the National Academy of Sciences</u> **96**: 8461-8466.

Kosa, T., Maruyama, T. and Otagiri, M. (1998). "Species differences of serum albumins: II. chemical and thermal stability." <u>Pharmaceutical Research</u> **15**(3): 449-454.

Kumi, G., Yanez, C. O., Belfield, K. D. and Fourkas, J. T. (2010). "High-speed multiphoton absorption polymerization: fabrication of microfluidic channels with arbitrary cross-sections and high aspect ratios." <u>Lab Chip</u> **10**(8): 1057-1060.

Kumi, G., Yanez, C. O., Belfield, K. D. and Fourkas, J. T. (2010). "High-speed multiphoton absorption polymerization: fabrication of microfluidic channels with arbitrary cross-sections and high aspect ratios." <u>Lab on a Chip</u> **10**(8): 1057-1060.

Kuroda, D., Zhang, Y., Wang, J., Kaji, N., Tokeshi, M. and Baba, Y. (2008). "A viscosity-tunable polymer for DNA separation by microchip electrophoresis." <u>Analytical Bioanalytical Chemistry</u> **391**(7): 2543-2549.

Lafratta, C. N., Baldacchini, T., Farrer, R. A., Fourkas, J. T., Teich, M. C., Saleh, B. E. A. and Naughton, M. J. (2004). "Replication of two-photon-polymerized structures with extremely high aspect ratios and large overhangs." <u>Journal of Physical Chemistry B</u> **108**: 11256-11258.

Lafratta, C. N., Li, L. and Fourkas, J. T. (2006). "Soft-lithographic replication of 3D microstructures with closed loops " <u>Proceedings of the National Academy of Sciences</u> **103**(23): 8589-8594.

Lapos, J. A. and Ewing, A. G. (2000). "Injection of fluorescently labeled analytes into microfabricated chips using optically gated electrophoresis." <u>Analytical Chemisry</u> **72**: 4598-4602.

Leach, J., Bivens, K., Patrick, C. and Schmidt, C. E. (2003). "Photocrosslinked hyaluronic acid hydrogels: natural, biodegradable tissue engineering scaffolds." <u>Biotechnology and Bioengineering</u> **82**: 578-589.

Ledermann, A., Cademartiri, L. and Hermatschweiler, M. (2006). "Three-dimensional silicon inverse photonic quasicrystals for infrared wavelengths." <u>Nature Materials</u> **5**: 942-945.

Li, L., Gattass, R., Gershgoren, E., Hwang, H. and Fourkas, J. (2009). "Achieving {lambda}/20 resolution by one-color initiation and deactivation of polymerization." <u>Science</u> **324**: 910-913.

Li, M., Keller, P., Li, B., Wang, X. and Brunet, M. (2003). "Light-driven side-on nematic elastomer actuators." <u>Advanced Materials</u> **15**: 569-572.

Liu, Z. and Calvert, P. (2000). "Multilayer hydrogels as muscle-like actuators." <u>Advanced Materials</u> **12**(4): 288-291.

Maruo, S. and Inoue, H. (2006). "Optically driven micropump produced by three-dimensional two-photon microfabrication." Applied Physics Letters **89**: 144101.

Mcclain, M. A., Culbertson, C. T., Jacobson, S. C., Allbritton, N. L., Sims, C. E. and Ramsey, J. M. (2003). "Microfluidic devices for the high-throughput chemical analysis of cells." Analytical Chemistry **75**(21): 5646-5655.

Miller, C. C. (1924). "The Stokes-Einstein law for diffusion in solution." Proceedings of the Royal Society of London. Series A, Containing Papers of a Mathematical and Physical Character **106**: 724-749.

Monnig, C. A. and Jorgenson, J. W. (1991). "On-column sample gating for high-speed capillary zone electrophoresis." Anal. Chem. **63**: 802-807.

Nielson, R., Kaehr, B. and Shear, J. (2009). "Microreplication and design of biological architectures using dynamic-mask multiphoton lithography." Small **5**: 120-125.

Park, K. (2001). "Environment-sensitive hydrogels for drug delivery." Advanced Drug Delivery Reviews **53**: 321-339.

Parsek, M. and Greenberg, E. (2005). "Sociomicrobiology: the connections between quorum sensing and biofilms." Trends in Microbiology **13**: 27-33.

Peters, T. (1985). "Serum albumin." Advances in Protein Chemistry **37**: 161-245.

Pettit, D. L., Wang, S. S.-H., Gee, K. R. and Augustine, G. J. (1997). "Chemical two-photon uncaging: a novel approach to mapping glutamate receptors." Neuron **19**: 465-471.

Pilobello, K., Krishnamoorthy, L., Slawek, D. and Mahal, L. K. (2005). "Development of a lectin microarray for the rapid analysis of protein glycopatterns." ChemBioChem **6**: 985-989.

Pitts, J. D., Campagnola, P. J., Epling, G. A. and Goodman, S. L. (2000). "Submicron multiphoton free-form fabrication of proteins and polymers: studies of reaction efficiencies and applications in sustained release." Macromolecules **33**: 1514-1523.

Plenert, M. and Shear, J. (2003). "Microsecond electrophoresis." Proceedings of the National Academy of Sciences **100**(7): 3853-3857.

Pramanick, D. and Mukherjee, D. (1993). "Molecular interaction of methylene blue with Triton X-100 in reverse micellar media." Journal of Colloid and Interface Science **157**: 131-134.

Rajadhyaksha, M., Grossman, M. and Esterowitz, D. (1995). "In vivo confocal scanning laser microscopy of human skin: melanin provides strong contrast." Journal of Investigative Dermatology **104**: 946-952.

Redfield, R. J. (2002). "Is quorum sensing a side effect of diffusion sensing?" Trends in Microbiology **10**: 365-370.

Ritschdorff, E. T., Plenert, M. and Shear, J. B. (2009). "Microsecond analysis of transient molecules using bi-directional capillary electrophoresis." <u>Analytical Chemistry</u> **81**: 8790-8796.

Rock, R., Hansen, K., Larsen, R. and Chan, S. (2004). "Rapid photochemical triggering of protein unfolding in a nondenaturing environment." <u>Chemical Physics</u>.

Schild, H. G. (1992). "Poly (N-Isopropylacrylamide) - Experiment, Theory and Application." <u>Progress in Polymer Science</u> **17**: 163-249.

Seidlits, S. K., Schmidt, C. E. and Shear, J. B. (2009). "High-resolution patterning of hydrogels in three dimensions using direct-write photofabrication for cell guidance." <u>Advanced Functional Materials</u> **19**: 3543-3551.

Shear, J., Xu, C. and Webb, W. (1997). "Multiphoton-excited visible emission by serotonin solutions." <u>Photochemistry and Photobiology</u> **65**: 931-936.

Shear, J. B. (1999). "Multi-photon excited fluorescence in bioanalytical chemistry." <u>Analytical Chemistry</u> **71**: 598A-605A.

Sidorenko, A., Krupenkin, T., Taylor, A., Fratzl, P. and Aizenberg, J. (2007). "Reversible switching of hydrogel-actuated nanostructures into complex micropatterns." <u>Science</u> **315**: 487 - 490.

Sidorenko, A., Krupenkinb, T. and Aizenberg, J. (2008). "Controlled switching of the wetting behavior of biomimetic surfaces with hydrogel-supported nanostructures." <u>Journal of Materials Chemistry</u> **18**: 3841-3846.

Spikes, J. D., Shen, H., Kopeckova, P. and Kopecek, J. (1999). "Photodynamic crosslinking of proteins. 111. Kinetics of the FMN-and rose bengal-sensitized photooxidation and intermolecular crosslinking of modeI tyrosine-containing M(2-hydroxypropyI)methacryIamide copolymers." <u>Photochemistry and Photobiology</u> **70**: 130-137.

Sun, H., Matsuo, S. and Misawa, H. (1999). "Three-dimensional photonic crystal structures achieved with two-photon-absorption photopolymerization of resin." <u>Applied Physics Letters</u> **74**: 786-788.

Sun, H., Tanaka, T. and Kawata, S. (2002). "Three-dimensional focal spots related to two-photon excitation." <u>Applied Physics Letters</u> **80**: 3673-3675.

Takeda, K., Wada, A., Yamamoto, K., Moriyama, Y. and Aoki, K. (1989). "Conformational change of bovine serum albumin by heat treatment." <u>Journal of Protein Chemistry</u> **8**(5): 653-659.

Tao, L., Thompson, J. E. and Kennedy, R. T. (1998). "Optically gated capillary electrophoresis of o-phthalaldehyde/β-mercaptoethanol derivatives of amino acids for chemical monitoring " <u>Analytical Chemisry</u> **70**: 4015-4022.

Tirumala, V., Divan, R., Ocola, L. and Mancini, D. C. (2005). "Direct-write e-beam patterning of stimuli-responsive hydrogel nanostructures." <u>Journal of Vacuum Technology</u> **23**: 3124-3128.

Tokarev, I. and Minko, S. (2009). "Multiresponsive, hierarchically structured membranes: new, challenging, biomimetic materials for biosensors, controlled release, biochemical gates, and nanoreactors." <u>Advanced Materials</u> **21**: 241-247.

Tseng, S. C. G. and Zhang, S. H. (1995). "Interaction between rose bengal and different protein components." <u>Cornea</u> **14**(4): 427-435.

Vauthey, E. and Henseler, A. (1995). "Picosecond transient thermal phase grating study of a photoinduced electron transfer reaction in solution." <u>Journal of Physical Chemistry</u> **99**: 8652-8660.

Volk, M. (2001). "Fast initiation of peptide and protein folding processes." <u>European Journal of Organic Chemistry</u>.

Wang, I., Bouriau, M., Baldeck, P., Martineau, C. and Andraud, C. (2002). "Three-dimensional microfabrication by two-photon-initiated polymerization with a low-cost microlaser." <u>Optics Letters</u> **27**(15): 1348-1350.

Watanabe, T., Akiyama, M., Totani, K., Kuebler, S. M., Stellacci, F., Wenseleers, W., Braun, K., Marder, S. R. and Perry, J. W. (2002). "Photoresponsive hydrogel microstructure fabricated by two-photon initiated polymerization." <u>Advanced Functional Materials</u> **12**(9): 611-614.

Wu, C., Liu, T., Chu, B., Schneider, D. K. and Graziano, V. (1997). "Characterization of the PEO-PPO-PEO triblock copolymer and its application as a separation medium in capillary electrophoresis." <u>Macromolecules</u> **30**(16): 4574-4583.

Wu, C., Liu, T., White, H. and Chu, B. (2000). "Atomic force microscopy study of $E_{99}P_{69}E_{99}$ triblock copolymer chains on silicon surface." <u>Langmuir</u> **16**(2): 656-661.

Xu, C. and Webb, W. (1996). "Measurement of two-photon excitation cross sections of molecular fluorophores with data from 690 to 1050 nm" <u>Journal of the Optical Society of America B</u> **13**: 481-491.

Xu, C., Zipfel, W., Shear, J., Williams, R. and Webb, W. (1996). "Multiphoton fluorescence excitation: new spectral windows for biological nonlinear microscopy." <u>Proceedings of the National Academy of Sciences</u> **93**: 10763-10768.

Yamasaki, M. and Yano, H. (1990). "Differential scanning calorimetric studies on bovine serum albumin: I. Effects of pH and ionic strength." <u>International Journal of Biological Macromolecules</u> **12**: 263-268.

Yanik, M. F., Cinar, H., Cinar, H. N., Chisholm, A. D., Jin, Y. and Ben-Yakar, A. (2004). "Functional regeneration after laser axotomy." <u>Nature</u> **432**: 822.

Younse, J. (1995). "Projection display systems based on the digital micromirror device (DMD)." <u>Proceedings of SPIE</u> **2641**: 64-75.

Zhang, Y. and Gorner, H. (2009). "Photoprocesses of xanthene dyes bound to lysozyme or serum albumin." Photochemistry and Photobiology **85**: 677-685.

Zhao, B. and Moore, J. (2001). "Fast pH-and ionic strength-responsive hydrogels in microchannels." Langmuir **17**: 4758-4763.

Zipfel, W. R., Williams, R. M., Christie, R., Nikitin, A. Y., Hyman, B. T. and Webb, W. W. (2003). "Live tissue intrinsic emission microscopy using multiphoton-excited native fluorescence and second harmonic generation." Proceedings of the National Academy of Sciences **100**: 7075-7080.

Zumbusch, A., Holtom, G. and Xie, X. (1999). "Three-dimensional vibrational imaging by coherent anti-stokes raman scattering." Physical Review Letters **82**: 4142-4145.

Vita

Eric Thomas Ritschdorff was born in Poughkeepsie, NY on February 17, 1981 to John and Joanne Ritschdorff. He completed his secondary education in 1999 at Our Lady of Lourdes High School in Poughkeepsie, NY. In 1999, he entered Marist College in Poughkeepsie, NY, and received a Bachelor of Science in Chemistry in 2004. In the fall of 2004, he enrolled in the Analytical Chemistry graduate program at the University of Texas at Austin.

Permanent address: 11 Miron Drive Poughkeepsie, NY 12603

This dissertation was typed by the author.